

Southern Illinois University Carbondale

OpenSIUC

Theses

Theses and Dissertations

12-2020

Rare Earth Elements and Yttrium in Acid Mine Drainages of the Illinois Basin

Kyle Klitzing

Southern Illinois University Carbondale

Follow this and additional works at: <https://opensiuc.lib.siu.edu/theses>

Related Files

[Tables.xlsx](#) (3163 kB)

Recommended Citation

Klitzing, Kyle, "Rare Earth Elements and Yttrium in Acid Mine Drainages of the Illinois Basin" (2020).
Theses. 2808.

<https://opensiuc.lib.siu.edu/theses/2808>

This Open Access Thesis is brought to you for free and open access by the Theses and Dissertations at OpenSIUC. It has been accepted for inclusion in Theses by an authorized administrator of OpenSIUC. For more information, please contact opensiuc@lib.siu.edu.

RARE EARTH ELEMENTS AND YTTRIUM IN ACID MINE DRAINAGES OF THE
ILLINOIS BASIN

by

Kyle Klitzing

B.S., Southern Illinois University, 2015

A Thesis

Submitted in Partial Fulfillment of the Requirements for the
Master of Science Degree

Department of Geology
in the Graduate School
Southern Illinois University Carbondale
December 2020

THESIS APPROVAL

RARE EARTH ELEMENTS AND YTTRIUM IN ACID MINE DRAINAGES OF THE
ILLINOIS BASIN

by

Kyle Klitzing

A Thesis Submitted in Partial
Fulfillment of the Requirements
for the Degree of
Master of Science
in the field of Geology

Approved by:

Dr. Liliana Leticariu, Chair

Dr. Steven Esling

Dr. Daniel Hummer

Graduate School
Southern Illinois University Carbondale
November 05, 2020

AN ABSTRACT OF THE THESIS OF

Kyle Klitzing, for the Master of Science degree in Geology, presented on November 5, 2020, at Southern Illinois University Carbondale.

TITLE: RARE EARTH ELEMENTS AND YTTRIUM IN ACID MINE DRAINAGES OF THE ILLINOIS BASIN

MAJOR PROFESSOR: Dr. Liliana Lefticariu

Coal has been an important natural resource of energy in the Illinois Basin for generations. In addition to the organic macerals in coal, there is inorganic matter containing minerals and trace elements. With growing demand for economic and critical metals including Rare Earth Elements and Yttrium (REY), coals containing anomalously high concentrations of trace elements, as well as their associated coal mine wastes, and drainages have been explored as promising secondary resources, but there were no former studies of REY in Illinois basin CMD.

CMD samples were collected from 35 abandoned coal mine sites from three regions of the Illinois basin. Region 1 (R1) the southern extent of the basin extending west along the cottage grove fault system and includes Hicks dome, a nexus of regional hydrothermal activity and provenance of the Illinois Kentucky Fluorite District (IKFD) ore deposits; Region 2 (R2) comprised locations situated in western Illinois along the Du Quoin Monocline; and Region 3 (R3) comprised locations situated in northern Illinois, farthest from the Hicks Dome.

Two hypotheses were tested in this study: (1) that pH and Σ REY would share an inverse correlation, with the greatest abundances of REY found in the most acidic drainages; and (2) hydrothermal activity associated with Hicks Dome in southern Illinois was the source of REY enrichment in the coals, and so, REY abundance and pattern would reflect proximity to the cryptoexplosive complex, with the greatest enrichments expected in R1, closest to Hicks Dome.

The geochemical data of 42 CMD samples was examined was analyzed to test these two

hypotheses. Samples ranged from extremely acidic (pH=1.93) to circumneutral (pH=7.6) with an average pH value of 3.4. Total REY values (\sum REY) averaged 1,057 $\mu\text{g/L}$ across all samples and ranged from 0.4-9,879 $\mu\text{g/L}$ while \sum *critical*-REY abundances (Nd, Eu, Tb, Dy, and Y) averaged 611 $\mu\text{g/L}$ and ranged from 0.2-7,213 $\mu\text{g/L}$. Furthermore, there are significant direct correlations of \sum REY with Al, Si, SO_4 , Zn, Ni, Cu, Cd, Co and no correlations with Fe, Ca, P, Ba, and V. In the course of investigation, it was found that pH and linear concentration values for REY correlate poorly. However, logarithmic values of REY concentrations (i.e., $\log[\sum\text{REY}]$), as well as the above trace metals have strong inverse correlations with pH ($r=-0.84$, $p<0.005$). The data for Illinois CMD is agreeable with contemporary studies, where appreciable \sum REY abundance has been found only in acidic drainages (pH<4.5). The second hypothesis, that \sum REY abundances would be greatest within the region of Hicks Dome, proved false. The greatest \sum REY (and \sum *critical*-REY) contents were found in R3-CMD farthest from Hicks Dome, with the second greatest abundances found in R2. There were additional distinguishing regional characteristics, namely, notable concentrations of *critical*-REY, Li, Be, and other trace metals in R3; enrichments of Ba within R1-CMD; and enrichments of B in R2 along with greater relative abundances of La, Ce, Pr, and Nd. Furthermore, in this study it was found that Sr was directly correlated with LREY enrichment; accordingly, Sr in Illinois CMD is associated with a less economically attractive (low in *critical*-REY) abundance pattern. Altogether, the geochemical data suggests that REY enrichment in the Illinois basin is secondary to infiltration of the host rocks with metal rich, hydrothermal fluids.

ACKNOWLEDGMENTS

My deepest gratitude to Dr. Liliana Leticariu, whose encouragement and support made this thesis possible. Thank you also to Angie Mick, who was always willing to share her experience and knowledge of these sites and whose assistance in the field was invaluable. My thanks also to the Porter Jobling foundation, who provided the funding for analyses. And finally, much appreciation is due to my committee, who have kept me on track through it all.

DEDICATION

To my dearest wife Lucy Klitzing who has been my rock through it all, whose love makes every task sweeter, every moment happier, every pain bearable, every night calmer, and the stars seem touchable. This work is also dedicated to my parents, Mike and Maria Klitzing, who have been there for me since the beginning with boundless, unconditional love and support.

TABLE OF CONTENTS

<u>CHAPTER</u>	<u>PAGE</u>
ABSTRACT.....	i
ACKNOWLEDGMENTS	iii
DEDICATION.....	iv
LIST OF TABLES.....	viii
LIST OF FIGURES	ix
CHAPTERS	
CHAPTER 1 Introduction.....	1
1.1 Introduction.....	1
1.2 Regional REY Enrichment	1
1.3 Acid Mine Drainages (AMD) as REY Resources	1
1.4 Coal Mining AMD.....	3
1.5 Project Motivation	5
1.6 Hypotheses.....	6
1.7 REY Resources	6
1.8 REY Importance	7
1.9 Alternative REY Resources	8
1.10 Geologic History of Illinois Basin	11
CHAPTER 2 Methodology.....	14
2.1 Sampling Sites	14
2.2 Site Selection	15
2.3 Field Measurements	16

2.4 Sample Collection.....	16
2.5 Laboratory Methods.....	17
2.5.1 Filtration.....	17
2.5.2 Acidification	17
2.5.3 Sulfate Determination	18
2.5.4 Dilutions.....	18
2.6 Data Analysis Methods.....	20
CHAPTER 3 Results.....	21
3.1 Geochemistry of Coal Mine Discharge (CMD).....	21
3.1.1 Acidity.....	21
3.2 Rare Earth Elements and Yttrium (REY)	21
3.2.1 NASC Normalized REY Pattern.....	22
3.2.2 Regional Variations in REY Pattern.....	22
3.2.3 REY Distribution	27
3.3 REY and pH.....	36
3.4 Major and Trace Elements	36
3.4.1 Anion Makeup	36
3.4.2 Bulk Cations.....	38
3.4.3 Heavy Metals and Other Trace Elements	44
3.4.4 Trace Metal Correlations	53
CHAPTER 4 Discussion.....	57
4.1 Hypothesis 1: Cumulative REY Abundance vs pH.....	57
4.2 Hypothesis 2: Proximity to Hicks Dome vs Σ REY	61

4.3 <i>Critical</i> -REY Correlations	62
4.4 Additional Provenance for REY	67
4.5 Tab Simco CMD	68
4.6 Comparison with Spanish AMD.....	72
4.7 Comparison with Appalachian CMD.....	72
CHAPTER 5 Summary and Recommendations	74
5.1 Summary	74
5.2 Comments and Future Considerations	75
5.3 Economic Viability	76
REFERENCES	78
APPENDICES	
APPENDIX A Maps	85
APPENDIX B Copyright Permissions.....	88
VITA.....	95

LIST OF TABLES

<u>TABLE</u>	<u>PAGE</u>
Table 1.1: Modes of REY Enrichment	9
Table 3.1: Regional REY Statistics	34
Table 3.2: Bulk Elements.....	43
Table 3.3: Trace Elements	52

LIST OF FIGURES

<u>FIGURE</u>	<u>PAGE</u>
Figure 1.1: Chondrite-normalized REY values of samples in the Hick’s Dome area	2
Figure 1.2: (a) Enrichment of Spanish AMD relative to natural waters, and (b) MREE enrichment compared to parent ore body	2
Figure 1.3: (a) pH - Σ REY correlations in Appalachian AMD (b) Discrepancies of REY abundance between precipitates from acidic and circumneutral Appalachian CMD..	3
Figure 1.4: NASC normalized samples of Appalachian CMD.....	4
Figure 1.5: Speciation of REY with and without dissolved sulfate.....	4
Figure 1.6: 2018 Global REY production and reserves.....	8
Figure 1.7: Map of major structural features in Southern Illinois and surrounding area.....	11
Figure 1.8: Schematic of proposed ore genesis model for the IKFD.....	13
Figure 2.1: Sampling locations across the Illinois Basin.....	14
Figure 2.2: Organization of study area into three regions	14
Figure 2.3: Photograph of workbench setup for sample dilution and acidification.....	19
Figure 3.1: Regional and frequency distribution of sample pH values.....	21
Figure 3.2: Regional NASC normalized abundances of REY	23
Figure 3.3: Regional variation in REY composition	25
Figure 3.4: Examples of the two modalities of REY enrichment	26
Figure 3.5: Box and whisker diagrams showing regional variations of REY	31
Figure 3.6: Plots of individual REY concentrations vs pH.....	35
Figure 3.7: Regional variations of Cl and P and their plots against Σ REY abundance	37

Figure 3.8: Composite Figure of regional values of TDS and % contribution of the major analytes to bulk anion chemistry as well as their plots against \sum REY abundance ...	40
Figure 3.9: Regional distribution of trace metal abundance values.....	49
Figure 3.10: Correlations of Co with (a) SO ₄ and (b) As	54
Figure 3.11: Trace element correlations with \sum REY abundance values	56
Figure 4.1: Graph plotting cumulative REY abundance with pH values	57
Figure 4.2: Linear correlations of SO ₄ with Fe and Co.....	60
Figure 4.3: (a) Correlation between \sum REY and \sum <i>critical</i> -REY (b) Correlation between pH and \sum <i>critical</i> -REY abundance	63
Figure 4.4: (a) Range of concentration values for the <i>critical</i> -REY (b) Percent contribution of individual <i>critical</i> -REY to the cumulative <i>critical</i> -REY abundance	63
Figure 4.5: Composite figure (a) Portion of \sum REY that are <i>critical</i> -REY (b) Range of Y contribution to cumulative abundances of <i>critical</i> -REY.....	64
Figure 4.6: (a) Plot of Y against \sum <i>critical</i> -REY (b) Plot of Y/Ce against % <i>critical</i> -REY.	65
Figure 4.7: (a) Plot of Y/Ce against \sum REY (b) Inverse correlation of Y/Ce with Sr.....	66
Figure 4.8: Map view of the Tab Simco site.....	68
Figure 4.9: View and schematic of bioreactor cell at Tab Simco.....	68
Figure 4.10: NASC normalized REY abundances between two samples from the Palzo mine...	70
Figure 4.11: Comparison of \sum REY values for Illinois and Appalachian CMD.....	73
Figure A1: Map of sampling locations across the greater Illinois Basin.....	85
Figure A2: Map illustrating the three sampling areas in the Illinois Basin	86
Figure A3: Depletions/enrichment effects of remediation at Tab Simco	87
Figure A4: Enrichment of TS main seep vs combined seeps	87

CHAPTER 1

INTRODUCTION

1.1 Introduction

The rare-earth elements (REE) are defined by IUPAC as the set of 17 chemical elements consisting of the fifteen lanthanides, scandium, and yttrium (IUPAC, 2005). Scandium and yttrium are grouped with the lanthanides because they are found to occur within the same ore deposits and additionally, they display similar chemical properties to the lanthanide elements. In diagrams showing concentrations of rare earth elements and yttrium (REY), Y is typically placed between Dy and Ho because they share very similar ionic radii as well as trivalent natures (Dai et al., 2016b).

1.2 Regional REY Enrichment

In the far southeastern part of Illinois, the cryptoexplosive igneous complex known as Hicks Dome is known to be a source of REY, with enrichments seen in minerals contained in the igneous intrusions associated with Hicks dome, the explosion breccia, as well as within the associated fluorite. Long et al. (2010) found REY enrichment in some sections of drill core through the breccia of the Hicks Dome cryptoexplosive complex; these zones were cemented with fluorite, calcite, galena sphalerite, and pyrite. Denny et al. (2015) also found significant REY enrichment in fluorite ore and igneous rocks (Figure 1.1) and identified the REY mineral of one of the samples to be synchysite, one of numerous REY-bearing fluorocarbonates intergrown in these types of deposits.

1.3 Acid Mine Drainages (AMD) as REY Resources

AMD associated with coal and metal mining operations could also be enriched in REY and other critical elements (Ayora et al., 2015; Stewart et al., 2017; Lefticariu *et al.*, 2020).

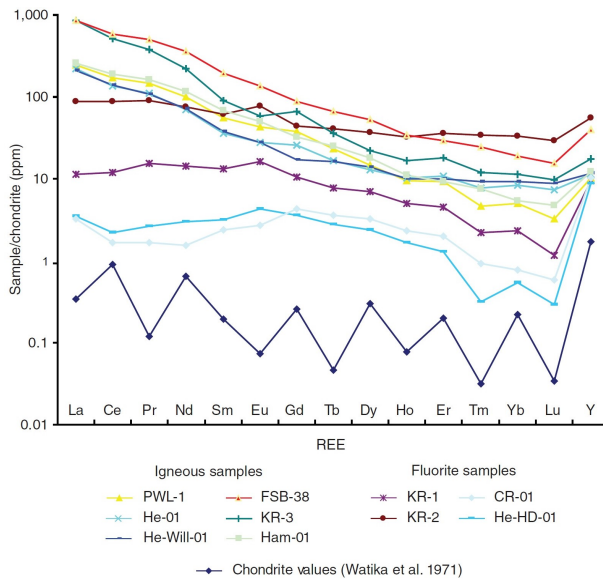


Figure 1.1 Chondrite-normalized REY values of samples in the Hick’s Dome area. Source: Illinois State Geological Survey (Denny et al., 2015). Reprinted with permission.

Studies of metal mine drainages in Spain by Ayora et al. (2015) revealed that many AMD can be significantly enriched in REY (Figure 1.2a), with total concentration values, Σ REY, of 4,000–80,000 picomol/L, several orders of magnitude greater than those of natural waters .

After normalization to the North American Shale Composite (NASC), the REY pattern in AMD showed a convex pattern of enrichment compared to the source mining refuse (Figure 1.2b) (Ayora et al., 2015). This middle REE enrichment was ascribed by the authors to the fractionation of REY during the adsorption of REY to the Fe precipitates (Ayora et al., 2015).

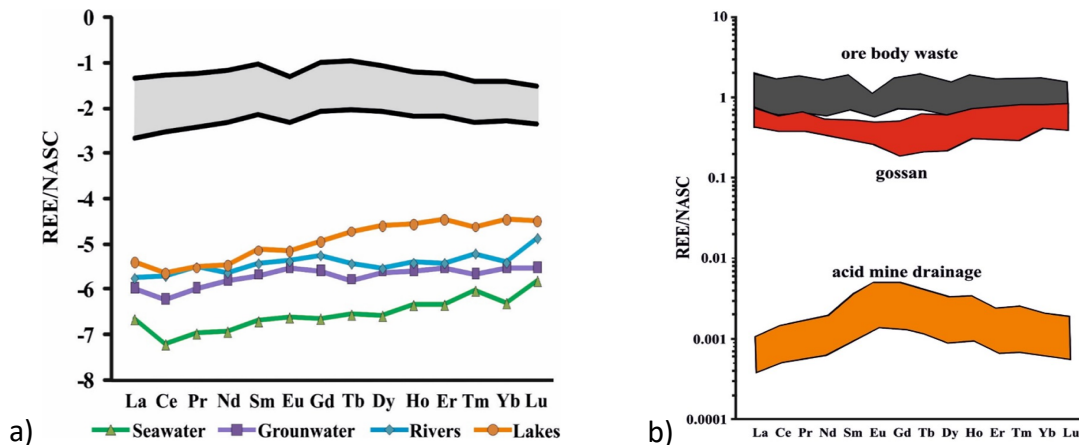


Figure 1.2: Figures from Ayora et al. (2015) showing (a) Enrichment of Spanish AMD relative to natural waters, and (b) MREE enrichment compared to parent ore body. Reprinted with permission.

1.4 Coal Mining AMD

In the 2017 study by Stewart et al., they evaluated the potential of coal mine drainages (CMD) in the Appalachian basin as a REY resource. In this study they reported results from 18 samples of coal mining drainages collected across the Appalachia Basin. The pH of coal mining drainages ranged from 2.8 to 6.6 and the Σ REY varied from 0.29-1,134 $\mu\text{g/L}$. For the Appalachian Basin, in terms of magnitude, they estimated an output of ~ 538 tons of REY per year from Appalachian CMD, 80% of that coming from AMD sites.

Stewart et al. (2017) found a direct correlation between discharge pH and REY abundance in Appalachian coal mine drainages (Figure 1.3), with acidic mine drainages being enriched with REY compared to neutral and alkaline ones, with total REY concentrations decreasing exponentially with increasing pH. This result was interpreted by the authors to suggest that at least some of the REY is sourced from minerals that are readily leached by acidic solutions, such as phosphates, carbonates, and some silicates (Stewart et al., 2017). A decrease of total REY concentration by several orders of magnitude in alkaline CMD (Figure 1.3B) is attributed to adsorption or co-precipitation with Al- and/or Fe-rich phases; at the same time, the

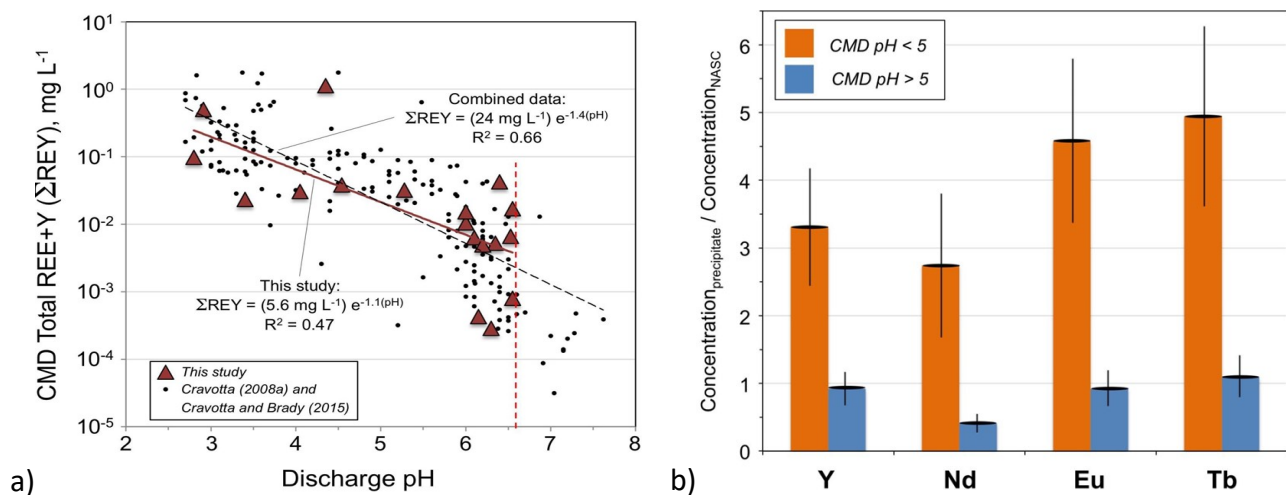


Figure 1.3 Results by Stewart et al., (2017) (a) identifying inverse correlation between pH and REY abundance in Appalachian CMD and (b) discrepancies of REY abundance of precipitates between acidic and circumneutral Appalachian CMD. Figures reprinted with permission.

solutions with neutral and alkaline pH values have limited dissolution capacity of REY bearing minerals (Stewart et al., 2017).

In this study, in addition to CMD samples, solid samples of the precipitates were also collected at various Appalachian AMD treatment sites. The Al-rich, Ca-Mg-rich, and Fe-rich precipitates were found to be slightly depleted in the LREE, but with an REY enrichment pattern otherwise like that of the parent AMD. The patterns of REY normalized to the NASC (Figure 1.4) for both the AMD and the precipitates showed depletions of LREE relative to HREE (Stewart et al., 2017). Overall, the Appalachian AMD described by Stewart et al. (2017), showed a MREY enrichment (Figure 1.4), similar to that reported by Ayora et al. in AMD from Spain (2015). The drainages were characterized by low pH and abundant sulfate with REY present primarily as complexes with sulfate (LnSO_4^+) and, to a lesser degree, as free ions, Ln^{3+} (Figure 1.5).

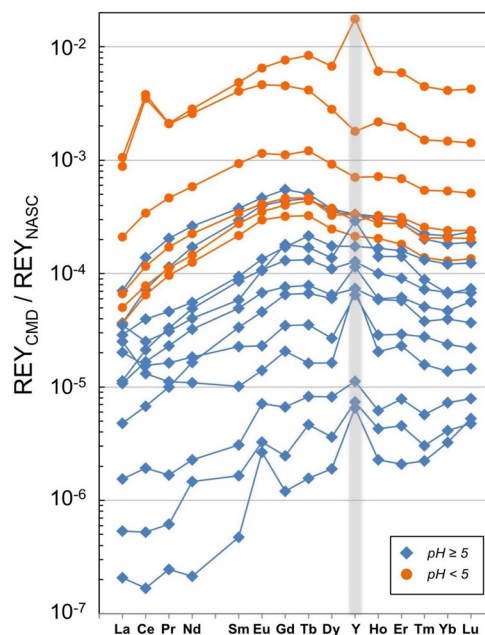


Figure 1.4 NASC normalized samples of Appalachian CMD from Stewart et al., (2017). Reprinted with permission.

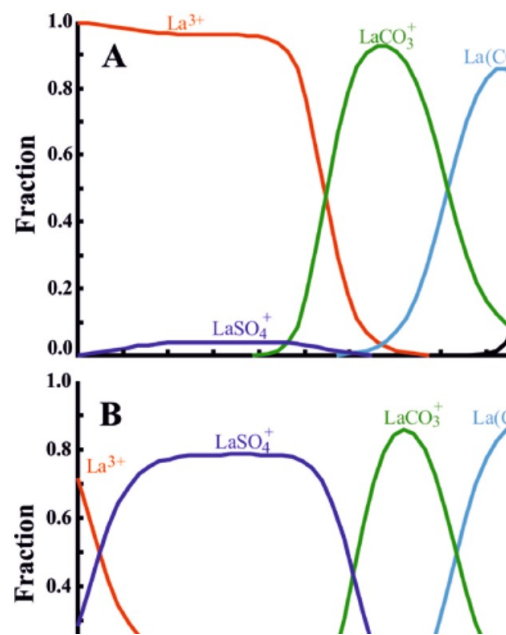


Figure 1.5 Speciation of REY in solution without (a) and within (b) the presence of dissolved sulfate. Figures by Ayora et al., (2015); reprinted with permission.

1.5 Project Motivation

By the time the Surface Mining Control and Reclamation Act passed in 1977, over 200,000 acres had been affected by mining operations in Illinois, with over 10% having since been recognized as “problem acreage”: negatively affected water and land including tippie sites, exposed refuse and goaf, toxic and barren spoil banks, etc. (IDNR). While many mine remediation efforts can have lasting effects, AMD sites typically must be revisited continually as more permanent treatment solutions are still being developed. AMD is particularly damaging to the environment and treatment is a high priority, though poorly funded effort. The cost of AMD remediation is not a static value since it involves the cost of the initial AMD treatment technology as well as the perpetual costs of maintenance. This may be ameliorated, however, if AMD is identified as a resource of REY in the Illinois basin.

Coal in the Illinois basin could be an economic source of REY. The most likely host of REY is the inorganic fraction of coal, dominantly within the clays but also as detrital minerals like the phosphate mineral monazite. In the Illinois Basin, the organic matter fraction in coals (i.e., macerals), have not been shown to be enriched in REY (Kolker et al., 2020). REY have been found with abundance in other coals, e.g. those in Eastern Kentucky by Hower et al (1999) and the hydrothermally altered coals studied by Seredin and Dai (Seredin and Dai, 2012a). In the Illinois Basin, some coals have been affected by hydrothermal mineralization and they are enriched in metals such as Zn, Pb, Cu (Moorehead, 2013) . Such coal seams containing hydrothermal mineralization are commonly seen in different coal seams in the southern Illinois basin (Cobb, 1981; Hower et al., 2000). Additionally, the weathering of hydrothermally- affected coal mining refuse at various abandoned coal mine sites might produce AMD with excessively high concentrations of sulfate and metals (Lefticariu et al., 2020). Such metal-rich AMD could

also have high concentrations of REY since REY-rich hydrothermal solutions could have induced enrichments in the sedimentary sequences.

While the coal and coal mining products of eastern Kentucky, Far Eastern Russia, and China have attracted the most research and attention due to their anomalously high REY concentrations, coal mine drainage is another avenue by which coal wastes can potentially be tapped for REY and Illinois has these in abundance. Coupling AMD remediation with recovery of REY is an attractive prospect with both environmental and economic benefits.

1.6 Hypotheses

With these considerations, this project tested the following hypotheses:

H1: The total concentration of REY, Σ REY, in AMD from abandoned coal mining sites across the Illinois Basin are inversely correlated with the pH of the AMD, such that the highest Σ REY concentrations will be found in AMD with the lowest pH values.

H2: Hydrothermal activity in southern Illinois, associated with Hicks Dome, enriched the coal seams from this region in REY. Therefore, a spatial relationship should be seen between REY distribution pattern and proximity to Hicks Dome, such that the AMD with the highest Σ REY concentrations will be found in close proximity to the Hicks Dome; the further the AMD site is from the Hicks Dome, the lower the Σ REY concentrations in AMD.

1.7 REY Resources

Despite the name, REY are not particularly rare in terms of abundance within the Earth's crust (Weng et al., 2015), but rather they are not concentrated in economically minable concentrations and thus are scarce relative to most other metals such as Zn, Cu, etc.. To date, REY ore deposits have been identified within two geologic environments, namely: (1) magmatic REY deposits, which include (1a) carbonatite deposits (i.e., Mountain Pass, CA; Bear Lodge

WY), (1b) Peralkaline deposits (i.e., Bokan Mountain, AK) AND (1c) Pegmatitic deposits (apatite deposits Mineville, NY) and (2) sedimentary REY deposits, which include (2a) monazite-xenotime-bearing placer deposits (i.e., Elliot Lake Mining District, GA), (2b) phosphorite deposits (i.e., phosphate deposits, FL) and (2c) regolith-hosted (i.e., Southern China, Madagascar, Brazil) ion-adsorption clay deposits. Ion-adsorption clay (IAC) deposits are formed as the result of surface weathering of igneous rocks when REY are released from igneous minerals and reabsorbed by clay minerals (Weng et al., 2015; USGS, 2019). The IAC deposits are the leading source of production for heavy REY (HREY) such as Gd, Lu, and Y. The production of light rare earth elements (LREY) on the other hand typically comes from carbonatite and placer deposits. (USGS, 2019).

1.8 REY Importance

REY are increasingly ubiquitous in high technologies and are used in semiconductors, catalysts, in power generation and storage, alloys, optics, lighting, and numerous other technologies with scientific, commercial and military applications (Bauer et al., 2010). REY containing materials have highly valuable properties and whilst substitutes are available for many applications, they are generally less effective (Dai et al., 2016b; USGS, 2019).

Significantly, the national demand of REY is projected to increase rapidly within the next several decades and many REY with high criticality, so called critical-REY, namely Nd, Eu, Tb, Dy, and Y (Bauer et al., 2010; Goodenough et al., 2018; USGS, 2019), are already in high demand (Alonso et al., 2012; USGS, 2019). The primary uses of the *critical*-REY are within permanent magnets, such as those used in wind turbines and electric vehicles, and as phosphors in the production of energy efficient lighting (Generalic; King; Chu, 2011).

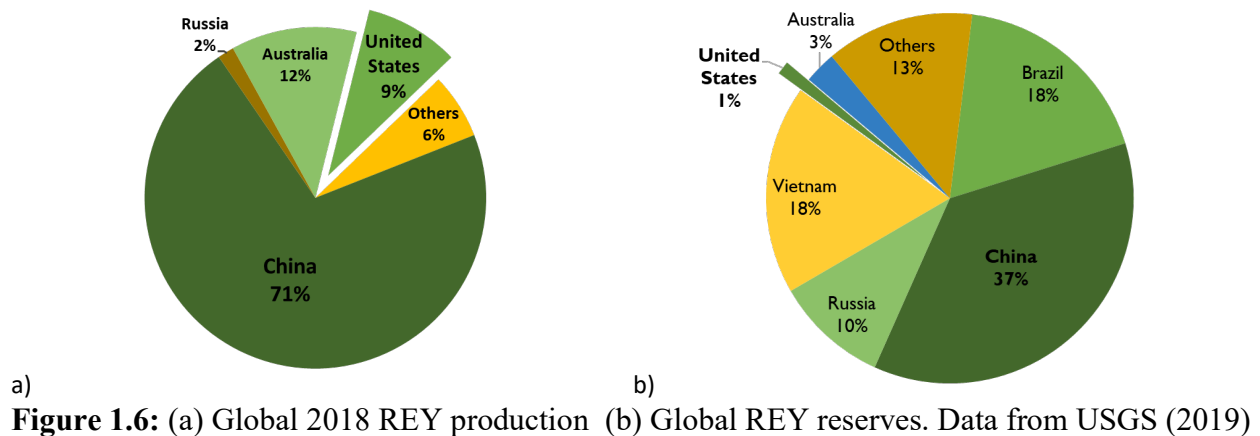
China was responsible for 71% of the world production of REY in 2018. Furthermore,

China was responsible for virtually all of the world’s Y supply, from its weathered clay ion-adsorption ore deposits in the southern Provinces—primarily Fujian, Guangdong, and Jiangxi—and from a lesser number of deposits in Guangxi and Hunan Provinces (USGS, 2019). With the reopening of the REY mine in Mountain Pass, CA in the first quarter of 2018, the United States is no longer wholly reliant on REY imports; the United States accounted for roughly ~9% of 2018 world REY (USGS, 2019).

An examination of worldwide REY reserves reveals further reason for concern. The United States holds only 1% of identified reserves (Figure 1.6), whereas China contains 38% (USGS, 2019). Furthermore, global annual demand is increasing by >5% (USGS, 2019). All of these factors bespeak the economic necessity of identifying additional REY resources to avoid disruption of REY, as a result of increasing demand and/or changes in trade or political climates, which could put the United States at a strategic and economic disadvantage (USGS, 2019).

1.9 Alternative REY Resources

Thus, alternative sources of REY are continuously being sought out (Bauer et al., 2010; Weng et al., 2015). In recent years, the enrichment of REY within coal and coal mining wastes (i.e., overburden and underburden rocks related to coal seams) have been investigated as resources of REY. The most well studied coal deposits are those of China (Zhao et al., 2007;



Yang et al., 2012; Dai et al., 2016a), far Eastern Russia (Seredin and Dai, 2012a; Dai et al., 2016a)), and the U.S.A. (Schatzel and Stewart, 2003; Hower et al., 2016b; Stewart et al., 2017).

Seredin and Dai (2012) identified four main genetic types of REY enrichment in coals (Table 1.1:): the Terrigenous type reflects accumulation of REY into peat by way of surface waters; Tuffaceous enrichment is associated with the incorporation of volcanic ash into the peat; an Infiltrational genetic origin denotes interactions with meteoric groundwater, similar to that seen in uranium deposits; and Hydrothermal genetic enrichment entails the interaction of deep, hot fluids with coal deposits at various stages of development.

The major REY coal deposits of South China and far Eastern Russia are characterized by tuffaceous and hydrothermal and mixed tuffaceous/hydrothermal genetic styles of enrichment (Dai et al., 2016a). Based on experimental extractions of REY from low rank Russian coals, Seredin and Dai (Seredin and Dai, 2012b) determined the cut-off grade for a coal seam, at 2004 REY prices, to be $\geq 1000 \mu\text{g/g}$ REO in the coal ash or 800-900 $\mu\text{g/g}$ for a coal seam with thickness over 5 meters and relatively thick benches having REO $\geq 1000 \mu\text{g/g}$ that can be preferentially mined.

REY has been found to be present in coal in three association types: (1) REY-rich detrital minerals such as zircon and apatite, (2) REY-rich authigenic minerals such as goyazite, and (3) adsorbed onto organic matter (Seredin and Dai, 2012b). Authigenic minerals host the highest

Table 1.1: Modes of REY Enrichment (after Seredin and Dai, 2012)

Enrichment Type	REO content in ash	Associated elements	Example deposit
Terrigenous	0.1-0.4%	Al, Ga, Ba, Sr	Jungar, China (Dai et al., 2006; Dai et al., 2008)
Tuffaceous	0.1-0.5%	Zr, Hf, Nb, Ta, Ga	Dean, USA (Mardon and Hower, 2004)
Infiltrational	0.1-1.2%	U, Mo, Se, Re	Aduunchulun, Mongolia (Arbuzov and Mashen'kin, 2007)
Hydrothermal	0.1-1.5	As, Sb, Hg, Ag, Au, etc.	Rettikhovka, Russia (Seredin, 2004)

amounts of REY in coal, mostly as alunite minerals and phosphates. In hydrothermally enriched coals, REY-rich carbonates (i.e., kimuraite, lanthanite) and fluorocarbonates (i.e., bastnaesite) are common and may reflect both epigenetic (introduced in coal by hydrothermal solutions which precipitated REY-rich minerals as veins) and diagenetic (diagenetic changes of the sedimentary deposit after deposition) origins (Seredin and Dai, 2012b).

Within the major metalliferous coal deposits of East Asia, the REY were found to be associated with clay and organic matter as well as with primary REY-bearing magmatic minerals. The fraction of REY bound to organic matter can be significant. For example, in the Vanchin and Luzanovka coal deposits in far Eastern Russia, the humic matter accounts for ~50% of REY (Seredin and Dai, 2012b). They also found that rather than the coal itself, other sedimentary strata associated with the coal deposits, such as the overburden and underburden, may be preferentially enriched in REY, most probable by hydrothermal fluids.

In the U.S.A., a significant number of studies have concentrated on determining the REY contents in coal from various basins, including Appalachia (Stewart et al., 2017) Illinois (Denny et al., 2015; Lefticariu et al., 2020), and Wyoming (Palmer et al., 2001; Huang et al., 2020).

Hower et al., (2016a) reported varying but appreciable Σ REY values in four eastern Kentucky coal beds. Values ranged from 40-103 ppm on a whole coal basis (569-944 ppm on a coal ash basis with greatest abundances found in the so-called fireclay member, which is notable enriched in REY. The fireclay member is the host to thin lenticulate pyroclastic deposits of volcanic ash called tonsteins. These tonsteins have REY bearing minerals such as zircon, apatite, crandallite and monazite, and the underlying coal seams contain between 1,965-4,198 ppm Σ REY on an ash basis. (Hower et al., 1999). This tuffaceous enrichment can be a notable influence on REY contents, even in sections of coal where an ash layer did not visibly survive

coal diagenesis, like the contemporaneous Dean coal member where the tonstein layer did not persist and the only evidence of the tuffaceous enrichment is the age of the strata and the elevated levels of REY, (Hower et al., 2016b). Hower et al (2016a) concluded that REY abundance in these US coals happened by way of multiple modes of enrichment, with some, as with the Fire Clay member, likely the result of all four genetic types. Recovery of REEs from clay-rich rocks associated with coal seams (i.e., tonstein, coal mining waste materials) are one of the more promising approaches to REE recovery.

1.10 Geologic History of Illinois Basin

The Illinois Basin contains some of the most important coal resources in the U. S. This Paleozoic sedimentary basin is an intracratonic basin that covers ~34 million acres in Illinois, Southwestern Indiana, and Western Kentucky. Coal and coal mining products in the Illinois basin are a potential domestic REY coal-based resources.

The history of the Illinois basin begins with the breakup of Rodinia, in the late Proterozoic. At this time, a failed intracontinental rift in southeastern Illinois produced the Reelfoot rift and the Rough Creek graben, intersecting at the Lusk Creek fault zone (Figure 1.7),

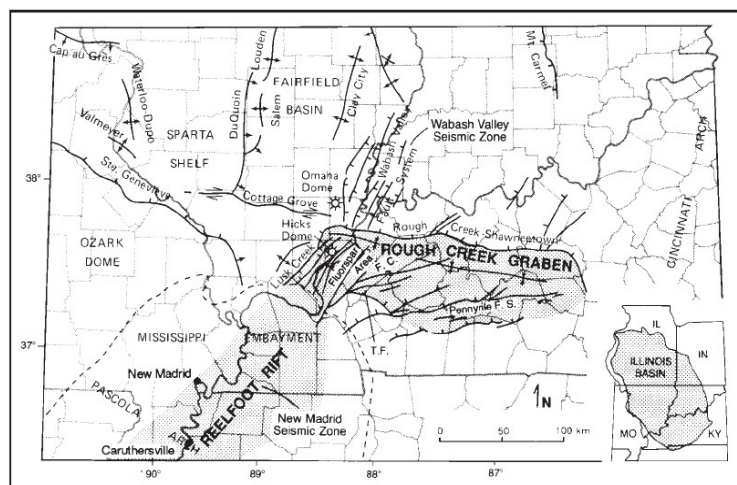


Figure 1.7: Map by Kolata and Nelson, 1997, showing the major structural features in Southern Illinois and surrounding area. Reprinted with permission.

with deep basement cutting faults, and graben blocks (Kolata and Nelson, 1997). These faults reactivated in the late Paleozoic, and from the Late Cambrian to Early Ordovician the basin depocenter extended across the rift system, followed by the deposition of approximately 2,500 meters of mostly carbonate rock (Kolata and Nelson, 1997). The New Albany Shale was deposited in the Upper Devonian (~385-360 Ma) and coal deposition in the basin took place during the Pennsylvanian, 300-320 Ma (Plumlee et al., 1995).

During the Permian period, oil began migrating from the New Albany shale (Plumlee et al., 1995). The mafic igneous intrusions at the Hicks Dome formed near the end of the Permian period (Bradbury et al., 1992; Plumlee et al., 1995). As the alkaline ultramafic magma ascended, the explosive release of CO₂ and other magmatic gases caused extensive brecciation and fractures within the host sedimentary rocks (Bradbury et al., 1992) The magma intruded into the tension fractures in the radial network of fractures in the area of Hicks Dome, the NW trending Tolu Arch, as well as into the recently formed Cottage Grove fault system (Kolata and Nelson, 1997). The intrusions are porphyritic in nature and can generally be classified as alnöite, a Si-poor rock that can grade into either kimberlite (more forsterite, less augite) or carbonatite (greater amounts of carbonate) (Denny et al., 2015).

The IKFD is a Mississippi Valley Type deposit located within the Illinois basin, extending over an area of roughly 2,600 km² over southeastern Illinois and western Kentucky that is thought to have formed near the end of the Permian (Plumlee et al., 1995). Unlike other regional MVT deposits, the Illinois Kentucky fluorspar district is dominated by fluorite mineralization: run-of-mine ore contains 30-40% fluorite, 2-3% zinc, and minor Pb mineralization (Seid et al., 2013). Since all of the carbonatite complexes around the world show evidence of late stage magmatism that is rich in REY and F, the fluorspar district in Southern

Illinois and Kentucky is thought to be directly related to the Hicks Dome based on the anomalous amounts of acidity and fluorine witnessed in the mineralogical evidence (Plumlee et al., 1995).

The IKFD formed after the main intrusive event of the Hicks Dome cryptoexplosive complex. A more gradual release of magmatic gases would have continued as alkaline magmatism died down (Plumlee et al., 1995). Hydrofluoric acid and CO₂ rich gases titrated into brines drawn down by a convective hydrothermal system along basement faults (Figure 1.8). These saturated, acidified brines then migrated vertically and laterally along fault zones and as they migrated away from Hicks Dome, distal ore mineralization occurred (Plumlee et al., 1995).

Based on fluorite inclusions, this mineralization primarily took place at temperatures below 150°C and by three different mechanisms: by cooling, during mixing with other basinal brines, or injection into and reaction with carbonates. These processes resulted in the three major modes of fluorite mineralization seen: fissure-filling veins, flat stratabound replacements of limestones, and cementation of the breccias at Hicks Dome. Lastly, the removal of metals from the brine by sulfide precipitation was likely aided by additional H₂S from the magmatic gases (Plumlee et al., 1995).

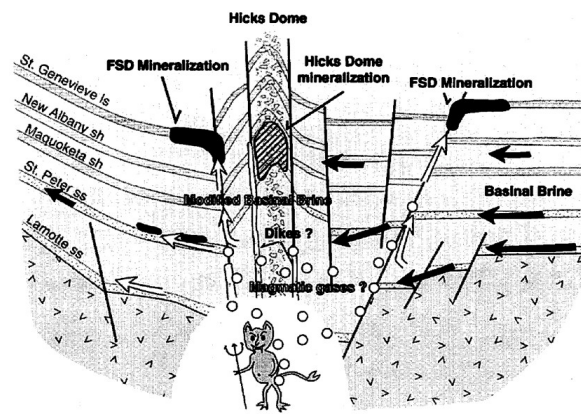


Figure 1.8: Schematic by Plumlee et al., (1995) of their proposed ore genesis model for the IKFD. Reprinted with permission.

CHAPTER 2

METHODOLOGY

Sampling and Analytical Procedures:

2.1 Sampling Sites

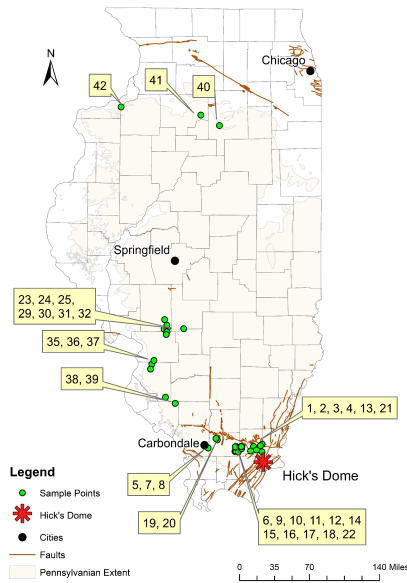


Figure 2.1: Sampling locations across the Illinois Basin. Larger view in Appendix A.

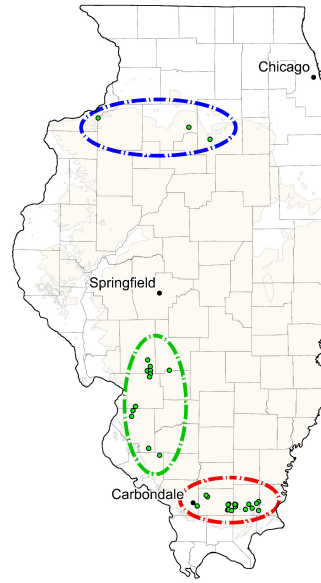


Figure 2.2: Organization of study area into three regions. Larger view in Appendix A.

In total, 42 drainages were sampled across the Illinois Basin. Of these, 37 were chosen to be analyzed as part of this study. Site selection was done with intent of providing samples that would most fully represent coal mine drainages (CMD) of the Illinois basin, with considerations to aqueous chemistry, proximity to Hick's Dome, and geographic breadth (Figure 2.1).

Based on the proximity to the Hicks Dome, we defined three distinct regions found on the southern, western, and northern margins (Figure 2.2): (1) Region 1 (R1) comprised locations situated in southern and southeastern Illinois, in close proximity to the Hicks Dome, with most sampling sites situated along the Cottage Grove fault system. (2) Region 2 (R2) comprised locations situated in western Illinois along the Du Quoin Monocline (3) Region 3 (R3) comprised

locations situated in northern Illinois, farthest from the Hicks Dome. The Tab Simco site, an abandoned coal mine site with extreme AMD is just southeast of Carbondale, IL, has frequently captured the attention of SIU researchers. TS-CMD was considered separately from R1-CMD in terms of regional data (averages, trends) in order to try to further investigate how Tab Simco might compare in regional trends as well to gauge the level of heterogeneity between samples from a site arising from the course of time, sampling of different seeps, and last but not least, the result of remediation efforts.

2.2 Site Selection

Sampling sites were selected from locations recognized by the Illinois Department of Natural Resources (IDNR) as a Problem Area Drainage (PAD). These sites were chosen under the guidance of IDNR, with an attempt to be representative of Illinois CMD, covering the broad spectrum of water chemistries that have resulted from the interaction of ground and meteoric water with the varying source coals found in the Illinois basin (e.g., Springfield No. 5, Herrin No 6) as well as their associated mining wastes. In consideration of the hypotheses being tested, factors influencing site selection were the acidity (pH) of AMD and the proximity of the AMD site to the Hicks Dome igneous complex as well as the presence of hydrothermal mineralization in the coalmine weathering rocks (i.e., high concentrations of Zn, Pb, Cu in the AMD), the discharge flow rate, and the overall geographic breadth (Figure 2.2). The field campaign to collect AMD samples took place from February to October 2017. The five complementary TS-CMD samples were collected from May to July of 2013.

A team of professionals that included Angie Mick from IDNR and at times Paul Behum from OSMRE, and occasionally accompanied by Thor Lindquist, also from IDNR. accompanied the SIU team during sample collections. In parallel with the SIU team, the IDNR team performed

field measurements and collected AMD samples which were then analyzed at the IDNR Geochemistry Lab in Benton Illinois. I had access to all the data that IDNR team collected. The IDNR dataset was not included in this thesis because the overall values were very similar to those measured by SIU team. However, the fact that the two datasets generated by two different teams/labs produced very similar results, particularly for AMD with extreme REY values, assure us that the data reported in this thesis are accurate.

2.3 Field Measurements

At each AMD site, the GPS coordinates were recorded using an iPhone 6s Plus, and photographs of the sampling site as well as the local area were taken using the same device. During each of the field sampling campaigns, measurements of the field parameters, including pH, temperature, specific conductance (SC), oxygen reduction potential (ORP), and dissolved oxygen (DO), were performed on unfiltered samples immediately following sample collection using a Hanna® multi-sensor probe. The pH electrode Hanna HI769828-1 field probe (pH/ORP) was calibrated with Orion pH buffers at 1.68, 4.01, and 7.00 and then checked against a pH 10 buffer. The ORP was measured using a factory calibrated Hanna HI769828-1 Ag/AgCl probe and a single point calibration was performed using a Hamilton redox (ORP) buffer (475 ± 5 mV). Dissolved oxygen was determined with a Hanna HI769828-2 amperometric probe calibrated to on-site atmospheric oxygen as 100% DO. The location of the CMD samples and the field parameters are presented within the supplementary Excel workbook, in worksheet Table S1.

2.4 Sample Collection

Aqueous samples were collected in 250-mL high-density linear polyethylene (HDPE) sample bottles which were thoroughly precleaned using trace hydrochloric acid and DI water procedures before being transported to the field. Where possible, the bottles where simply

submerged in the AMD stream. Site specific factors required a different methodology at times: Surface instability / inaccessibility at some sites necessitated the use of a telescoping pole with a large open bottle attached at its end. This collector was rinsed by filling and emptying it multiple times before using it to fill a sample bottle. At other sites, lack of adequate effluent to simply submerge the sample bottle required the use of a plastic syringe, rinsed thoroughly before with the effluent and afterwards with distilled water. After collection, the fluid samples were placed immediately into an ice-filled cooler $\sim 4^{\circ}\text{C}$ in order to minimize microbial activity and transported directly to the SIUC Geochemical Laboratory.

2.5 Laboratory Methods

2.5.1 Filtration

Upon arrival to the lab, effluent samples were immediately filtered with $0.45\ \mu\text{m}$ cellulose acetate filter papers (Millipore® HAW) to ensure future analyses would represent dissolved constituents only. As filtration took place, the collection bottle was rinsed thoroughly of all sediment, vegetative matter, etc. with a jet of distilled water. The bottle was shaken vigorously to remove excess water and left upside down to dry until the filtration of the sample had completed. Once all the liquid had passed through the filter, the vacuum line was removed along with the feed reservoir / filter. To remove any lingering water drops, the collection bottle was shaken once more before filling it with the filtrate. The filtrate and feed reservoirs were then rinsed with distilled water, shaken, and left to drip dry.

2.5.2 Acidification

The sample, now filtered, was acidified by the addition of 15N HNO_3 using a clean pipette. After $\sim 4\text{mL}$ had been added, the sample bottle was capped and shaken by hand to mix. Standard pH test strips were then used to verify acidic conditions. The bottle containing the

filtered and acidified effluent was appropriately marked and then stored in the laboratory refrigerator.

2.5.3 Sulfate Determination

Sulfate contents of the samples were determined gravimetrically by precipitation of barium sulfate in accordance with the procedure outlined in EPA method 375.3.

Samples were transferred into 50mL volumetric flasks and then heated to 80 °C on a hotplate. When the solution reached the set temperature, an aliquot of saturated BaCl₂ solution was added to the beaker to induce BaSO₄ precipitation (the solution became white as a result of BaSO₄ formation). Aliquots of BaCl₂ solution was added to the solution until all BaSO₄ precipitated (the solution was clear). Transferring the precipitated BaSO₄ from the beaker was accomplished by pipetting off the solution above the precipitate. The precipitate and the residual solution were then transferred to a pre-weighed and labeled vial using the pipette, rinsing the beaker multiple times with DDI water to make sure that no BaSO₄ was left in the beaker. After the BaSO₄ settled out of suspension within the vial, excess liquid was pipetted away and discarded. The vials were placed together within a large beaker and placed in an oven to dry at 75 °C. After samples were dry, the beaker was removed from the oven and immediately covered with plastic wrap to minimize sorption of water vapor from air. It was left to sit for 1 hour to return to room temperature. Vials were placed one at a time on a Mettler AE100 analytical balance and their masses were measured. The containing beaker was recovered with the plastic wrap between individual measurements.

2.5.4 Dilutions

Liquid samples were sent to an outside lab, Bureau Veritas Commodities Canada Ltd., for analysis by ICP-MS for heavy and trace metal concentrations, including the REY suite. Prior to

shipping, the liquid samples were diluted to the TDS required by the lab (0.1%), as necessary (Figure 2.3).

Samples for cation analysis, including REY were acidified to a 5 wt./v% trace-metal grade HNO₃ (ACS certified) solution and analyzed on a contract basis by the ACME Laboratories, Inc. (Bureau Veritas Commodities), Vancouver, British Columbia, Canada (Table S2). All samples were analyzed by ICP-MS, including two field replicates and one blank (18.2MΩcm-1 water) for all the CMD samples, in low-, medium-, and high-resolution modes, depending on individual element spectral values. A mixture of single-element standard solutions (STD TMDA-70 and STD TMDA-70.2) was used for instrument calibration.

The analytical precision ($\pm 1\sigma$) of standard concentration values was within 1%, whereas sample reproducibility was typically $< \pm 3\%$. All blanks were below detection. Recent research showed that accurate Eu concentration measurements by ICP-MS of coal and coal-related materials can be affected by high Ba concentrations if the Ba/Eu concentration ratios are > 1000 (Yan et al., 2018). However, most of the CMD samples have Ba/Eu ratios < 20 , with only one sample (S1) having a high Ba/Eu ratio of 1556, and therefore for the CMD samples considered in this study the reported Eu concentration values are accurate.

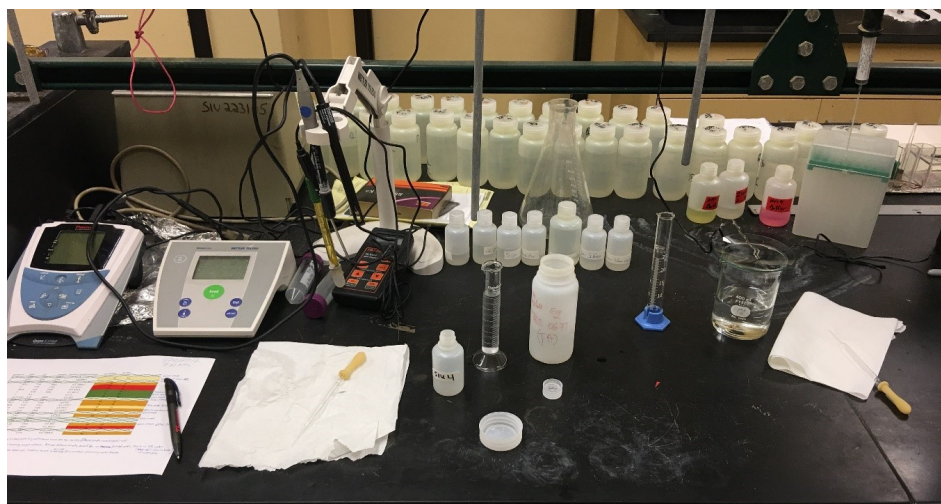


Figure 2.3: Workbench setup for sample dilution and acidification.

2.6 Data Analysis Methods

To identify relationships between different categories of data, Pearson correlation values were calculated with the significance level $\alpha=0.005$ or 0.5%. Box and whisker plot diagrams were constructed. Median was included in calculation of quartiles for the construction of box and whisker plot diagrams. Except where noted, analyte values that fell below the detection limit (BDL) of the laboratory equipment were treated as values of zero during calculation of statistics and correlations.

CHAPTER 3

RESULTS

3.1 Geochemistry of Coal Mine Discharge (CMD)

3.1.1 Acidity

The coal mine drainages (CMD) from the Illinois Basin that were analyzed in this study were largely acidic (Figure 3.1B), with an average of pH 3.4 across all samples, with a wide range of pH values for the CMD samples (Figure 3.1A), ranging from extremely acidic (pH=1.93) to circumneutral (pH=7.6). Within R1-CMD samples, pH values averaged 4.2 and ranged from 2.8-7.6. At Tab Simco (TS), pH values averaged 3.2 while ranging from a circumneutral 6.2 in the bioreactor outlet flow to a rather acidic pH 2.5 at a source seep. Samples of R2-CMD were more acidic overall with an average pH of 2.4 and values ranging from 1.9-3.3. R3-CMD was similarly acidic, with an average pH of 2.7 and values ranging from 2.5-3.0. Overall, R2-CMD is most acidic, followed by R3-CMD, then R1-CMD. Concerning TS-CMD has similar pH values to R1-CMD.

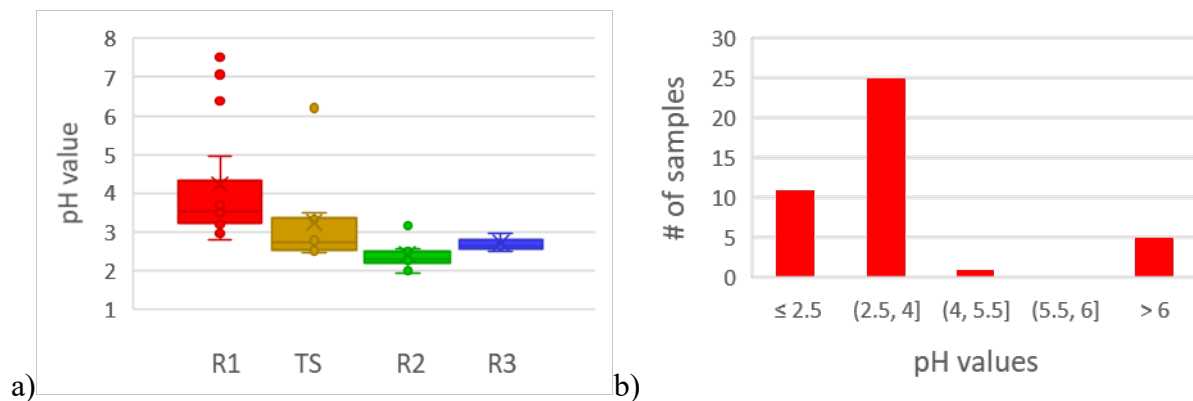


Figure 3.1: (a) regional distribution of pH values (b) frequency distribution of pH values.

3.2 Rare Earth Elements and Yttrium (REY)

In this study, we consider the REY within the context of conventional subgroups, namely light rare earth elements (LREE), which include the lanthanide elements between La ($z=57$) and

Eu ($z=63$), heavy rare earth elements (HREE), which include the elements from Gd ($z=64$) to Lu ($z=71$), as well as an intermediate, overlapping categorization, the middle rare earth elements (MREE), which span from Sm ($z=62$) to Ho ($z=67$). Despite the difference in mass, Y is included alongside HREE due to chemical similarities, having similar ionic radius with Dy and Ho. Total REY concentrations (Σ REY) averaged 1057 $\mu\text{g/L}$ across all samples (Table S2). Σ REY values varied between 0.6 and 9879 $\mu\text{g/L}$. In Region 1, Σ REY_{R1} values averaged 497.9 $\mu\text{g/L}$ and ranged from 0.6-1708 $\mu\text{g/L}$. Within R2-CMD, abundances averaged 1190 $\mu\text{g/L}$, ranging from 167.9-3851 $\mu\text{g/L}$. Concentrations were even higher in R3-CMD, averaging 4742 $\mu\text{g/L}$, due largely to an extraordinarily high value of 9879 $\mu\text{g/L}$ in SIU-41. SIU-41 was a statistical outlier for many elements, and found to be very concentrated in REY, in particular with MREY, with MREY values over 20x the study average (Table S2).

3.2.1 NASC Normalized REY Pattern

The North American Shale Composite (NASC; Gromet et al., 1984) was chosen as the normalization standard to represent the unenriched source material of the CMD. Because nominal amounts of REY are naturally present within these Paleozoic sediments, AMD from sites without appreciable enrichment in REY may show still baseline values, and so normalization against a standard is done to show enrichments due to external factors (Gromet et al., 1984; Dai et al., 2016b).

3.2.2 Regional Variations in REY Pattern

After normalization to the NASC, CMD from all 3 regions of the Illinois basin, including Tab Simco samples (Figure 4.2A-D), show enrichments in the middle REY, particularly Y and Gd, and to a lesser extent Tb, Dy, and Eu. These enrichments taper down as one goes through the HREY, with milder but still significant enrichments seen in all regions (Figure 3.2E).

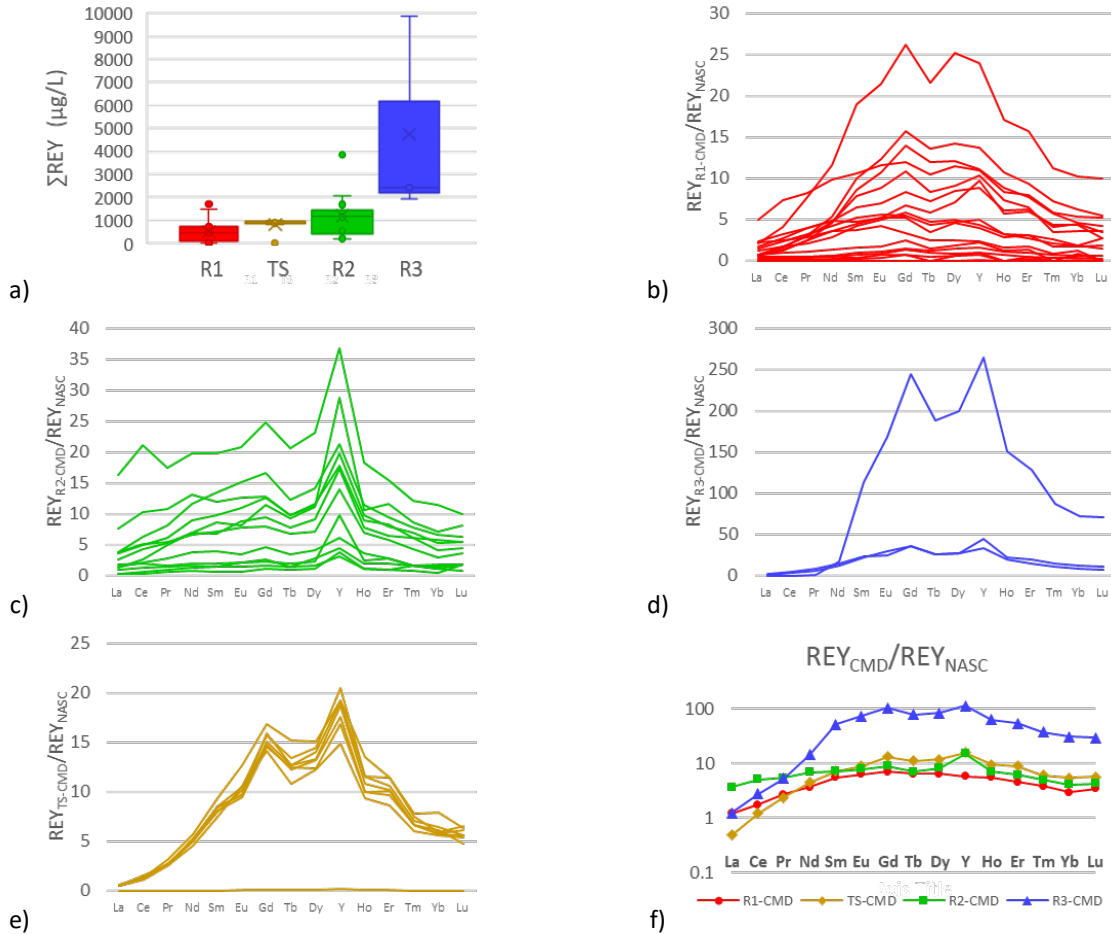


Figure 3.2: Composite figure of the NASC normalized REY abundances for (a) Region 1, (b) Region 2, (c) Region 3, (d) Tab Simco and (f) normalized regional averages of REY of R1, R2, and R3-CMD, absent the outlier SIU-41.

Greater LREY enrichment is seen in R2-CMD samples, with enrichments across individual REY largely in the same order of magnitude, with abundances dropping off toward the edges of the LREY and HREY and similar enrichments in both, and a notable bump in Y values (Figure 3.2B). Similar patterns in Y enrichment are seen for Tab Simco samples and R3-CMD, but not for R1-CMD (Figure 3.2E). The REY pattern of R1-CMD is gradual and smooth, with an enrichment curve that broadly peaks in the MREY before tapering off to a mild enrichment of the HREY (Figure 3.2A). Several samples from R1-CMD show notable enrichments in Dy over Y. The pattern of enrichment for normalized R3-CMD data has quite

minor enrichments in LREY, instead skewing heavily towards the MREY, especially Gd and Y with a milder enrichment in the HREY (Figure 3.2C).

Concentrations of the REY were BDL in multiple samples of R1-CMD 9 (Table 3.1:), an especially frequent occurrence in the circumneutral samples like SIU-18 (pH=7.55), where REY concentrations were almost entirely BDL, with the notable exception of Y. Though only a member of the lanthanide family honorarily, Y was the only REY present in every single sample. In another circumneutral sample, SIU-4 (pH=7.06), only values for Ce and Y were reported. The omnipresence of Y and Ce further reinforces their dominance in REY enrichment.

R2-CMD is where the greatest enrichments of the LREY are seen (Figure 3.2B), and where R1 and R2-CMD differ most in terms of REY pattern. The LREY are second most abundant in R3-CMD, with R1-CMD having the least enrichment in LREY ((Figure 3.2E).

MREY enrichment is most prominent in R3-CMD (Figure 3.2C), with similar ranges in concentrations found between the acidic samples of R1-CMD and R2-CMD. These elements are where the course of distinguishing the similarities between TS-CMD and regional drainages breaks down, with the notable exception of Y. There is a notable Y enrichment in R3-CMD, R2-CMD, and TS-CMD (Figure 3.2E). This enrichment is comparatively muted within much of R1-CMD.

HREY enrichment is seen in these drainages, but is especially prominent in R3-CMD (Figure 3.2C) and TS-CMD (Figure 3.2D), where a lack of LREY serves to highlight a moderate, but still significant enrichment of the HREY, at least in comparison to that of the MREY.

In R1-CMD (Figure 3.3D), largest concentrations and range of values were found for Y (24.4%) and Ce (22.3%), then Nd (15%), then with smaller range and abundances, La (6.8%) and Gd (5.2%).

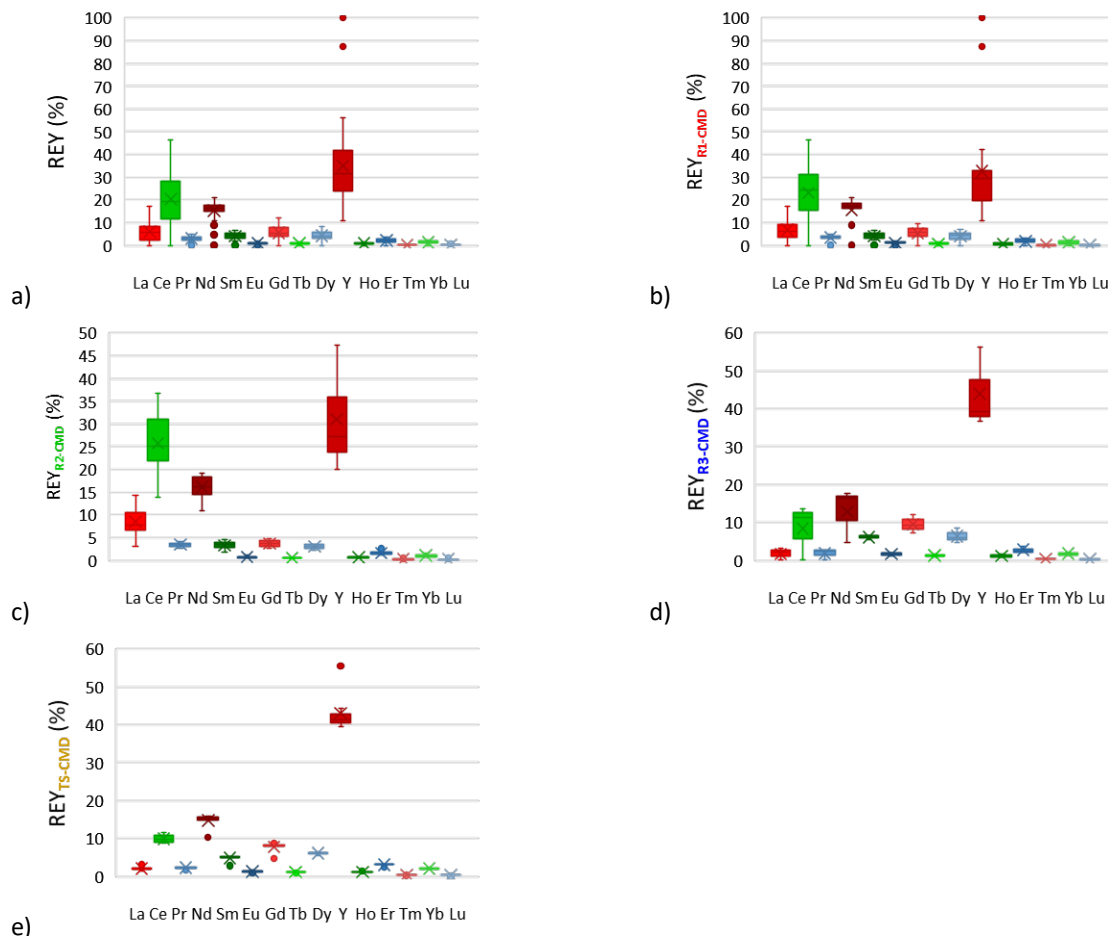


Figure 3.3: Composite figure displaying regional variations in REY composition in (a) the Illinois basin (b) Tab Simco CMD (c) R1-CMD (d) R2-CMD (e) R3-CMD.

In R2-CMD (Figure 3.3E), even greater concentrations of Y are present with values averaging 31% of the total REY load. Ce values are still codominant, but to a lesser extent making up on average 25.7% of the $\sum\text{REY}_{\text{R2-CMD}}$, followed by Nd (16.1%) and La (8.5%) and Gd (3.7%).

Within R3-CMD (Figure 3.3F), there is a strong preferential enrichment of Y, contributing on average 44% of the $\sum\text{REY}_{\text{R3-CMD}}$ concentrations, Nd is secondarily prominent accounting for 12.9% of $\sum\text{REY}_{\text{R3-CMD}}$ on average, followed by Gd (9.5%), Ce (8.4%) and Dy (6.4%).

REY within TS-CMD(Figure 3.3C) is characterized by a dominance of Y (43.1%)

followed by Nd (14.7%), Ce (10%), Gd (7.7%) and Dy (6.1%).

Overall, Y was the dominant element in terms of overall contribution to Σ REY (Figure 3.3A). This predominance is most notable in R3-CMD and R2-CMD (Figure 3.3E,D), which is also where Σ REY abundances were greatest. Cerium was dominant in R2-CMD (Figure 3.3D), followed by R1-CMD, then R3-CMD. Contribution of Nd to Σ REY abundance was greatest in R2-CMD, then R1-CMD, then R3-CMD. These contributions (in terms of %) were relatively constant across regions (Figure 3.3C-F), so although Nd is the second most dominant REY in R3-CMD and TS-CMD, it seems to result from visible shift in these regions toward MREY over LREY enrichment, rather than enrichments of Nd in particular.

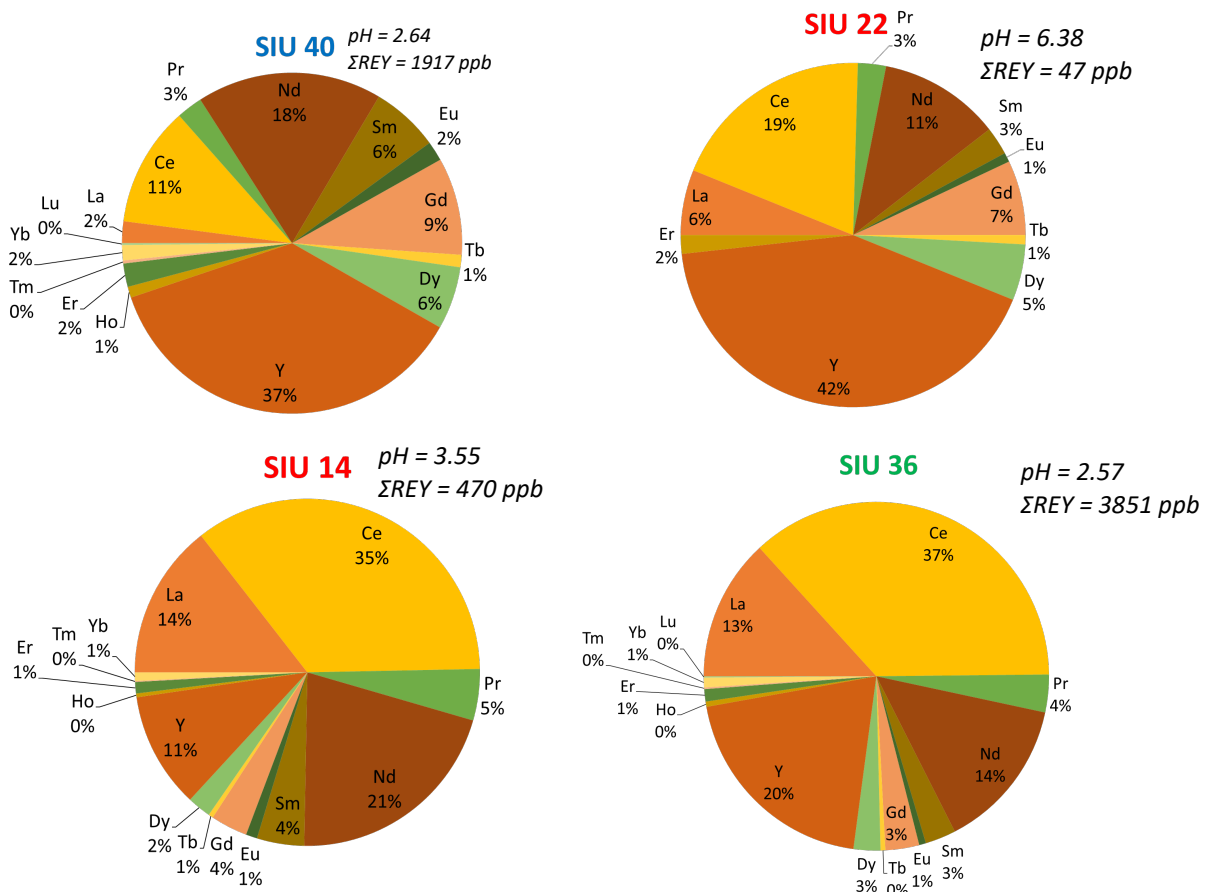


Figure 3.4: Examples of the two modalities of REY enrichment seen in this study, with Y dominant examples at top and Ce dominant examples on the bottom.

Overall there appear to be two modes of REY enrichment (Figure 3.4), Y dominant (e.g. SIU 22 and SIU 40), and Ce dominant (e.g., SIU 14 and SIU 36). Either mode of enrichment can be found between samples with varying pH and Σ REY abundances. Though none were identified within R3-CMD, it is quite possible that this is a consequence of the limited number of CMD samples.

3.2.3 REY Distribution

3.2.3.1 Lanthanum

Across the basin, La concentrations (Figure 3.5A) averaged 53.6 $\mu\text{g/L}$. Within R1-CMD, La values were BDL in two samples, with an overall average of 33.7 $\mu\text{g/L}$. The remaining 17 R1-CMD samples averaged 38 $\mu\text{g/L}$ and ranged from 0.03-154.8 $\mu\text{g/L}$. La abundances within TS-CMD averaged 15.2 $\mu\text{g/L}$ and ranged from 0.2-19.6 $\mu\text{g/L}$; similar to that seen in R1-CMD. La concentrations in R2-CMD averaged 114 $\mu\text{g/L}$ and ranged from 10.0-507.5 $\mu\text{g/L}$. Within R3-CMD, La values averaged 38.6 $\mu\text{g/L}$ and ranged from 1.7-74.6 $\mu\text{g/L}$. Overall, La is most abundant within R2-CMD, followed by R3-CMD then R1-CMD.

3.2.3.2 Cerium

Across the Illinois Basin, Ce concentrations (Figure 3.5B) averaged 177.9 $\mu\text{g/L}$. Within R1-CMD, Ce abundance was BDL in one sample, with an overall average of 113.0 $\mu\text{g/L}$, with values in the remaining R1-CMD averaging 119.3 $\mu\text{g/L}$ and ranging from 0.26-494 $\mu\text{g/L}$. The Ce concentrations seen in TS-CMD were similar, averaging 81.3 $\mu\text{g/L}$ with values ranging from 0.64-106 $\mu\text{g/L}$. Ce concentrations within R2-CMD averaged 342.9 $\mu\text{g/L}$ and ranged from 27.1-1,412 $\mu\text{g/L}$. Within R3-CMD, values averaged 186.3 $\mu\text{g/L}$, and ranged from 9.6-330.8 $\mu\text{g/L}$. Overall, Ce abundances are greatest in R2-CMD, followed by R3-CMD, then R1-CMD.

3.2.3.3 Praseodymium

Basin wide Pr concentrations (Figure 3.5C) averaged 27.0 µg/L. Within R1-CMD, Pr values were BDL in one sample, with an overall average of 18.7 µg/L, with values of the other 18 R1-CMD samples averaging 20.9 µg/L, ranging from 0.020-63.4 µg/L. The Pr values of TS-CMD were similar to resembles R1-CMD, with an average concentration of 18.6 µg/L in TS-CMD averaged 18.6 µg/L and ranged from 0.12-24.6 µg/L. Pr values in R2-CMD averaged 42.3 µg/L and ranged from 4.6-137 µg/L. Average concentrations in R3-CMD were similar, 41.3 µg/L, but the range of values (8.3-67.9 µg/L) was half of that for R2-CMD. Overall, the greatest range in Pr values and average abundance was found in R2-CMD, followed by R3-CMD, then R1-CMD.

3.2.3.4 Neodymium

Across the basin, Nd concentration (Figure 3.5D) values averaged 148 µg/L. Nd concentrations were BDL in 2 samples of R1-CMD, with an overall average of 91.5 µg/L and the remaining 17 values averaging 102 µg/L and ranging from 0.050-317 µg/L. In R2-CMD, Nd abundances averaged 192 µg/L and ranged from 24.6-545 µg/L. In R3-CMD, concentrations averaged 399 µg/L with values ranging from 338-462 µg/L. Overall, Nd was particularly abundant in R3-CMD, with lesser concentrations found in R2-CMD, then R1-CMD. Nd values within TS-CMD averaged 123 µg/L and ranged from 0.74-158 µg/L. The Nd concentrations in TS-CMD are in line with those in R1-CMD.

3.2.3.5 Samarium

Across the basin, Sm concentrations (Figure 3.5E) averaged 52.4 µg/L. Within R1-CMD samples, Sm abundances were BDL in three samples of R1-CMD, with a regional average of 26.2 µg/L. Concentrations averaged 31.1 µg/L in the other sixteen samples from the region. Sm

abundances in TS-CMD averaged 40.9 µg/L with values ranging from 0.20-52.1 µg/L. Within R2-CMD, Sm concentrations averaged 40.7 µg/L, with values ranging from 3.8-111 µg/L. In R3-CMD, Sm values were markedly higher, averaging 295 µg/L and ranging from 124-632 µg/L. Overall, Sm was most abundant in R3-CMD, followed by R2-CMD, then R1-CMD.

3.2.3.6 Europium

Across the basin, Eu concentrations (Figure 3.5F) averaged 13.9 µg/L. Within R1, Eu abundances were BDL in 3 drainages, with an overall regional average of 6.4 µg/L. The remaining 16 R1-CMD drainages averaged 7.6 µg/L together, and had values ranging from 0.417-25.4 µg/L. Eu abundances in TS-CMD averaged 10.8 µg/L and ranged from 0.06-15.0 µg/L. In R2-CMD, Eu values averaged 9.3 µg/L and ranged from 0.83-24.6 µg/L. Within R3-CMD, Eu abundances averaged 88.1 µg/L with values ranging from 28.8-199.6 µg/L. Overall, Eu was most abundant in R3-CMD, followed by R2-CMD then R1-CMD.

3.2.3.7 Gadolinium

Across the basin, Gd concentrations (Figure 3.5G) averaged 76.1 µg/L. Within R1-CMD, Gd values were BDL in two samples, for an overall regional average of 31.0 µg/L. The remaining R1-CMD samples averaged 34.7 µg/L and had values ranging from 0.010-128.3 µg/L. Gd concentrations in TS-CMD averaged 65.6 µg/L and ranged from 0.34-82.5 µg/L. Within R2-CMD, Gd values averaged 44.1 µg/L and ranged from 5.83-122 µg/L. Within R3-CMD, Gd values were much higher, averaging 517 µg/L and ranging from 176-1,199 µg/L. Overall, Gd was quite abundant in R3-CMD, with lesser concentrations in R2, then R1.

3.2.3.8 Terbium

Concentrations of Tb (Figure 3.5H) across the basin averaged 10.4 µg/L. Within R1-CMD, Tb abundances were BDL in four samples, leading to an overall regional average of 4.4

µg/L. The remaining fifteen R1-CMD samples together averaged 5.6 µg/L with values ranging from 0.42-18.3 µg/L. Tb values in R2-CMD averaged 6.1 µg/L and ranged from 0.83-17.5 µg/L. Within R3-CMD, Tb concentrations averaged 68.3 µg/L, ranging from 22.5-160 µg/L. Overall, the greatest abundances of Tb are found in R3-CMD, followed by R2 and R1-CMD. Tb concentrations in TS-CMD averaged 9.5 µg/L and ranged from 0.06-12.9 µg/L.

3.2.3.9 Dysprosium

Dy concentrations averaged 55.6 µg/L across the basin (Figure 3.5I). Within R1-CMD, Dy values were BDL in two drainages, for an overall regional average of 24.1 µg/L, with concentrations in the remaining seventeen drainages averaging 27.0 µg/L and ranging from 0.010-105 µg/L. Within R2-CMD, average concentrations of 34.8 µg/L were seen with Dy values ranging from 5.0-96.7 µg/L. Within R3-CMD, Dy values averaged 354 µg/L and ranged from 114-833 µg/L. Overall, Dy was most abundant in R3-CMD, followed by R2-CMD, then R1-CMD. Abundances of Dy within TS-CMD averaged 49.5 µg/L and ranged from 0.40-62.9 µg/L. The values of Dy for TS-CMD tend towards those seen within R2-CMD.

3.2.3.10 Yttrium

Though only a member of the lanthanide family honorarily, Y (Figure 3.5J) was the only REY present in every single sample, with an overall average concentration of 383 µg/L. In R1-CMD, Y values averaged 123 µg/L and ranged from 0.17-503 µg/L. Y abundances within TS-CMD averaged 334 µg/L and ranged from 3.98-430 µg/L. Within R2-CMD, Y concentrations were higher, averaging 321 µg/L and ranging from 65.4-773 µg/L. Values were even greater within R3-CMD, averaging 2,404 µg/L and ranging from 702-5,558 µg/L. Overall, Y was the most abundant REY, with concentrations highest within R3-CMD, then R2-CMD, then lastly R1-CMD.

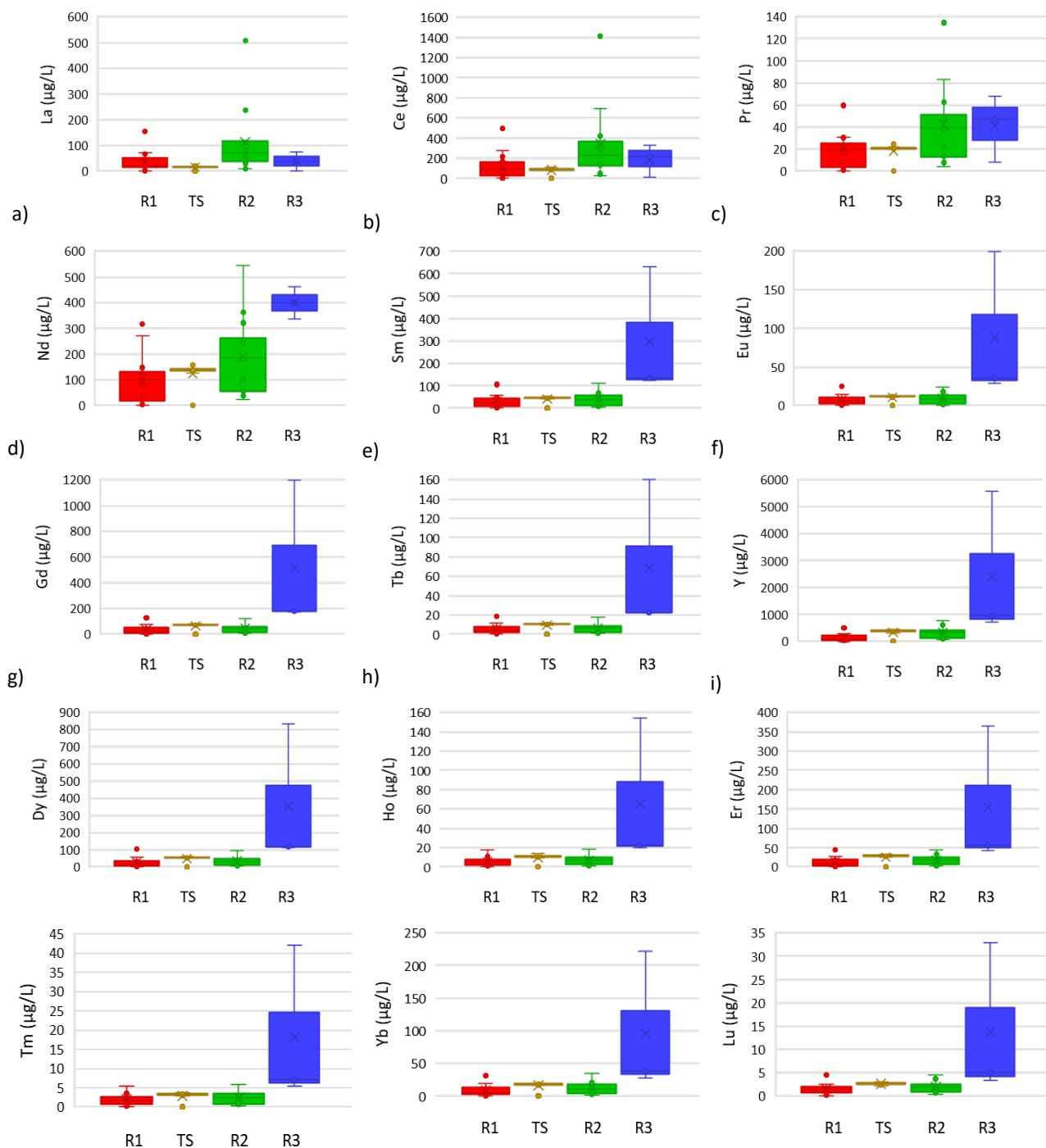


Figure 3.5: Composite Figure: Box and whisker diagrams showing regional variations of REY: (a) La, lanthanum (b) Ce, cerium (c) Pr, praseodymium (d) Nd, neodymium (e) Sm, samarium (f) Eu, europium, (g) Gd, gadolinium (h) Tb, terbium (i) Y, yttrium (j) Dy, dysprosium (k) Ho, holmium (l) Er, erbium (m) Tm, thulium (n) Yb, ytterbium (o) Lu, lutetium

3.2.3.11 Holmium

Concentrations of Ho (Figure 3.5K) averaged 10.5 µg/L across the basin. Within R1-CMD, Ho values were BDL in five samples, for an overall regional average of 4.2 µg/L. Concentrations in the remaining fourteen R1-CMD averaged 5.7 µg/L and ranged from 0.70-17.5 µg/L. Ho abundances within TS-CMD averaged 9.8 µg/L and ranged from 0.08-13.8 µg/L. Within R2-CMD, Ho concentrations were slightly higher, averaging 7.2 µg/L and ranging from 1.26-18.8 µg/L. Abundances were much greater in R3-CMD, where values averaged 65.6 µg/L and ranged from 20.0-154 µg/L. Overall, Ho was most prevalent in R3-CMD, then R2-CMD, followed closely by R1-CMD.

3.2.3.12 Erbium

Across the basin, Er abundances (Figure 3.5L) averaged 26.0 µg/L. In R1-CMD, Er concentrations were BDL in three drainages, leading to an overall regional average of 11.0 µg/L with values in the other sixteen drainages averaging 13.1 µg/L and ranging from 0.83-44.6 µg/L. Abundances within TS-CMD averaged 25.6 µg/L and ranged from 0.18-32.6 µg/L. Within R2-CMD, Er values were mostly similar, with a slightly higher concentration average of 17.8 µg/L and values ranged from 2.9-44.2 µg/L. Within R3-CMD, Er values averaged 155 µg/L with values ranging from 42.6-365 µg/L. Er concentrations are greatest in R3-CMD, followed by R2 and R1-CMD.

3.2.3.13 Thulium

Abundances of Tm (Figure 3.5M) across the basin averaged 3.1 µg/L. Within R1-CMD, Tm concentrations were BDL in six samples, for an overall regional average of 1.3 µg/L. Tm values in the remaining eleven R1-CMD samples averaged 1.9 µg/L and ranged from 0.19-5.4 µg/L. Within R2-CMD, Tm concentrations averaged 2.4 µg/L and ranged from 0.42-5.8 µg/L.

Within R3-CMD, values were highest, averaging 18.2 µg/L and ranging from 5.4-42.1 µg/L.

Overall, Tm abundances are greatest in R3-CMD, followed by R2, then R1-CMD.

Concentration values in TS-CMD averaged 2.9 µg/L and ranged from 0.020-3.8 µg/L. The Tm values in TS-CMD are most like those in R2-CMD.

3.2.3.14 Ytterbium

Across the basin, abundances of Yb (Figure 3.5N) averaged 17.1 µg/L. Within R1-CMD, Yb concentrations were BDL in three drainages, for an overall regional average of 7.7 µg/L. The remaining sixteen R1-CMD samples averaged 9.1 µg/L together, and ranged from 0.010-31.3 µg/L. Abundances of Yb in TS-CMD averaged 16.7 µg/L and ranged from 0.14-24.2 µg/L. Within R2-CMD, Yb values averaged 12.6 µg/L and ranged from 1.25-35.0 µg/L. Within R3-CMD, Yb was more abundant, with concentrations averaging 96.3 µg/L and ranging from 27.9-222 µg/L. Overall, Yb is most abundant in R3-CMD, followed by R2, then R1-CMD.

3.2.3.15 Lutetium

Lu was the least abundant REY (Figure 3.5O) with an average concentration of 2.45 µg/L across the basin. Within R1-CMD, Lu concentrations were BDL in seven drainages. Like the other HREY, the greatest Lu abundances were seen in R3-CMD, where they averaged 13.8 µg/L and ranged from 3.3-32.9 µg/L. Overall, Lu abundances are greatest in R3-CMD followed by R2 then R1-CMD.

Table 3.1: Regional REY Statistics

Unit			Region 1	Tab Simco		Region 2	Region 3	All samples
				Untreated Samples	All samples			
La	µg/L	Average	33.7	17.4	15.2	114.3	38.6	53.6
		Range	BDL		0.2	10.0	1.7	BDL
		Min. Max.	154.8		19.6	507.5	74.6	507.5
Ce	µg/L	Average	113.0	92.8	81.3	342.9	186.3	177.9
		Range	BDL		0.6	27.1	9.6	BDL
		Min. Max.	494.0		106.2	1412.1	330.8	1412.1
Pr	µg/L	Average	18.7	21.3	18.6	42.3	41.3	27.0
		Range	BDL		0.1	4.6	8.3	BDL
		Min. Max.	63.4		24.6	134.6	67.9	134.6
Nd	µg/L	Average	91.5	140.8	123.3	192.3	399.3	148.3
		Range	BDL		0.7	24.6	337.5	BDL
		Min. Max.	317.1		157.5	545.0	462.1	545.0
Sm	µg/L	Average	26.2	46.7	40.9	40.7	296.4	52.4
		Range	BDL		0.2	3.8	123.8	BDL
		Min. Max.	106.3		52.1	110.8	632.1	632.1
Eu	µg/L	Average	6.4	12.3	10.8	9.3	88.1	13.9
		Range	BDL		0.1	0.8	28.8	BDL
		Min. Max.	25.4		15.0	24.6	199.6	199.6
Gd	µg/L	Average	31.0	74.9	65.6	44.1	517.2	76.1
		Range	BDL		0.3	5.8	175.8	BDL
		Min. Max.	128.3		82.5	121.7	1198.8	1198.8
Tb	µg/L	Average	4.4	10.9	9.5	6.1	68.3	10.4
		Range	BDL		0.1	0.8	22.5	BDL
		Min. Max.	18.3		12.9	17.5	160.0	160.0
Dy	µg/L	Average	24.1	56.5	49.5	34.8	354.3	55.6
		Range	BDL		0.4	5.0	114.2	BDL
		Min. Max.	105.4		62.9	96.7	832.5	832.5
Y	µg/L	Average	122.8	381.1	334.0	320.9	2403.6	382.5
		Range	0.2		4.0	65.4	701.7	0.2
		Min. Max.	502.9		430.2	772.5	5558.3	5558.3
Ho	µg/L	Average	4.2	11.2	9.8	7.2	65.6	10.5
		Range	BDL		0.1	1.3	20.0	BDL
		Min. Max.	17.5		13.8	18.8	154.2	154.2
Er	µg/L	Average	11.0	29.2	25.6	17.8	154.7	26.0
		Range	BDL		0.2	2.9	42.5	BDL
		Min. Max.	44.6		32.6	44.2	365.0	365.0
Tm	µg/L	Average	1.3	3.3	2.9	2.4	18.2	3.1
		Range	BDL		0.0	0.4	5.4	BDL
		Min. Max.	5.4		3.8	5.8	42.1	42.1
Yb	µg/L	Average	7.7	19.1	16.7	12.6	96.3	17.1
		Range	BDL		0.1	1.3	27.9	BDL
		Min. Max.	31.3		24.2	35.0	222.1	222.1
Lu	µg/L	Average	1.0	2.7	2.3	2.0	13.8	2.4
		Range	BDL		BDL	0.4	3.3	BDL
		Min. Max.	4.6		3.0	4.6	32.9	32.9
ΣREY	µg/L	Average	497.0	920.1	806.0	1189.5	4741.8	1056.9
		Range	0.4		7.2	167.9	1917.1	0.4
		Min. Max.	1707.5		1001.3	3851.3	9879.2	9879.2
Σcritical-REY	µg/L	Average	249.2	601.6	527.1	563.3	3313.6	610.8
		Range	0.2		5.2	110.0	1211.7	0.2
		Min. Max.	969.2		659.0	1456.3	7212.5	7212.5
% critical	%	Average	53.6	65.3	66.3	51.5	66.2	56.3
		Range	35.3		64.4	37.8	62.4	35.3
		Min. Max.	100.0		73.0	66.4	73.0	100.0
Y/Ce		Average	1.6	4.1	4.4	1.4	3.0	2.2
		Range	0.3		3.6	0.5	2.9	0.3
		Min. Max.	7.0		6.2	3.4	3.2	7.0

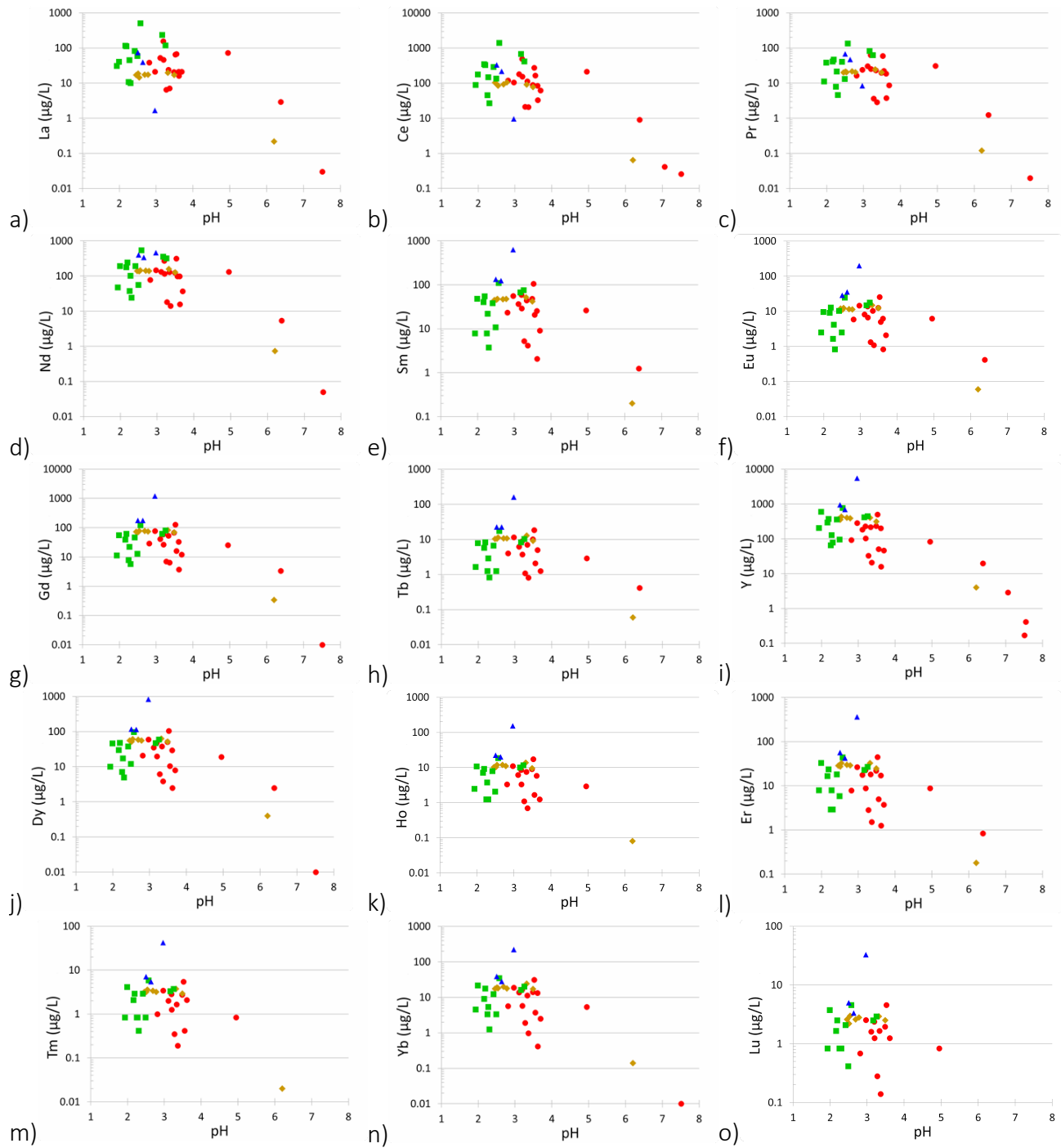


Figure 3.6: Composite Figure: Plots of individual REY values vs pH.
 (a) La, lanthanum (b) Ce, cerium (c) Pr, praseodymium (d)Nd, neodymium (e) Sm, samarium (f) Eu, europium (g) Gd, gadolinium (h) Tb, terbium (i) Y, yttrium (j) Dy, dysprosium (k) Ho, holmium (l) Er, erbium (m)Tm, thulium (n) Yb, ytterbium (o) Lu, lutetium.

3.3 REY and pH

Most of the AMD showed enrichment in Y, Ce, Nd, Gd, Dy, Tb, and Ce. However, no correlation was identified between pH and linear analyte concentration (i.e., unadjusted) values for most REY, with the exception of borderline mild inverse correlations between linear analyte concentration values and pH for Pr ($r=-0.37$, $p=0.016$) (Table S4) and Nd ($r=-0.41$, $p=0.007$).

A moderate inverse correlation was seen between pH and log adjusted values of La ($r=-0.68$, $p<0.005$), Ce ($r=-0.76$, $p<0.005$), Pr ($r=-0.74$, $p<0.005$), Nd ($r=-0.58$, $p<0.00008$), Sm ($r=-0.53$, $p<0.005$), Eu ($r=-0.50$, $p<0.005$), Gd ($r=-0.69$, $p<0.005$), Tb ($r=-0.49$, $p<0.005$), (r=-0.82, $p<0.005$) Dy ($r=-0.69$, $p<0.005$), Er ($r=-0.54$, $p<0.005$), Tm ($r=-0.48$, $p<0.005$), Yb ($r=-0.67$, $p<0.005$), and strongest inverse correlation seen for log adjusted values of Y ($r=-0.82$, $p<0.005$).

Unlike most REY, no statistical correlation was evident between log-adjusted Lu values $\log[\text{Lu}]$ and pH ($r=-0.09$, $p=0.61$), similarly, correlation between log-adjusted Ho values and pH were borderline ($r=-0.44$, $p=0.0059$).

3.4 Major and Trace Elements

The CMD sample chemistry was characterized by a wide range of values for major and trace elements, with wide ranges for SO_4 (500-12,000 mg/L), Al (0.2-1,386 mg/L), and Fe (2-3632.5 mg/L) (Table 3.2:), composing the main constituents in the Illinois CMD. Furthermore, among major and non-REY trace elements, only Si had statistically significant inverse correlation with pH in both linear (Si : pH) and logarithmic, i.e., $\log[\text{Si}]$: pH, considerations ($r=-0.58$, $p<0.005$) and ($r=-0.68$, $p<0.005$) (Table S4).

3.4.1 Anion Makeup

Sulfate is the dominant anion across all samples with values ranging from 474 mg/L (SIU-15) to 35,875 (SIU 41), averaging 4318 mg/L (Table 3.2: Bulk Elements). Across

regions, SO_4 concentrations were lowest in region 1, averaging 1950 mg/L compared to the average values of 4,363 mg/L for Tab Simco, 5,510 mg/L for R2-CMD, and 14,417 mg/L for R3-CMD samples (Table 3.2:). Cl and F input was minor, in fact only 8 samples had Cl values above the detection limit. The contribution of Cl to the anion makeup was most notable in SIU-37 (167 mg/L), with not only the highest concentration, but also the greatest proportion, comprising 4.1% of the anions on a combined weight basis. No statistical correlation between Cl and pH was found ($r=-0.01$, $p=0.94$), nor between Cl and $\sum\text{REY}$ ($r=-0.1$, $p=0.53$).

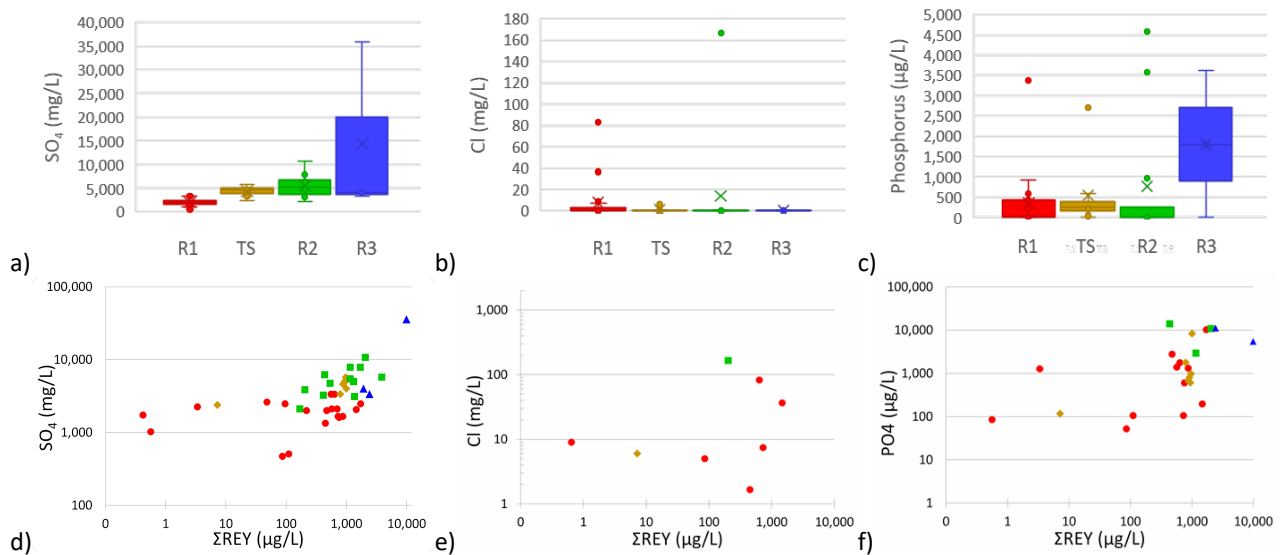


Figure 3.7: Composite figure of a) plot of Cl concentrations vs pH b) regional distribution of Cl concentrations c) plot of P concentrations vs $\sum\text{REY}$ d) regional distribution of P concentrations.

Phosphorus values were BDL in 18 of the 42 basin drainages, averaging 606 $\mu\text{g/L}$ across all samples. Between P and $\sum\text{REY}$, no correlation was evident ($r=0.28$, $p=0.071$). In R1-CMD, P concentrations averaged 345 $\mu\text{g/L}$ overall, but was present in only 12 of 19 samples, which averaged 547 $\mu\text{g/L}$ and ranged from 17.0-3,375 $\mu\text{g/L}$. Concentrations within TS-CMD averaged 541 $\mu\text{g/L}$ overall, but were BDL in 1 sample, averaging within the 7 remaining 619 $\mu\text{g/L}$ and ranging from 38.0-2,708 $\mu\text{g/L}$. P abundances in TS-CMD are in line with those of R1-CMD. R2-CMD was more abundant on average (760 $\mu\text{g/L}$), even though it was present in only 3 of 12

samples, which averaged 3,042 $\mu\text{g/L}$ and ranged from 958-4,583 $\mu\text{g/L}$. P values in R3-CMD averaged 1,806 $\mu\text{g/L}$ overall, with one sample, SIU-40 BDL. The remaining samples, SIU-41 and SIU-42 had values of 1,792 $\mu\text{g/L}$ and 3,625 $\mu\text{g/L}$ respectively (averaging 2,708 $\mu\text{g/L}$). P concentrations were highest in R3-CMD, on average, though the greatest values are notably seen within R2-CMD. With P concentrations BDL in so many, it becomes suffice to say that concentrations were generally highest in R3 and R2 and lower but more ubiquitous in R1-CMD.

3.4.2 Bulk Cations

The major cations in Illinois CMD, in order of their abundance, are Fe, Ca, Mg, Al, Na, Si, Mn, and K. Cation chemistry in CMD across the Illinois basin was largely heterogeneous, with wide ranges of concentration values for many elements, but especially for Fe (1.8-3,633 ppm), Mn (3.1-399.9 ppm), Zn (0.02-269 ppm), Si (5.8-72.5 ppm), and Li (0.04-37.8 ppm). One drainage site SIU-41 was marked by extremely high concentrations of certain elements, namely SO_4 , Al, Mg, Mn, Li, Ni, Cd, Co, and Be. The uniqueness of this drainage, combined with the factor of R3-CMD being composed of just 3 samples, makes authoritative distinctions in regional trends of ranges and abundances difficult.

3.4.2.1 Iron

Fe was both the widest ranging (1.8-3633 mg/L) and most abundant cation, averaging 585.0 mg/L across all samples. In R1-CMD, Fe concentrations averaged 213.1 mg/L, ranging from 1.8-878 mg/L. Fe values averaged 541.2 mg/L in TS-CMD, where sample values ranged from 170.0-891.1 mg/L. Concentrations within R2-CMD, averaged 1282 mg/L, ranging from 88.0-3633 mg/L. Within R3-CMD, values averaged 270.3 mg/L and ranged from 115.7-514.5 mg/L. Overall, Fe concentrations were greatest (and most variable) in R2-CMD with lesser abundance in R3, then R1 (Figure 3.8C).

3.4.2.2 Calcium

Ca concentrations averaged 451.3 mg/L across all samples. R1 CMD values averaged 381.5 mg/L, ranging from 75.7-595.4 mg/L. Ca concentrations in TS-CMD averaged 466.9 mg/L, ranging from drainages ranged from 390.8-745.1 mg/L. In R2-CMD, Ca values averaged 531.1 mg/L and ranged from 420.0-615.0 mg/L. R3-CMD concentrations averaged 532.9 mg/L, ranging from 410.8-596.7 mg/L. Overall, the highest concentrations of Ca were found in R3-CMD, followed by R2, TS, then R1.

3.4.2.3 Magnesium

Mg concentrations averaged 333.9 mg/L across the basin. R1-CMD Mg values averaged 118.8 mg/L and ranged from 36.8-376.7 mg/L. Mg values averaged 207.0 mg/L in TS-CMD and ranged from 175.5-230.8 mg/L. In R2-CMD, Mg concentrations averaged 226.2 mg/L and ranged from 64.2-369.6 mg/L. In R3-CMD, concentrations averaged 2,465 mg/L, ranging from 94.2 mg/L to an exceptional 6,890 mg/L in SIU-41, ~40x higher than the sample average. Overall, Mg values and ranges are highest within R3-CMD, with lesser abundances in R2-CMD then R1-CMD.

3.4.2.4 Aluminum

Al concentrations averaged 125.1 mg/L across all samples. Within R1-CMD, Al concentrations averaged 40.1 mg/L, ranging from 0.02-151.2 mg/L. In /L, ranging from 14.5-571.4 mg/L. On a per region basis, R3-CMD had the largest Al concentrations and range of values. In R3-CMD, concentrations averaged 579.6 mg/L and ranged from 163.7-1386 mg/L., followed by TS-CMD, then R2-CMD, values averaged 133.7 mg, and lastly, R1-CMD. There is a strong direct correlation between ΣREY and Al ($r=0.91$, $p<0.005$) (Table S4) (Figure 3.8N).

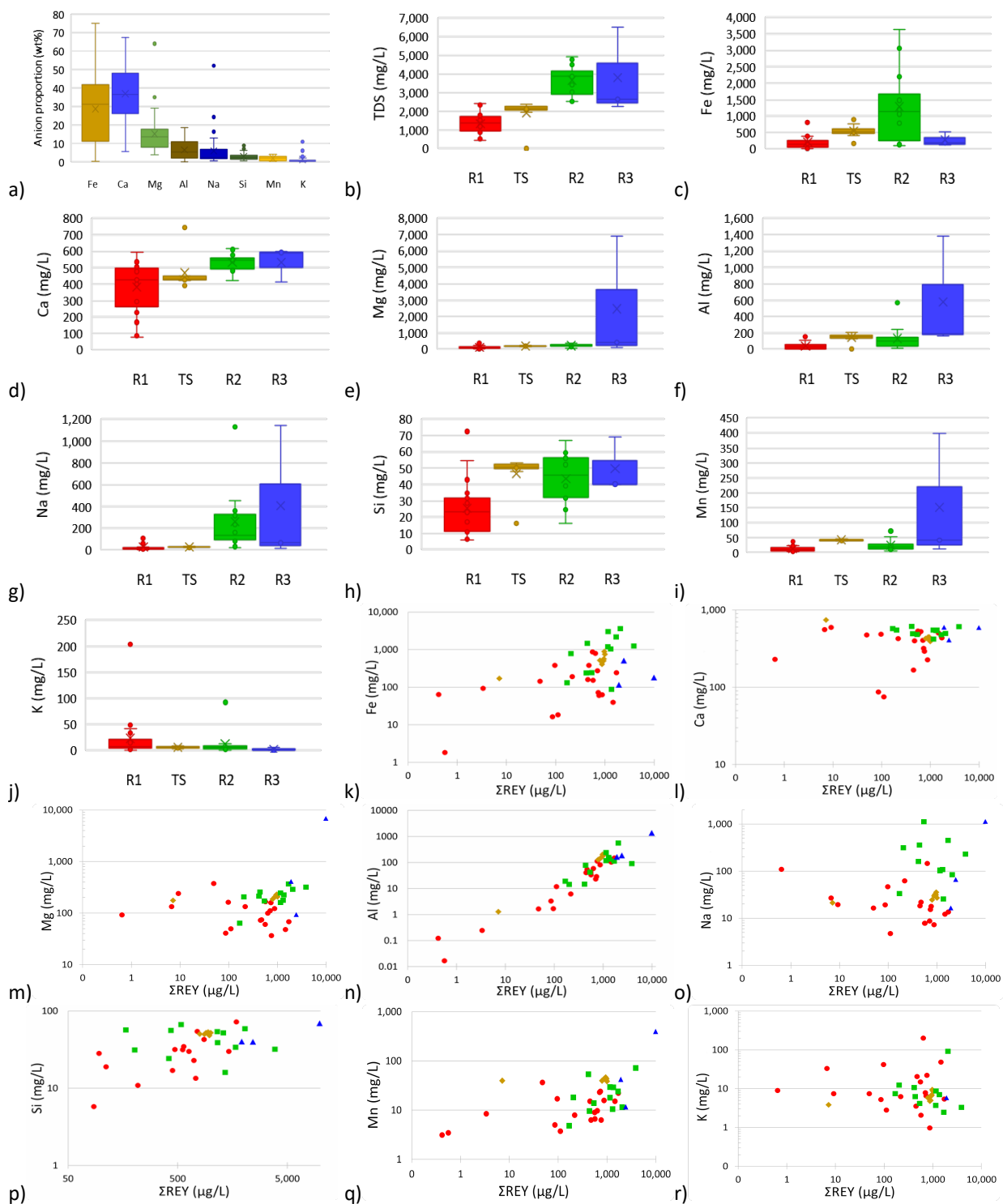


Figure 3.8: Composite Figure: (a) Contribution of the major analytes to bulk anion chemistry. (b) Regional values of TDS. (c-j): Regional abundances of (c) Fe, iron (d) Ca, calcium (e) Mg, magnesium (f) Al, aluminum (g) Na, sodium (h) Si, silicon (i) Mn, Manganese and (j) K, potassium. (k-r): Σ REY against major cations (k) Fe, iron (l) Ca, calcium (m) Mg, magnesium (n) Al, aluminum (o) Na, sodium (p) Si, silicon (q) Mn, manganese (r) K, potassium.

3.4.2.5 Sodium

Na concentrations averaged 123 mg/L across the basin. Within R1-CMD, Na values averaged 30.8 mg/L, ranging from 4.8-146.3 mg/L. Within R2-CMD, Na values averaged 260.1 mg/L, ranging from 25.8-1130.4 mg/L. Within R3-CMD, concentrations averaged 408.6 mg/L, ranging from 16.7-1,142.5 mg/L. Overall, Na concentrations are greatest in R3-CMD, then R2-CMD, then R1-CMD. Na concentrations in TS-CMD averaged 29.2 mg/L, and ranged from 21.4-35.8 mg/L; in regard to Na, TS-CMD resembles R1-CMD.

3.4.2.6 Silicon

Si concentrations averaged 36.3 mg/L across the basin. Within R1-CMD, Si values averaged 25.3 mg/L, and ranged from 5.82 mg/L in SIU 15 to 72.5 mg/L in SIU 11. Within TS-CMD, Si concentrations averaged 46.7 mg/L, ranging from 15.2-53.3 mg/L, placing TS-CMD in line with Si values for R2-CMD. R2-CMD contained on average 43.5 mg/L Si, ranging from 16.1-66.8 mg/L. R3-CMD was even more abundant, with an average Si value of 49.8 mg/L, ranging from 40.0-69.1 mg/L. Overall, Si was most abundant in R3, then R2, then R1.

Correlations between Si and the other elements are relatively fewer. Aside from the aforementioned correlations for SO₄ (r=0.46) and Al (r=0.50), Si only has moderate correlations with a few elements, Cu (r=0.44, p<0.005), Ni (r=0.43, p<0.005), and one of the few elements to have correlations with P (r=0.46, p<0.005).

3.4.2.7 Manganese

Mn concentrations averaged 31.7 mg/L across the basin. Mn concentrations with R1-CMD averaged 12.7 mg/L, ranging from 3.1-36.9 mg/L. In R2-CMD, values averaged 24.7 mg/L, ranging from 4.9-72.4 mg/L. Mn concentrations were even higher within R3-CMD, where values averaged 151.2 mg/L, ranging from 11.7 mg/L to an exceptional 399.9 mg/L within

sample SIU-41. Within TS-CMD, Mn values averaged 42.5 mg/L and ranged from 38.8-46.0 mg/L. Overall, Mn was most abundant in R3, then R2, and lastly R1. Mn values within TS-CMD resemble those in R2-CMD.

3.4.2.8 Potassium

K was present in 39 of 42 samples, with an overall average concentration of 15.9 mg/L. Within R1-CMD, concentrations averaged 23.7 mg/L, ranging from 1.0-203.3 mg/L. K concentrations in TS-CMD averaged 5.4 mg/L and ranged from 3.9-9.4 mg/L. In R2-CMD, K concentrations were BDL for one site (SIU-25), averaging 13.3 mg/L overall. K was even more elusive in R3-CMD, with 2 samples BDL, and a value of 5.8 mg/L in sample SIU-40. Overall, K was most abundant in R1-CMD, followed by R2, then R3.

Table 3.2: Bulk Elements

Unit		Region 1	Tab Simco		Region 2	Region 3	All samples
			Untreated Samples	All samples			
pH	Average	4.2	2.8	3.2	2.4	2.7	3.4
	Range	Min.	2.8	2.5	1.9	2.5	1.9
		Max.	7.6	6.2	3.3	3.0	7.6
ΣREY	Average	497.0	920.1	806.0	1189.5	4741.8	1056.9
	Range	Min.	0.4	7.2	167.9	1917.1	0.4
		Max.	1707.5	1001.3	3851.3	9879.2	9879.2
SO ₄	Average	1950.2	4645.8	4363.6	5510.4	14416.7	4317.5
	Range	Min.	474.0	2388.0	2125.0	3375.0	474.0
		Max.	3377.7	5700.0	10750.0	35875.0	35875.0
Cl	Average	7.5	BDL	0.8	13.9	BDL	7.5
	Range	Min.	BDL	BDL	BDL	BDL	BDL
		Max.	83.3	6.0	166.7	BDL	166.7
P	Average	345.4	613.1	541.2	760.4	1805.6	605.6
	Range	Min.	BDL	BDL	BDL	BDL	BDL
		Max.	3375.0	2708.3	4583.3	3625.0	4583.3
Al	Average	40.1	163.8	143.5	133.7	579.6	125.1
	Range	Min.	0.0	1.3	14.5	163.7	0.0
		Max.	151.2	205.6	571.4	1386.0	1386.0
Si	Average	25.3	51.0	46.7	43.5	49.8	36.3
	Range	Min.	5.8	16.2	16.1	40.0	5.8
		Max.	72.5	53.3	66.8	69.1	72.5
Fe	Average	213.1	594.2	541.2	1281.8	270.3	585.0
	Range	Min.	1.8	170.0	88.0	115.7	1.8
		Max.	878.0	891.1	3632.5	514.5	3632.5
Ca	Average	381.5	427.1	466.9	531.1	532.9	451.3
	Range	Min.	75.7	390.8	420.0	410.8	75.7
		Max.	595.4	745.1	615.0	596.7	745.1
Mg	Average	118.8	211.5	207.0	226.2	2464.7	333.9
	Range	Min.	36.8	175.5	64.2	94.2	36.8
		Max.	376.7	230.8	369.6	6890.0	6890.0
Mn	Average	12679.1	42874.1	42497.9	24692.5	151227.6	31687.6
	Range	Min.	3139.2	38832.1	4860.8	11725.4	3139.2
		Max.	36899.2	46034.8	72441.7	399852.5	399852.5
Na	Average	30.8	30.3	29.2	260.1	408.6	123.0
	Range	Min.	4.8	21.4	25.8	16.7	4.8
		Max.	146.3	35.8	1130.4	1142.5	1142.5
K	Average	23.7	6.8	6.4	13.3	1.9	15.9
	Range	Min.	1.0	3.9	BDL	BDL	BDL
		Max.	203.3	9.4	92.5	5.8	203.3

3.4.3 Heavy Metals and Other Trace Elements

The CMD drainages in the Illinois Basin were enriched in many economically valuable metals, particularly in average concentrations for Zn (9,150 µg/L), Ni (1,321 µg/L), and Co (457 µg/L) (Table 3.3:). Some alkali and alkaline earth metals also appeared with widely varying degrees of concentration, especially for Li (39.9-37,804 µg/L) and Sr (6.7-2,492 µg/L).

3.4.3.1 Lithium

Li concentrations (Figure 3.9A) in Illinois CMD averaged 1,220 µg/L. Within R1-CMD, Li values averaged 152 µg/L, ranging from 39.9-322 µg/L. Li concentrations within TS-CMD averaged 572 µg/L, and ranged from 371-652 µg/L. Concentrations in R2-CMD averaged 379 µg/L and ranged from 371-652 µg/L. Within R3-CMD, Li values averaged 13,074 µg/L, ranging from 213 µg/L, to an extreme value of 37,804 µg/L in SIU-41. Overall, Li was most abundant in R3 drainages, followed by R2, then R1.

3.4.3.2 Strontium

Sr concentrations (Figure 3.9B) across the basin averaged 599.5 µg/L. Within R1-CMD, concentrations averaged 590.3 µg/L, ranging from 32.7-1,322.9 µg/L. Sr abundances within TS-CMD averaged 248.1 µg/L, ranging from 127.5-929.4 µg/L. Values in R2-CMD averaged 974.8 µg/L and ranged from 174.2-2,492 µg/L. R3-CMD concentrations were much lower, averaging 93.1 µg/L and ranging from 6.7-151.3 µg/L.

3.4.3.3 Rubidium

Rb concentrations (Figure 3.9C) across the basin averaged 47.9 µg/L. In R1-CMD, Rb values averaged 29.1 µg/L and ranged from 5.6-289.6 µg/L. Within TS-CMD, Rb concentrations averaged 27.5 µg/L and ranged from 12.6-35.6 µg/L. Rb was most abundant within R2-CMD, where abundances averaged 82.7 µg/L and ranged from 17.9-537.5 µg/L.

Within R3-CMD, values averaged 18.8 µg/L and ranged from 5.8-30.4 µg/L. Rb was most abundant in R2-CMD, then R1-CMD, followed by R3-CMD.

3.4.3.4 Barium

Across the Illinois basin, Ba concentrations (Figure 3.9D) averaged 30.6 µg/L overall, and were below the detection limit (BDL) in just one drainage, SIU-40. Concentrations in R1-CMD averaged 36.8 µg/L, ranging from 4.1-305.4 µg/L. Ba concentrations in TS-CMD were among the highest of the basin, averaged 60.2 µg/L and ranging from 11.3-127.0 µg/L. TS-CMD is rather like R1-CMD concerning Ba. Within R2-CMD, values averaged 8.2 µg/L, ranging from 2.1-24.2 µg/L. Abundances were even lower in R3-CMD, where one drainage was BDL and the other two had reported values of 2.5 µg/L for both. Overall Ba was most abundant in R1-CMD, followed by R2-CMD, then R3-CMD.

3.4.3.5 Beryllium

Beryllium (Figure 3.9E) was present in only 36 of 42 samples, with an overall average concentration of 18.6 µg/L. In R1-CMD, Be concentrations averaged 8.6 µg/L overall, but was present in only 14 of 19 samples, which averaged 11.6 µg/L and ranged from 0.8-31.0 µg/L. Within TS-CMD, Be values averaged 14.2 µg/L and ranged from 0.7 µg/L-19.2 µg/L. Be concentrations in R2-CMD averaged 16.0 µg/L overall, and was present in 11 of 12 samples, in which the average was 17.4 µg/L and whose values ranged from 2.1-43.8 µg/L. Within R3-CMD, concentrations averaged 103.9 and ranged from 42.5-222.5 µg/L. Overall, Be is most abundant within R3-CMD, followed by R2-CMD, then R1-CMD.

3.4.3.6 Cesium

Across the basin, Cs (Figure 3.9F) was absent in only one sample (SIU-17), with an overall average of 1.5 µg/L. Within R1, Cs concentrations averaged 1.0 µg/L, ranging from BDL

to 4.2 µg/L. Cs abundances in TS-CMD were similarly small, averaging 0.9 µg/L and ranging from 0.1-1.7 µg/L. Within R2-CMD, concentrations averaged 2.7 µg/L, ranging from 0.4-8.3 µg/L. Lastly, concentrations within R3-CMD averaged 1.8 µg/L, ranging from 1.3-2.5 µg/L. Overall, Cs was most abundant in R2, followed by R3, then R1.

3.4.3.7 Zinc

Zn was an abundant element within the Illinois CMD (Figure 3.9G), with an average concentration of 9,150 µg/L. For R1-CMD, Zn values averaged 4,154 µg/L with concentrations ranging from 20.9-22,233 µg/L. Zn abundances within TS-CMD averaged 3,145 µg/L and ranged from 89.4-7,150 µg/L. Within R2-CMD, Zn concentrations averaged 17,939 µg/L and ranged from 1,154-68,992 µg/L. R3-CMD Zn concentrations averaged 21,646 µg/L with values ranging from 4,800-30,079 µg/L. Overall, the R3-CMD was richest in Zn, followed by R2-CMD and then R1-CMD.

3.4.3.8 Nickel

Ni was prominent in many samples (Figure 3.9H), with an overall concentration of 1,321 µg/L. Concentrations within R1-CMD averaged 423 µg/L and ranged from 10.9-1,942 µg/L. Ni concentrations in TS-CMD ranged from 42.0-1,914 µg/L and averaged 1,419 µg/L, which are similar to the average R2-CMD. Within R2-CMD, Ni values averaged 1,045 µg/L, ranging from 75.0 -2,596 µg/L. The greatest abundances were seen in R3-CMD, with Ni values averaging 7,844 µg/L, ranging from 1,992-18,588 µg/L. Overall, Ni was most abundant in R3-CMD, followed by R2-CMD, then R1-CMD.

Ni has direct strong correlations with REY, the *critical*-REY, and other elements associated with Σ REY enrichment, namely SO₄ (r=0.93, p<0.005) Al (r=0.91, p<0.005), Mg (r=0.96, p<0.005), Mn (r=0.94, p<0.005), Li (r=0.97, p<0.005), and Be (r=0.94, p<0.005), Cd

($r=0.96$, $p<0.005$), and Co ($r=0.94$, $p<0.005$), with more mild correlations for U ($r=0.86$, $p<0.005$),) and lesser direct correlations with Cu ($r=0.71$, $p<0.005$) and Na ($r=0.62$, $p<0.005$)

3.4.3.9 Boron

B was present in only 32 of the 42 samples, with an overall average of 944 $\mu\text{g/L}$. In R1-CMD, B concentrations averaged 109.0 $\mu\text{g/L}$ overall, and was present in only 11 of 19 samples whose values averaged 188.2 $\mu\text{g/L}$ and ranged from 34.0-500.0 $\mu\text{g/L}$. B concentrations within TS-CMD averaged 165.8 $\mu\text{g/L}$ overall, and was identified in only 6 of 8 samples, which in themselves averaged 221.0 $\mu\text{g/L}$ and ranged from 126.0-260.0 $\mu\text{g/L}$. B was present in all R2-CMD, averaging 2,607 $\mu\text{g/L}$, and ranged from 1,250-4000 $\mu\text{g/L}$, as well as in all R3-CMD, with an average concentration of 1,653 $\mu\text{g/L}$, ranging from 458.3-3,667 $\mu\text{g/L}$. Overall, B was most abundant in R2-CMD, followed by R3-CMD, then R1-CMD (Figure 3.9I).

3.4.3.10 Cobalt

Co was present within all drainages, with an average concentration of 457.3 $\mu\text{g/L}$. In R1-CMD, Co values averaged 155 $\mu\text{g/L}$ and ranged from 2.7-361.3 $\mu\text{g/L}$. Co concentrations within TS-CMD averaged 404 $\mu\text{g/L}$ and ranged from 19.8-494 $\mu\text{g/L}$. Within R2-CMD, concentrations averaged 189 $\mu\text{g/L}$ and ranged from 6.7-509 $\mu\text{g/L}$. Co values within R3-CMD averaged 3,589 $\mu\text{g/L}$ and ranged from 780-8,925 $\mu\text{g/L}$. Overall, Co is most abundant in R3-CMD, followed by R2-CMD, then R1-CMD (Figure 3.9J).

3.4.3.11 Copper

Cu was present in all drainages, with an average concentration of 67.6 $\mu\text{g/L}$. In R1-CMD, Cu values averaged 41.6 $\mu\text{g/L}$ and ranged from 7.0-221 $\mu\text{g/L}$. Cu concentrations in TS-CMD averaged 74.8 $\mu\text{g/L}$ and ranged from 25.0-98.0 $\mu\text{g/L}$. Within R2-CMD, average concentrations of 57.6 $\mu\text{g/L}$ were found, with values ranging from 16.7-167 $\mu\text{g/L}$. In R3-CMD,

Cu values averaged 253 µg/L and ranged from 58.3-379 µg/L. Overall, Cu is most abundant in R3-CMD, followed by R2-CMD, then R1-CMD (Figure 3.9K).

3.4.3.12 Cadmium

Cd (Figure 3.9L) was present in only 34 of the 42 samples, with an overall average concentration of 36.5 µg/L. In R1-CMD, Cd was BDL in 5 samples, with a total average of 22.3 µg/L, with the other 14 samples averaging 30.3 µg/L and ranging from 0.1-162.1 µg/L. Within R2-CMD, Cd values were BDL in 3 samples, for an overall regional average of 14.8 µg/L, with values at the other 9 sites averaging 19.7 µg/L and ranging from 3.3-45.0 µg/L. Within R3-CMD, Cd concentrations averaged 267 µg/L and ranged from 32.9-688 µg/L. Overall, Cd is most abundant in R3-CMD, followed by R1-CMD, then R2-CMD; Cd concentrations in TS-CMD averaged 16.3 µg/L, was BDL at the bio-reactor outlet (SIU-8) with the other 7 samples averaging 18.7 µg/L, ranging from 16.7-22.1 µg/L.

3.4.3.13 Vanadium

V concentrations (Figure 3.9M) were 20.2 µg/L overall, though found to be BDL in ~43% of samples. In R1-CMD, overall V concentrations averaged 9.0 µg/L, 13 of 19 samples were BDL and the remaining 6 samples ranged from 0.5-125 µg/L, averaging 28.5 µg/L. V concentrations in TS-CMD averaged 25.9 µg/L overall, with 2 samples BDL, and the other 6 samples ranged from 4.0-104.2 µg/L, averaging 34.5 µg/L. V values within R2-CMD averaged 31.9 µg/L, being above BDL in only 5 of the 12 samples, which averaged 76.7 µg/L and ranged from 8.3-275.0 µg/L. Within R3-CMD, V was only found in sample SIU-42, at a concentration of 87.5 µg/L. Overall, V most abundant R2-CMD, followed by R3-CMD, then R1-CMD.

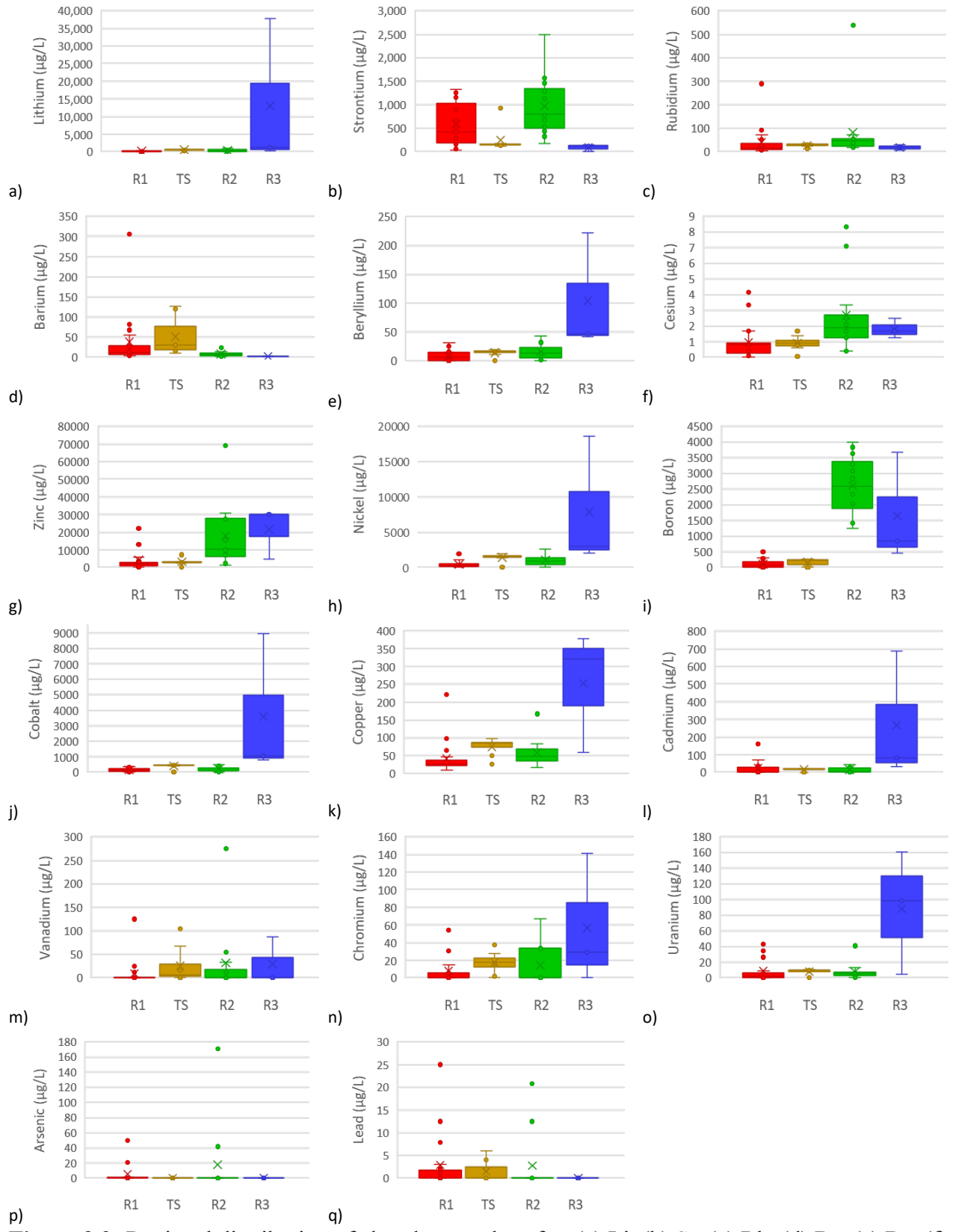


Figure 3.9: Regional distribution of abundance values for: (a) Li, (b) Sr, (c) Rb, (d) Ba, (e) Be, (f) Cs, (g) Zn, (h) Ni, (i) B, (j) Co, (k) Cu, (l) Cd, (m) V, (n) Cr, (o) U, (p) As, (q) Pb

3.4.3.14 Chromium

Cr was absent in 50% of samples and averaged 15.0 µg/L across all samples. Within the Cr containing samples (Figure 3.9N), values averaged 29.9 µg/L, ranging from 0.8-142µg/L. Within R1-CMD, Cr concentrations were BDL for 11 samples, with an average of 7.8 µg/L overall, with the remaining 8 sample values averaging 18.4 µg/L and ranging from 0.8-54.2 µg/L. Within TS-CMD, Cr concentrations averaged 17.4 µg/L overall, SIU-7 was BDL with other values ranging from 1.8-37.5 µg/L, averaging 19.9 µg/L. Within R2-CMD, Cr concentrations were BDL for 8 samples, but averaged 14.2 µg/L overall, with the remaining 4 samples averaging 42.7 µg/L and ranging from 33.3-66.7 µg/L. Within R3-CMD, Cr was BDL in one sample (SIU-40), with an overall average of 56.9 µg/L, with values of 29.2 µg/L in SIU-41 and a maximum of 142 µg/L within SIU-42 averaging 85.4 µg/L between them. Overall, Cr contents were greatest in R3-CMD, then R2-CMD, followed by R1-CMD.

3.4.3.15 Uranium

U concentrations across the basin (Figure 3.9O) averaged 14.3 µg/L for all samples. U values in R1-CMD averaged 9.0 µg/L overall, though values were BDL for 3 samples, with the remaining averaging 10.7 µg/L and ranging from 0.1-42.9 µg/L. U concentrations within TS-CMD averaged 8.0 µg/L and ranged from 0.4-10.8 µg/L. R2-CMD had average U concentrations of 8.1 µg/L overall; one location (SIU-37) was BDL, with the remaining averaging 8.8 µg/L, ranging from 0.8-40.8 µg/L. Within R3-CMD, values averaged 88.2 µg/L and ranged from 5.0-160.8 µg/L. Overall, U is most abundant in R3-CMD, with lesser abundances found in both R1-CMD then R2-CMD.

3.4.3.16 Arsenic

As (Figure 3.9P) was found in only 9 of the 42 drainages, with an overall average

concentration of 7.5 µg/L. Within R1-CMD, As concentrations averaged 5.5 µg/L with 12 samples BDL, with the remaining 7 averaging 14.8 µg/L, ranging from 0.8-50.7 µg/L. Within R2-CMD, As values averaged 17.7 µg/L overall, but was detected only within two samples, at a concentration of 41.7 µg/L in SIU-30 and 170.8 µg/L in SIU-23 (averaging 106.3 µg/L). As abundances were BDL for both TS-CMD and R3-CMD. Overall, R2-CMD has greater amounts of As than R1-CMD, and As is seemingly absent from R3-CMD.

3.4.3.17 Lead

Pb concentrations (Figure 3.9Q) were BDL in 1/3 of all samples, with an entire sample average of 2.4 µg/L. It was most prevalent within R1-CMD, averaging 2.9 µg/L overall, though it appeared in only 9 of the 19 samples, which averaged 6.1 µg/L and ranged from 0.5 µg/L to a max of 25.0 µg/L in SIU-14. R2-CMD Pb concentrations were 2.8 µg/L on average, with 10 of 12 samples BDL; the latter two samples, SIU 29 (12.5 µg/L) and SIU-38 (20.8 µg/L), averaged 16.7 µg/L. All R3-CMD samples were BDL for Pb. Overall, Pb values are highest in R1-CMD, followed by R2-CMD, then R3-CMD. TS-CMD averaged 1.5 µg/L, with 5 samples BDL; the remaining 3 samples ranged from 2.0-6.0 µg/L, averaging 4.0 µg/L.

Table 3.3: Trace Elements

Unit			Region 1	Tab Simco		Region 2	Region 3	All Samples
				Untreated Samples	All samples			
Li	µg/L	Average	151.9	600.7	571.9	379.2	13073.6	1219.8
		Range	39.9		370.6	83.3	212.5	39.9
		Min. Max.	322.4		652.0	950.0	37804.2	37804.2
Sr	µg/L	Average	590.3	150.7	248.1	974.8	93.1	599.5
		Range	32.7		127.5	174.2	6.7	6.7
		Min. Max.	1322.9		929.4	2492.1	151.3	2492.1
Rb	µg/L	Average	39.1	29.7	27.5	82.7	18.8	47.9
		Range	5.6		12.6	17.9	5.8	5.6
		Min. Max.	289.6		35.6	537.5	30.4	537.5
Ba	µg/L	Average	36.8	64.1	60.2	8.2	1.7	30.6
		Range	4.1		11.3	2.1	BDL	BDL
		Min. Max.	305.4		127.0	24.2	2.5	305.4
Be	µg/L	Average	8.6	16.2	14.2	16.0	103.9	18.6
		Range	BDL		0.7	BDL	42.5	BDL
		Min. Max.	31.0		19.2	43.8	222.5	222.5
Cs	µg/L	Average	1.0	1.0	0.9	2.7	1.8	1.5
		Range	BDL		0.1	0.4	1.3	BDL
		Min. Max.	4.2		1.7	8.3	2.5	8.3
Cu	µg/L	Average	41.6	81.9	74.8	57.6	252.8	67.6
		Range	7.9		25.0	16.7	58.3	7.9
		Min. Max.	220.8		98.0	166.7	379.2	379.2
Ni	µg/L	Average	423.3	1616.0	1419.2	1044.8	7844.4	1320.6
		Range	10.9		42.0	75.0	1991.7	10.9
		Min. Max.	1941.7		1914.0	2595.8	18587.5	18587.5
Cd	µg/L	Average	22.3	18.7	16.3	14.8	267.2	36.5
		Range	BDL		BDL	BDL	32.9	BDL
		Min. Max.	162.1		22.1	45.0	688.3	688.3
As	µg/L	Average	5.5	BDL	BDL	17.7	BDL	7.5
		Range	BDL		BDL	BDL	BDL	BDL
		Min. Max.	50.0		BDL	170.8	BDL	170.8
Co	µg/L	Average	155.0	458.7	403.9	188.5	3589.4	457.3
		Range	2.7		19.8	6.7	779.6	2.7
		Min. Max.	361.3		494.4	508.8	8924.6	8924.6
Cr	µg/L	Average	7.8	19.6	17.4	14.2	56.9	15.0
		Range	BDL		BDL	BDL	BDL	BDL
		Min. Max.	54.2		37.5	66.7	141.7	141.7
Pb	µg/L	Average	2.9	1.7	1.5	2.8	BDL	2.4
		Range	BDL		BDL	BDL	BDL	BDL
		Min. Max.	25.0		6.0	20.8	BDL	25.0
U	µg/L	Average	9.0	9.1	8.0	8.1	88.2	14.2
		Range	BDL		0.4	BDL	5.0	BDL
		Min. Max.	42.9		10.8	40.8	160.8	160.8
V	µg/L	Average	9.0	29.5	25.9	31.9	29.2	20.2
		Range	BDL		BDL	BDL	BDL	BDL
		Min. Max.	125.0		104.2	275.0	87.5	275.0
Zn	µg/L	Average	4153.5	3581.9	3145.3	17938.5	21645.8	9149.5
		Range	20.9		89.4	1154.2	4800.0	20.9
		Min. Max.	22233.3		7150.0	68991.7	30079.2	68991.7
B	µg/L	Average	109.0	171.4	165.8	2607.6	1652.8	944.0
		Range	BDL		BDL	1250.0	458.3	BDL
		Min. Max.	500.0		260.0	4000.0	3666.7	4000.0

3.4.4 Trace Metal Correlations

There are a number of inverse correlations of log adjusted concentrations of trace metals with pH, including Cu ($r=-0.44$, $p<0.005$), Ni ($r=-0.60$, $p<0.005$), Cd ($r=-0.53$, $p<0.005$), Co ($r=-0.48$, $p<0.005$), U ($r=-0.48$, $p<0.005$), and Zn ($r=-0.65$, $p<0.005$) (Table S4). Most of these metals also share strong correlations with the Σ REY, including Cu ($r=0.61$, $p<0.005$), Ni ($r=0.90$, $p<0.005$), Cd ($r=0.87$, $p<0.005$), Co ($r=0.91$, $p<0.005$), and U ($r=0.82$, $p<0.005$) (Figure 3.11H,J,K,L,O). Notably, despite the moderately inverse correlation seen between $\log[\text{Zn}]$ and pH ($r=-0.65$, $p<0.005$), no correlation was found between Zn and Σ REY abundances ($r=0.37$, $p=0.016$).

Graphs of trace element correlations are found in (Figure 3.11). There were also a number of trace elements that correlated well with Σ REY, but showed no correlations with pH (Table S4), such as the very strong direct correlation that were seen between Σ REY and Li (Figure 3.11A) ($r=0.88$, $p<0.005$), as well as Be (Figure 3.11E) ($r=0.96$, $p<0.005$), and B (Figure 3.11I) ($r=0.47$, $p<0.05$).

Unlike the majority of the trace metals, Cs, As, and V all failed to show correlations with either pH (in either consideration) or Σ REY (Table S4). No correlations whatsoever were found between Pb and Σ REY ($r=-0.14$, $p=0.37$) (Figure 3.11Q) nor between $\log[\text{Pb}]$ and pH ($r=-0.44$, $p=0.114$), nor were there correlations for any other analyte values (Table S3).

Concentration values of Co (Figure 3.10) (as well as the intercorrelated elements Li, Be, Cu, Ni, Cd, Co, U, B) all show statistically strong direct correlations with SO_4 ($r=0.92$, $p<0.005$) (Table S4), but not with As ($r=-0.07$, $p=0.65$) (Figure 3.10).

Sr and Fe are also well correlated with As, Rb, and K as well as the lighter REY (Table S4), notably both La and Ce as well as a further correlation of Fe with Pr ($r=0.49$, $p<0.005$).

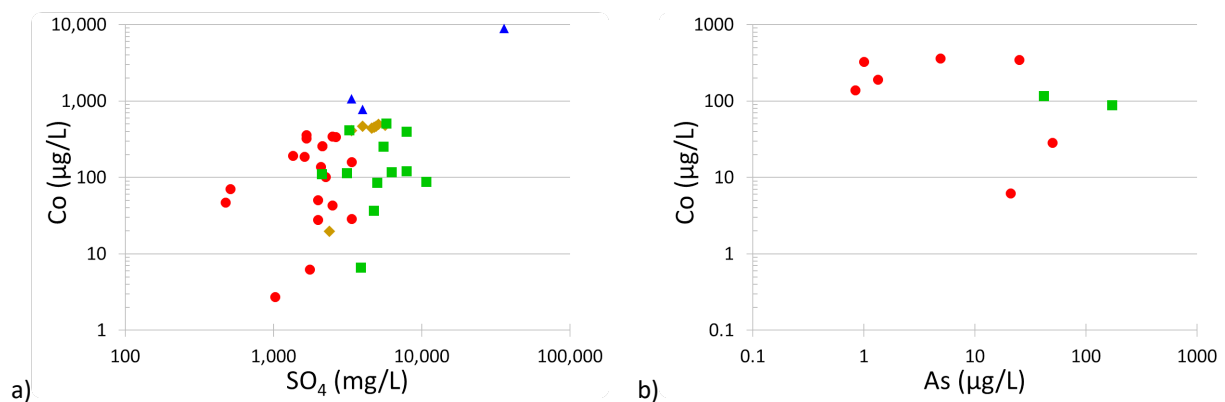


Figure 3.10: Correlations of Co with (a) SO_4 and (b) As.

Sr, Rb, As (Figure 3.11B,C,P), and K (Figure 3.8J), are distinct intercorrelated group that do not share correlations with pH nor with $\sum\text{REY}$, instead having few outside correlations, as in the mild direct correlations Sr with the La ($r=0.54$, $p<0.005$), and Ce ($r=0.49$, $p<0.005$), or the intercorrelations with Cs for both Rb ($r=0.68$, $p<0.005$) and As ($r=0.74$, $p<0.005$).

As, Rb, and Cs each have statistically sound moderate correlations with Fe ($r>0.6$, $p<0.005$) as well as with V with respective correlation coefficients $r=0.72$, $r=0.79$, and $r=0.52$. As and Cs also have moderate correlations with P ($r=0.54$, $p<0.005$ and $r=0.59$, $p<0.005$ respectively) Cs also has further correlations with Zn ($r=0.53$, $p<0.005$), and B ($r=0.59$, $p<0.005$)

Apart from the above mentioned correlations of V with Fe, As, Rb, Cs, and P, a moderate direct correlation is seen with Cr ($r=0.59$, $p<0.005$), and Cs ($r=0.52$, $p<0.005$). Like these other metals, no correlation could be made between Cr with $\sum\text{REY}$ or pH (Figure 3.11N). Aside from V and P ($r=0.59$, $p<0.005$), Cr only has statistically significant correlations with U ($r=0.58$, $p<0.005$) and Cu ($r=0.58$, $p<0.005$) (Table S4).

A strong statistical correlation was found between U (Figure 3.11O) and $\sum\text{REY}$ values ($r=0.82$, $p<0.005$). There was also a mild inverse correlation present between $\log[\text{U}]$ and pH ($r=-0.48$, $p<0.005$) (Table S4). The strongest correlations for U were for Cu, ($r=0.90$, $p<0.005$), Ni

($r=0.86$, $p<0.005$), Cd ($r=0.87$, $p<0.005$), and Co ($r=0.84$, $p<0.005$), Be ($r=0.85$, $p<0.005$), Li ($r=0.79$, $p<0.005$), SO₄ ($r=0.73$, $p<0.005$), Al ($r=0.79$, $p<0.005$), Mg ($r=0.78$, $p<0.005$), Mn ($r=0.74$, $p<0.005$), $p<0.005$), with lesser correlations for Cr ($r=0.58$, $p<0.005$) and Na ($r=0.46$, $p<0.005$) (Table S4).

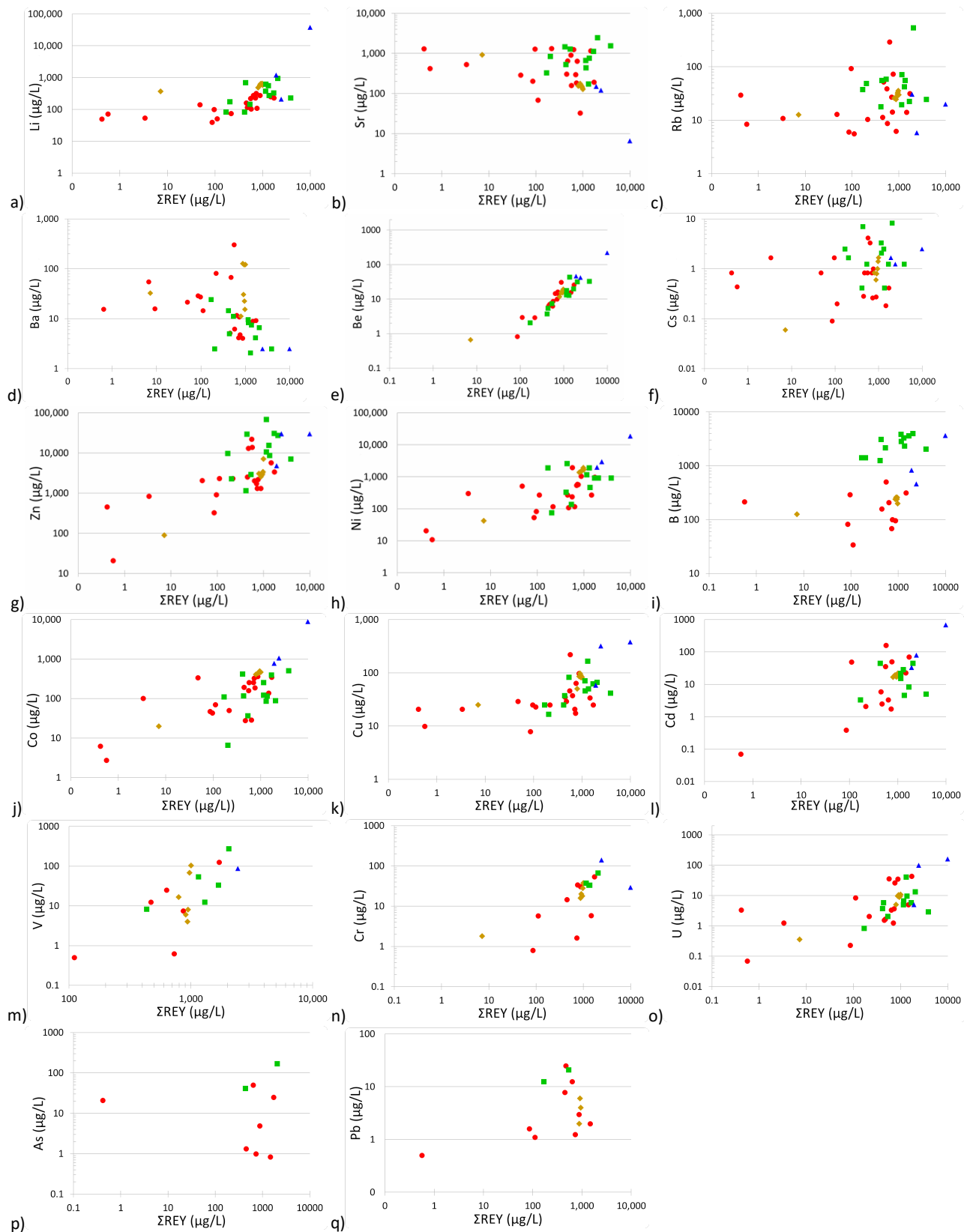


Figure 3.11 Trace element correlations with Σ REY abundance values: (a) Li, (b) Sr, (c) Rb, (d) Ba, (e) Be, (f) Cs, (g) Zn, (h) Ni, (i) B, (j) Co, (k) Cu, (l) Cd, (m) V, (n) Cr, (o) U, (p) As, (q) Pb

CHAPTER 4

DISCUSSION

4.1 Hypothesis 1: Cumulative REY Abundance vs pH

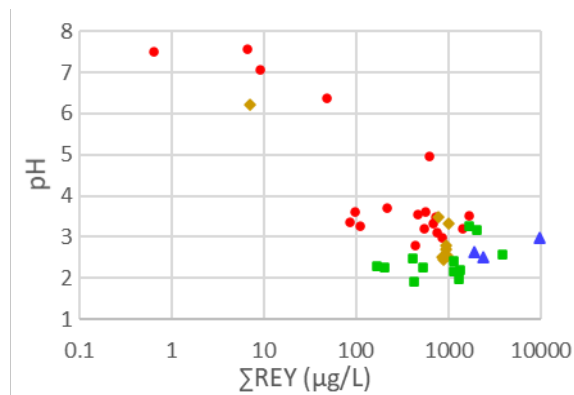


Figure 4.1: Graph plotting cumulative REY abundance with pH values.

In this study, partial support is found for the first hypothesis, that Σ REY abundances in AMD across the Illinois Basin are inversely correlated with the pH of the AMD. There is poor correlation between raw values of Σ REY abundance and pH ($r=-0.25$, $p=0.11$) with even worse correlation when considering only samples with pH value <5 , ($r=-0.08$, $p=0.66$), but when the REY data is transformed into logarithmic units, comparisons between the $\log[\Sigma\text{REY}_{\text{CMD}}]$ and pH reveal support for the hypothesis with strong inverse correlations between pH and $\log[\text{REY}]$ ($r=-0.84$, $p<0.005$) as well statistically robust correlations between pH and the majority of log-adjusted REY when taken individually, with the exception of Ho and Lu (Table S4). Correlations were similarly poor between unadjusted values individual REY, apart from mild inverse correlations seen for Pr ($r=-0.37$, $p=0.017$) and Nd ($r=-0.41$, $p=0.007$) (Table S3). This suggests that while low pH conditions are a necessary condition, there are other determining factors of Σ REY enrichment.

Because pH is a logarithmic expression of proton activity, while acid base reactions are stoichiometrically linear, it is therefore reasonable that correlations between H^+ and analyte

values are more convincing when both are expressed in like manner. Furthermore, primary REY enrichment likely happened by way of ingress of hydrothermal fluids rich in SO_4 and metals. Even so, REY is associated with SO_4 not because they occur together in a mineral phase, (Verplanck et al., 2004; Leticariu et al., 2017) but because REY and sulfide enrichment were both driven by hydrothermal processes (Cobb, 1981). Furthermore, acidity of a drainage is driven primarily by oxidation of pyrite and other sulfides, releasing Fe, H^+ and SO_4 (Gimeno Serrano et al., 2000). This increased acidity does not in itself affect REY, but previous AMD studies show that under conditions of low pH and abundant SO_4 , REY (lanthanide) speciation is dominated by sulfate complexation, primarily as mono-sulphate complexes (LnSO_4^+), followed $\text{Ln}(\text{SO}_4)_2^-$, with miniscule concentrations as a free ionic species (Gimeno Serrano et al., 2000; Verplanck et al., 2004; Zhao et al., 2007). Since sulfide phases are not a recognized mode of occurrence or origin for REY in either Asian or Appalachian metalliferous coals (Hower et al., 2016a; Dai et al., 2017), REY shares only hydrothermal provenance with these sulfides, and is not directly involved in their weathering processes and associated changes in aqueous chemistry, namely generation of H^+ and SO_4 during the weathering of sulfides as well as neutralizing effects of any site alkalinity from basement rock, remediation efforts, etc. REY contents were also indirectly effected by low pH conditions, because increasingly solutions will have a higher capacity for dissolution of REY-bearing as well as the non-REY bearing (i.e., sulfides) weathering materials (Stewart et al., 2017), as well as increased catalysis of aluminosilicates, (Pentrák et al., 2012). In this study, both Si and Al have strong correlations with $\sum\text{REY}$, ($r=0.91$, $p<0.005$), ($r=0.42$, $p=0.005$). Neither are redox sensitive and their concentrations are taken as a measure of bulk mineralogy of the weathering coal mine waste (Bigham and Nordstrom, 2000). The strong association of REY with Al and Si is thus likely tied to weathered

aluminosilicates. Clay minerals are produced as weathering products of aluminosilicates that are abundant at CMD sites both within the coal, (i.e., clay partings) and in overburden (Leticariu et al., 2017). Weathered clay minerals like illite and kaolinite, that are seen elsewhere to host REY, most notably clay ion adsorption REY deposits of southern China, orebodies from which comes most of the world's supply of Y (Williams-Jones et al., 2012; USGS, 2019). Gimeno Serrano et al., (2000) found that as sulfate concentrations increase, so does the degree of sulfate complexation. Greater amounts of this complexation stabilize aqueous REY, thereby limiting sorption to clays leading to greater concentrations of REY within AMD. Furthermore, REY will generally readily form stable complexes with fluorine. The presence of aluminum within AMD prevents this, due to the preferential association of aluminum with the fluorine anion, inhibiting REY-fluoride complexation that might otherwise occur (Gimeno Serrano et al., 2000; Ayora et al., 2015). Lastly, complexation and mobilization of REY by complexation with SO_4 is seen to occur without appreciable fractionation (Gimeno Serrano et al., 2000). Accordingly, REY are likely to accompany sulfur during weathering of and migration from coal and coal wastes as REY-sulfate complexes.

Even though Fe and SO_4 (Figure 4.2) together lead overall sample ion abundances, no statistical correlation is seen across the entire sample set ($r=0.27$, $p=0.08$) (Table S4), however, when values for SIU-41 are excluded from the calculation, a strong positive correlation is realized ($r=0.90$, $p=1.06\text{E-}14$). With knowledge that microorganisms are known to drive the cycling of Fe and S within the complex redox environment of CMD (Leticariu et al., 2017), there was concern that precipitation and dissolution of Fe might influence $\sum\text{REY}$, but no correlation was found between $\sum\text{REY}$ and Fe ($r=0.13$, $p=0.4$) (Table S4) This is compatible with findings that partitioning of REY into Fe-rich phases (i.e., jarosite, schwertmannite, goethite)

does not occur below pH 5, even for fresh Fe precipitates (Verplanck et al., 2004). Fe and SO₄ concentrations result from the weathering of sulfide minerals, pyrite mostly, but also sphalerite, schwertmannite, chalcopyrite and other sulfides highly associated with hydrothermal alteration of Illinois coal (Moorehead, 2013).

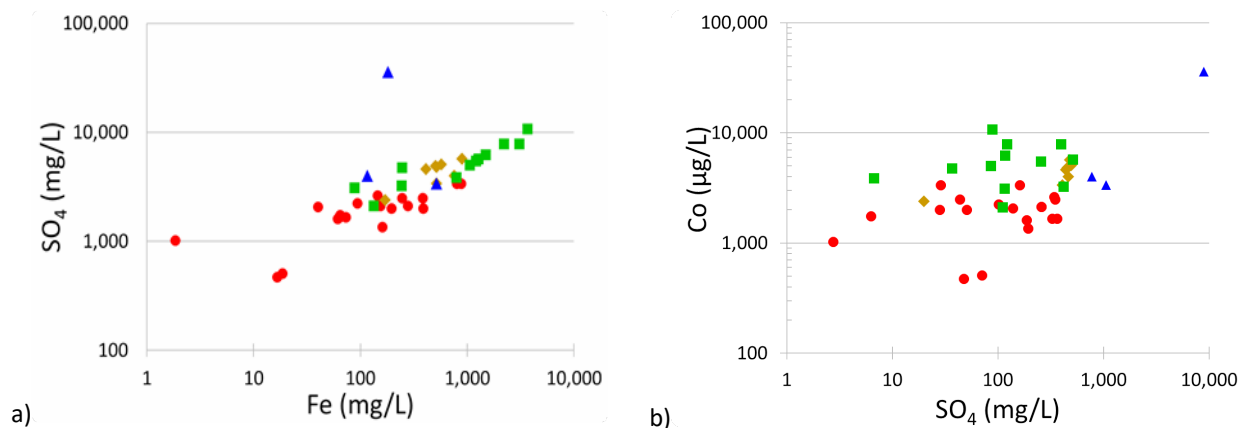


Figure 4.2: (a) plots of Fe and SO₄ concentrations trend in a mostly linear fashion and (b) SO₄ has direct linear correlations with Co as well as numerous other metals.

There are strong correlations for Σ REY (Table S3) with most metals, including Ni, Cu, Co, Cd which likewise share a strong correlation with SO₄ (Figure 4.2B). This enrichment likely came about from infiltration of the deposits by hydrothermal fluids which subsequently precipitated of reduced sulfur and metals as sulfides (galena, sphalerite, chalcopyrite). Hydrothermal provenance of metals in coals of the Illinois basin have been previously noted, with descriptions of hydrothermal enrichment of Hg and other metals within pyrite for some southern Illinois coals (Lefticariu et al., 2015; Manceau et al., 2018), as well in studies of coal seams further east in Union and Webster counties of Kentucky (Hower et al., 2000, 2001; Hower and Gayer, 2002). Hydrothermal enrichment of coal is also well studied in China and East Asia (Seredin and Dai, 2012a; Yang et al., 2012; Dai et al., 2016a). Surprisingly, despite associations of Zn metal with hydrothermal alteration, there were relatively poor correlative statistics between

Zn and REY ($r=0.37$, $p=0.016$) (Table S4), indicating that any hydrothermal solutions affecting coal and surrounding bedrock would increase metal contents, though not necessarily REY.

Ca, which, though it is ubiquitous in all CMD, failed to show statistically rigorous correlations with other elements (Table S4) and with lack of redox potential, Ca concentrations are a reflection of bulk composition at the site, with varying amounts of carbonate rocks (Behum et al., 2011). In addition to varying amounts of native carbonate rocks at CMD sites, there are also varying remediation efforts, where limestone is often used to provide bulk alkalinity to a site (Behum et al., 2011). Additionally, limestone aggregate is sometimes used as a road surface in many rural areas, which include these CMD sites.

4.2 Hypothesis 2: Proximity to Hicks Dome vs Σ REY

The second tested hypothesis supposed that since Hicks dome was known to be a great nexus of REY-rich geothermal fluids, (Denny et al., 2015), it may have served as the dominant source of REY enrichment for Illinois CMD, and if so, then the drainages closest to Hicks dome should be those most enriched in REY. Results of this study showed, however, that this hypothesis was false. In fact, the highest average abundances of REY were found furthest away from Hicks dome, with particularly high concentrations in R3 (average 4,742 $\mu\text{g/L}$, max 9,880 $\mu\text{g/L}$) in the northern part of the basin, followed by R2-CMD (1,190 $\mu\text{g/L}$, max 3,851 $\mu\text{g/L}$), in the southwestern margin of the basin. Region 1, which is home to Hicks dome had both the lowest average concentrations (497 $\mu\text{g/L}$) and lowest maximum (1,708 $\mu\text{g/L}$) of the study. Though Hicks dome may have been eliminated as the source of basin wide REY enrichment, there are some key regional differences.

In the course of the study, considerable amounts of Ba were identified in both TS and R1-CMD (Figure 3.9), this corresponds with the mineral barite, one of the main ore components

(along with calcite, sphalerite, and galena) of the MVT type mineralization seen in the IKFD (Denny et al., 2015). The alkaline cryptovolcanic complex at Hicks Dome is the likely source of the enrichments seen of K and especially Ba, enrichments which are absent or muted in other regions.

The mafic igneous rocks (MIR) that sporadically intrude Illinois coals are recognized as having significant \sum REY contents, which are dominated by the LREY (i.e., Ce, La, Nd), with correspondingly minor amounts of critical-REY, mostly consisting of Nd (Denny et al., 2015; Lefticariu et al., 2020). While they represent an overall minor fraction of weathering mine wastes, their presence may nonetheless correspond to the relative LREY enrichments seen in R2-CMD. Subsequent exposure of hydrothermal fluids to these MIR would enrich coals with LREY and differences in Misono softness would cause notable fractionation of Y and the LREY (Moorehead, 2013; Thompson et al., 2013) upon further fluid interactions with the MIR. The NASC normalized patterns of R2-CMD bear this out, where significant LREY enrichment is universally accompanied by anomalously high abundances of Y (Figure 3.2).

4.3 Critical-REY Correlations

Similar to that seen for \sum REY, unadjusted \sum critical-REY (Figure 4.3A) abundances had no correlation with pH ($r=-0.21$, $p=0.18$) (Table S3), but a statistically strong correlation was found between \log [critical-REY] and pH values ($r=0.83$, $p<0.005$) (Table S4). There is a nearly perfect correlation between the \sum critical-REY and \sum REY (Figure 4.3B) across all samples ($r=0.98$, $p<0.005$). Furthermore, there are strong direct inter-correlations ($r>0.896$, $p<0.005$) between the light rare earth elements La, Ce, and Pr, and Nd (Table S4). The middle and heavy rare earth elements (Sm-Lu) likewise have exceptionally strong intercorrelations ($r>0.99$, $p<0.005$) (Table S4).

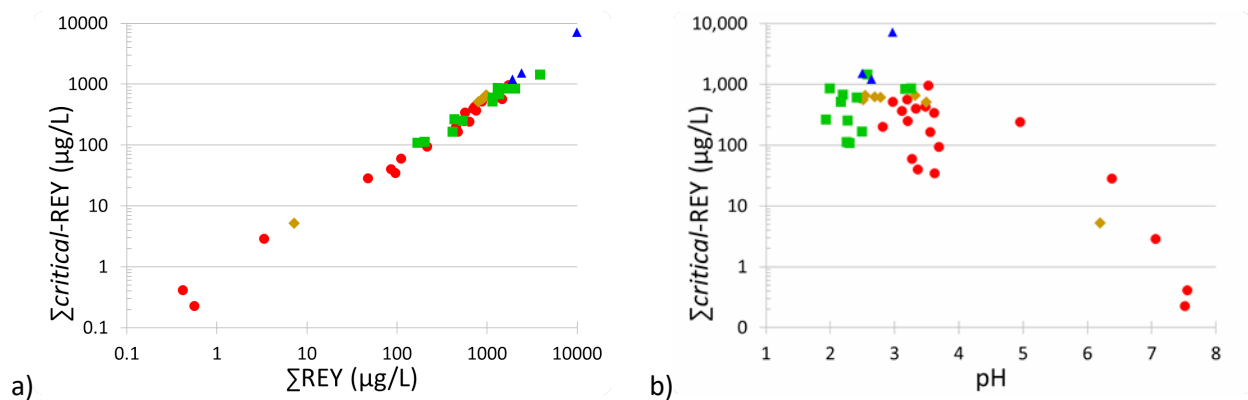


Figure 4.3: (a) a nearly perfect direct linear correlation between Σ REY and Σ critical-REY. (b) similar to total REY concentrations, Σ critical-REY abundances are greatest when $\text{pH} < 4$.

In terms of portional share of Σ critical-REY (Figure 4.4A), Y was dominant, with average contributions to Σ critical-REY (Figure 4.4B) ranging from 31% to up to 100% in the case of the circumneutral SIU-18. There is a moderately strong correlation between Y/Σ critical-REY and pH ($r=0.45, p<0.005$) which would accordingly mean that at higher pH, Y makes up a larger portion of the cumulative abundances of the *critical*-REY. Unfortunately, those higher pH are associated with lower concentrations of *critical*-REY, as discussed above. Among the *critical*-REY, Nd was the second most prominent, comprising an average of 29.8 % of the Σ critical-REY in a drainage and comprising anywhere from 0-59%. Proportion of Eu, Tb, and Dy, were much lower with average % contributions of 1.9%, 1.4%, and 7.7%.

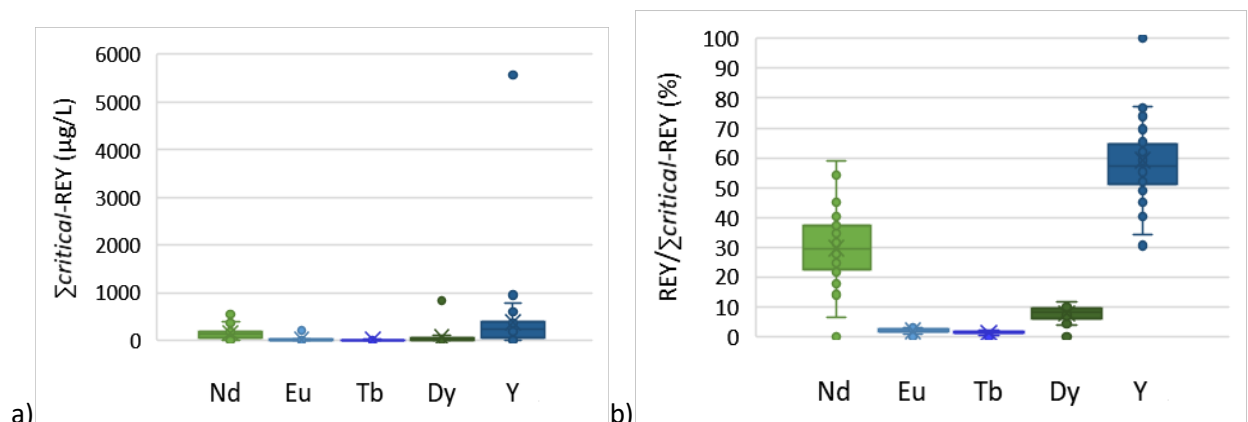


Figure 4.4: (a) range of concentration values for the critical-REY. (b) percent contribution of individual critical REY to the cumulative critical REY abundance.

In R3-CMD, Nd abundance (Figure 3.5D) was remarkably similar between drainages, despite changes in overall Σ REY and acidity values. The largest Nd values (and range of values) were found in R2-CMD, followed by R3-CMD, then R1-CMD. Enrichment in Y (Figure 3.5I), the dominant *critical*-REY in Illinois CMD, was greatest in R3-CMD (Figure 4.5B) where concentrations averaged 2,404 $\mu\text{g/L}$ with a study-wide maximum of 5,558 $\mu\text{g/L}$. Average concentrations for the *critical*-REY elements Eu (88 $\mu\text{g/L}$), Tb (68 $\mu\text{g/L}$), Dy (354 $\mu\text{g/L}$) were also at their greatest within R3-CMD (Figure 3.5F,H,J).

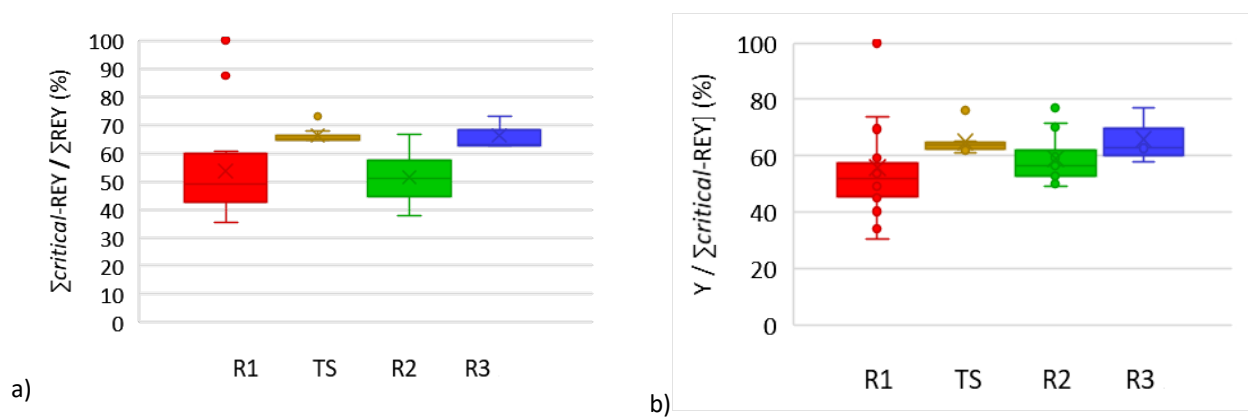


Figure 4.5: (a) range of values of the portion of Σ REY at each site are critical REY. (b) Range of Y contribution to cumulative abundances of critical REY.

Y (Figure 4.5B) made up an average of 59% of Σ *critical*-REY and 35% of Σ REY across all samples. There is a virtually perfect correlation ($r=0.995$, $p<0.005$) between Y and Σ *critical*-REY (Figure 4.6A). Though Y is included alongside the rare earth elements because it has similar physical and chemical properties (Bau and Dulski, 1995), there is a key difference, namely, trivalent Y^{3+} has the lowest covalency and ionization potential out of all the REY, a chemical characteristic known as the Misono softness parameter (Misono et al., 1967; Thompson et al., 2013). The anomalously low Misono softness parameter of Y leads to different chemical behaviors from the other REY (Bau, 1999), namely fractionation of Y and the other REY due to

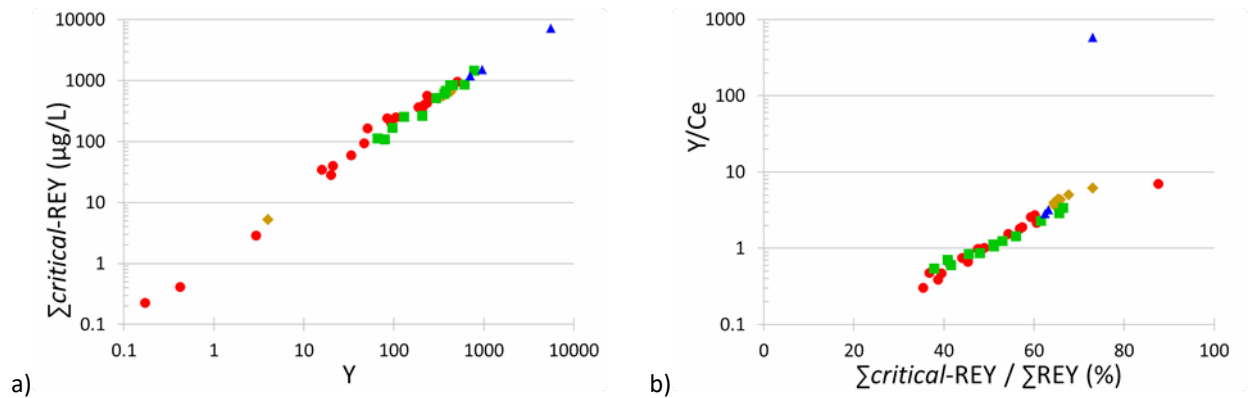


Figure 4.6: (a) almost perfectly linear plot of Y against $\Sigma_{critical-REY}$. (b) graph of Y/Ce (as proxy for degree of hydrothermal alteration) against percent of ΣREY that are *critical-REY*.

propensity of Y to remain in solution, even when other REY precipitate or are sorbed onto solid matrices (Thompson et al., 2013). The Misono softness parameter is a key factor that leads to initial Y enrichment during hydrothermal events, as well as during interactions with meteoric waters (i.e., weathering), causing further fractionation of Y and REY (Leticariu et al., 2020). In sharp contrast to Y, the Misono softness parameter of Ce is the second highest (Misono et al., 1967), thus we can use the values of the ratio of Y/Ce as a proxy for hydrothermal alteration extent, with increasing fractionation (enrichment) of Y into solution with increasingly longer periods of water-rock interaction (Williams-Jones et al., 2012; Thompson et al., 2013). With the exception of the extreme outlier SIU-41 (Y/Ce=580), sample Y/Ce ratios ranged from 0.3-7.0 (Table S2) and plot very neatly and linearly against $\Sigma_{critical-REY} / \Sigma REY$ (Figure 4.6B), with a strong direct correlation between Y/Ce and increasing portion of critical-REY to total ΣREY ($r=0.94$, $p<0.005$). With SIU-41 included (Table S4), the correlation statistic suffers dramatically ($r=0.25$, $p=0.11$), suggesting that additional factors at the site lead to the anomalous Y enrichment. Y/Ce varied regionally, with an average in Region 1 of $Y/Ce_{R1-CMD}=1.6$, an average in Region 2 of $Y/Ce_{R2-CMD}=1.4$, and in Region 3 $Y/Ce_{R3-CMD}=195.4$ with SIU-41, absent this outlier, the other two samples of the region have an average Y/Ce ratio of 3.0. The lower

value of Y/Ce for R1 and R2-CMD (Table 3.1:) agrees with our findings that R2-CMD shows an enrichment of the LREY, with respect to both the NASC and the abundances seen in R1 and R3.

It is important to distinguish however, that parameter shows no association with cumulative abundance of REY in Illinois AMD, with signs of varying degrees of “softness” driven fractionation of REY evident across all ranges of Σ REY (Figure 4.7A). Therefore, extent of water-rock interaction may be a predictor of economic REY patterns, but not necessarily an indicator of appreciable Σ REY values at a site. Even so, Y/Ce shares a strong direct linear correlation with $\Sigma_{critical}$ -REY ($r=0.94$, $p<0.005$) (Figure 4.6b). Thus, it seems that while Misono softness parameter is not the only factor effecting Σ REY abundance in Illinois, it is nonetheless an important factor because of its role in REY fractionation during both the initial enrichment of the site by hydrothermal fluids, as well as during subsequent weathering of coal mine materials. $\Sigma_{critical}$ -REY/ Σ REY or simply put, what proportion of the drainage is economically attractive, has moderately direct correlations with Si ($r=0.46$, $p<0.005$), Cu ($r=0.49$, $p<0.005$), and Ni ($r=0.48$, $p<0.005$) (Table S3), and bearing in mind that only acidic CMD will have Σ REY potential in Illinois, with circumneutral samples ($pH>5$) excluded, a strong inverse correlation with Sr ($r=-0.76$, $p=3.6E-8$) (Figure 4.7a). This means that high

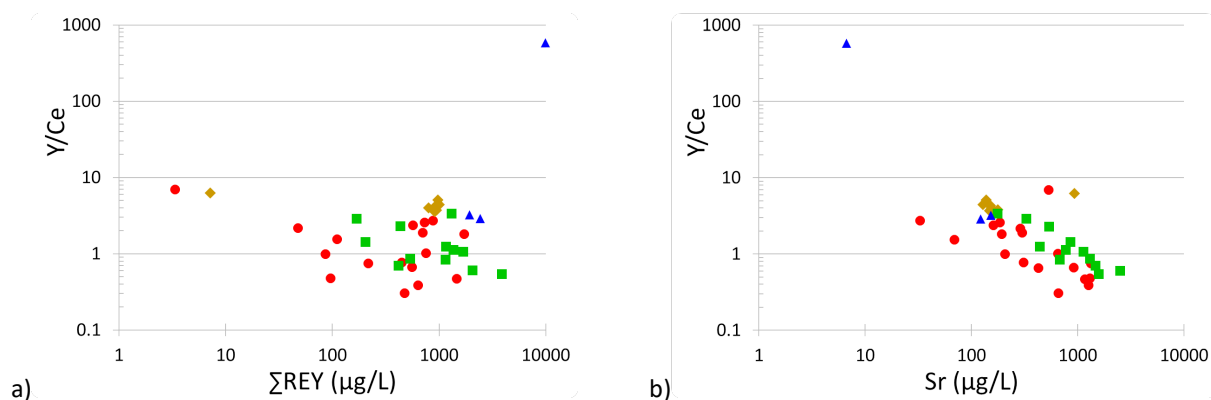


Figure 4.7: (a) graph showing wide range of Y/Ce across the range of Σ REY (b) graph showing decreasing Y/Ce values with greater concentrations of Sr.

concentrations of strontium in Illinois CMD are indicative of REY abundance patterns that are less economically attractive. Sr (Figure 4.7B) also shares this direct correlation with Y/Ce ($r=0.50$, $p=0.001$), absent the outliers SIU-41 and circumneutral SIU-18 where Y was the only Y reported with the remaining REY BDL. Thus, high concentrations of Sr appear to be present in AMD that did not suffer prolonged interactions with hydrothermal fluids.

4.4 Additional Provenance for REY

A large concern in this study was the impact of agricultural fertilizers on the REY content of samples. While the apatite group of minerals is primarily used as a source of phosphorous in the manufacture of fertilizers (USGS, 2019), some phosphates are significantly enriched in REY, to the extent that apatites are recognized as an ore mineral of REY (i.e., monazite) (Moorehead, 2013; Chehreh Chelgani and Hower, 2018; USGS, 2019). The data suggests that the contribution of REY from agriculture fertilizer to the Illinois CMD was minimal, if any. Phosphorus content was below the detection limit for most samples in the western sampling area. SIU 30 (also the most acidic sample) is the most notable outlier. This sample was collected from a blood-red pool of AMD at the Shale Lake winery, which was developed on the land of a former surface mine.

Apatite often contains U as well as REY, but U and P correlations were altogether mild ($r=0.42$, $p=0.006$) (Table S4). P also lacks the strong correlations seen for U with the hydrothermally associated Cu ($r=0.9$, $p<0.005$), Ni ($r=0.86$), Cd ($r=0.87$), Co ($r=0.84$) and Be ($r=0.85$). It therefore seems likely that U, P, and REY do not share a common provenance and more to the point, the lack of a strong correlation with phosphorus (Table S4) fails to point to a dominant apatitic source (much less agricultural provenance) of basinal REY enrichment. It is suspected by this author that the extremely high phosphorus content found here is the result of

fertilizer runoff from grape production and remediation efforts. P does have strong correlations with Si, Fe, Cs, Rb, Cr, and V (Table S4).

4.5 Tab Simco CMD

Tab Simco is an abandoned coal mining site local to SIU, roughly 6 km south east of Carbondale, IL. The central core of underground workings were mined from 1890-1955, followed by surface mining of the surrounding hill from 1960 until 1975 when it was abandoned, leaving exposed the underground workings along with huge mounds of weathering coal mine wastes (Lefticariu et al., 2017). Due to the low pH and high amounts of dissolved metals in the discharge, Tab Simco was recognized in 1996 as being one of the most contaminated sites in the mid-continental region (Smith, 2002). Today the site consists of a U shape around a hill (Figure 4.8), surrounded by steep gradient from surface mining (Behum et al., 2011). An AMD

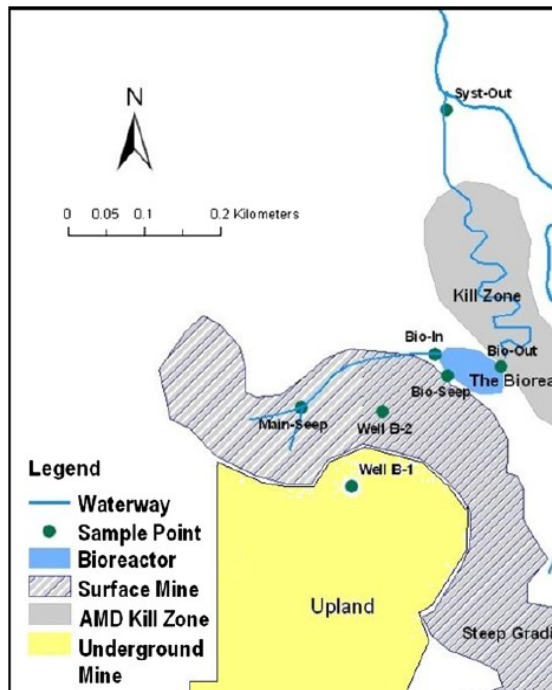


Figure 4.8: Map view of the Tab Simco site. Reprinted with permission (Behum et al., 2011).

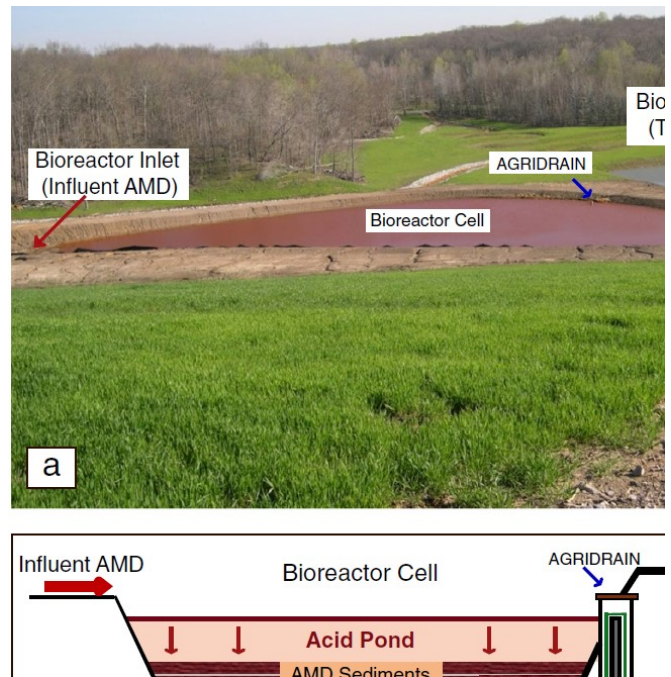


Figure 4.9: View (a) and schematic (b) of bioreactor cell, showing sampling locations and remediation design at Tab Simco. Reprinted with permission (Lefticariu et al., 2017).

treatment system was designed and constructed (Figure 4.9), consisting of a 3 km² bioreactor using wood chips, straw, yard waste, and powdered agricultural limestone as a substrate for microbial sulfate reduction (Behum et al., 2011; Lefticariu et al., 2017). After entering the bioreactor cell, the CMD filters through the organic substrate where it precipitates due to a combination of biological and abiotic processes, mostly as neoformed-nanoparticles of iron and sulfur precipitates on detrital particles of clay and quartz (Lefticariu et al., 2017)

One objective of this study was to comparatively examine the trace and bulk chemistry of TS-CMD to further elucidate hints of REY provenance, regional trends, and being on the far western extent of Region 1, to test whether it's grouping with R1-CMD was suitable. The samples of untreated AMD from Tab-Simco show little variation in REY abundance. The drainage was sampled at the main (most prominent) seep of the Tab-Simco site as well as at the bio-reactor inlet, which comprises an amalgamation of flows from multiple seeps. While most of the elemental abundances are enriched to the same degree, markedly higher concentrations of Ba, P, and V are at the main seep, suggesting heterogeneity within the same site due to AMD treatment across the site. Treatment of the polluted water showed an increase in pH from 3.49-5.20, a ~30% reduction in SO₄, 70% reduction in Si and Fe concentrations, as well as 99% reduction in Al values (Table S3). Water treatment at TS furthermore led to over 95% reduction in most trace metals (Table S3, Figure A3 in Appendix A) except for Cu (50% reduction) and the removal of over 99% of REY from the CMD. Site remediation also enriched the waters with respect to some of the elements, namely Ca (~74%), Ba (~190%), and especially Sr (505% increase) (Table S3).

Another strong example of local heterogeneity is found in samples SIU-10 and SIU-11 (Figure 4.10). These samples are both from the area of the old Palzo mine, where two types of

remediation were utilized. In the western area of the site, cement kiln dust was used to boost alkalinity. In the northeastern area of the site, sewage sludge was added as a carbon/electron source in efforts to utilize bacterial sulfate reduction to generate alkalinity. Oddly, As and V were BDL in SIU-10, but were identified in SIU-11, along with significant enrichments to P (~17x) as well as for Fe (4x), Mn (3.5x), and $\sum_{critical-REY}$ (2.63x).

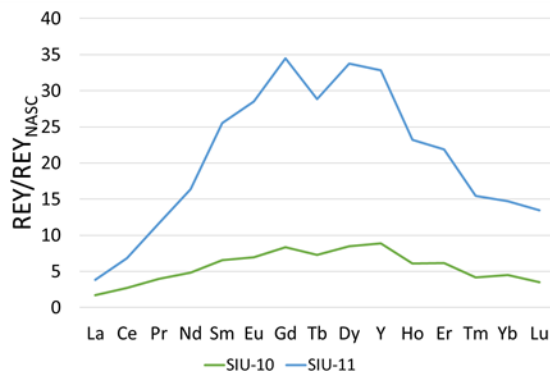


Figure 4.10: NASC normalized REY abundances between two samples from the Palzo mine.

Are the greater MREY abundances of SIU-11 (Figure 4.10) due to site heterogeneity, with larger amounts of REY in the fines, soil, strata, etc., in the effluent path? It might also be possible that instead the REY-bearing phases well distributed within the site, and these differences result from the liberation of heavy metals from the sewage sludge, elements which are absent in the cement kiln dust. Upon closer investigation, this site also presents a case where a more acidic drainage, SIU-10 (pH=3.11, $\sum REY=753 \mu g/L$) has lesser REY abundances than SIU-11 (pH=3.52, $\sum REY=1,708 \mu g/L$). A final key difference is the level of sulfate present. Sewage sludge is known to contain up to 2.3 wt.% S (Dewil et al., 2008), which could explain why the SO_4 concentrations in the sewage sludge seep SIU-11 (2,502 mg/L) are appreciably greater than concentrations in SIU-10 (1,620 mg/L). These greater amounts of dissolved sulfate likely led to increasing amount of sulfate-complexation and thus mobilization of REY as sulfate-complexes, as described in literature (Gimeno Serrano et al., 2000; Ayora et al., 2015). This

author purports that site-specific variables like these, that locally increase sulfate availability may lead to heightened REY extraction from an otherwise homogeneous substrate.

The heterogeneity of Σ REY enrichment is exemplified in sample outliers, whose results both confound analyses and whet the *apatite* of those searching for economically viable resources. There were distinct outliers found in samples from all regions, like SIU 23 from R2, standing out among R2-CMD for its high Rb (rubidium), Cs (cesium) and K content. R3-CMD held the most extreme outlier, SIU-41. Analyte values in sample SIU-41 were many times higher than the study averages for the major and trace elements: SO₄ (10x), Al (15x) Mg (40x), Mn (18x), Li (115x), Ni (21x), Cd (33x), Co (36x), and Be (16x), and U (15x). When correlating across the entire sample set, no correlation between pH and logarithmic Li was seen ($r=-0.37$, $p=0.016$), however when the outlier SIU-41 is excluded, the statistics were markedly improved with a mild inverse correlation ($r=-0.45$, $p=0.003$). After normalization to NASC, MREY abundances are 150-200x greater than NASC.

Overall, an examination of TS-CMD geochemistry shows that it overwhelmingly resembles other R1-CMD, especially with regards to Ba (Figure 3.9D). While there is a fair amount of variability in Ba concentrations within TS-CMD, the values recorded here are among the greatest for the basin. The abundances of Ba seen in TS-CMD and R1-CMD are not shared with R2-CMD and R3-CMD which contain comparatively paltry amounts. This is a good indication that Tab Simco site was exposed to fluids originating from Hicks Dome. Ba is one of the unusual signature elements of Hicks Dome and it is unlikely to be found in other regions of the Illinois Basin. Areas of similarity between TS-CMD and R2-CMD, such as shared elevations in Al and Mn concentrations, are in truth, associated with all REY enrichment across the basin. Additionally, while all regions show ubiquitously strong correlations of Σ REY with

hydrothermal metals, (Ni, Cu, Co, Cd), there are some trace elements that reveal great regional disparities. Namely, that TS and R1-CMD lack the abundances of Zn contained in R2 and R3-CMD (Figure 3.9G), and especially those of B (Figure 3.9I), of which unrivaled abundances are seen in R2-CMD, with even B values of R3-CMD middling in comparison, with similar minor abundances in TS-CMD and the rest of R1-CMD (Figure 3.9I). The strongest correlations for B were for Zn ($r=0.70$), Fe ($r=0.67$), followed by Cs ($r=0.59$), SO_4 ($r=0.58$) Na ($r=0.55$), Al ($r=0.49$), Nd ($r=0.47$), and lastly $\sum\text{REY}$ ($r=0.47$, $p<0.005$) (Table S3). While there was no correlation between $\log[\text{B}]$ and pH ($r=-0.42$, $p=0.015$) (Figure 3.11I), and it could be that this B enrichment is simply reflective of marine influence (Goodarzi and Swaine, 1994), it seems possible that B could still share a hydrothermal provenance with REY.

4.6 Comparison with Spanish AMD

Comparisons with AMD in Spain bring up some important differences, namely that rather than coal mines, these discharges were from metal mines in the Iberian Pyrite Belt. Ayora et al. (2015) reported an average REY load of 2.3 mg/L in Spanish AMD, with some drainages containing up to 13 mg/L, whereas Illinois AMD only contains ~ 1 mg/L REY on average. AMD from both regions showed enrichment in the MREY, but there are distinct negative Eu anomalies in Spanish AMD (Ayora et al., 2015) whereas negative Eu anomalies in Illinois CMD are almost entirely nonexistent.

4.7 Comparison with Appalachian CMD

In comparison with the Appalachian CMD reported by Stewart et al (2017), the average concentrations and ranges of $\sum\text{REY}$ in Illinois CMD are an order of magnitude higher, with a study average of 1057 $\mu\text{g/L}$, ranging from 0.42-9,980 $\mu\text{g/L}$, compared to those reported by Stewart et al, where samples averaged 109 $\mu\text{g/L}$ and ranged from 0.29-1,134 $\mu\text{g/L}$. As a further

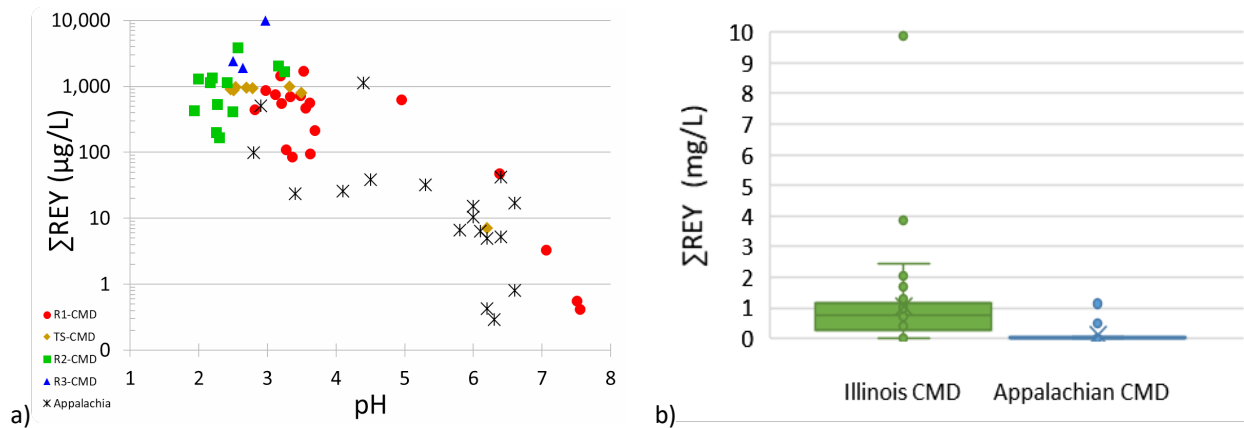


Figure 4.11: (a) Σ REY vs pH graph and (b) bar and whisker graph, comparing Σ REY values for both Illinois and Appalachian drainages. Data adapted from (Stewart et al., 2017).

point of comparison, this is slightly less than the third quartile of Σ REY values in this study ($Q3_{\Sigma\text{REY}} = 1,150 \mu\text{g/L}$). In terms of NASC-normalized abundance pattern, samples in this study displayed a prominent enrichment in the MREY elements, in particularly Sm-Er, with notable sample-to-sample enrichments in Y and Gd. In terms of critical REY, comparisons are similar with an order of magnitude larger average values for Σ critical-REY ($611 \mu\text{g/L}$ vs $59 \mu\text{g/L}$), and ranges of value (0.23 - $7,213 \mu\text{g/L}$ in Illinois CMD vs 0.23 - $714 \mu\text{g/L}$ in Appalachian CMD).

CHAPTER 5

SUMMARY AND RECOMMENDATIONS

5.1 Summary

The first hypothesis tested was the influence of pH on Σ REY abundance. What was found was a lack of correlation between the element concentration values and pH, for the REY as well as most elements. When abundances were converted into logarithmic values, however, multiple strong correlations were apparent for Σ REY, (including most individual REY and critical-REY), and major elements Al, Si, Fe, as well as the trace metals Cu, Ni, Cd, Co, U, and Zn. The preponderance of these metals indicate the interaction of hydrothermal fluids with these host rocks, and the strong associations of Σ REY (and furthermore the critical REY) have with Al, SO₄, Mg, Mn, Li, Be, Ni, Cd, and Co support enrichment by hydrothermal means. Simultaneously, we find that unfavorable REY profiles have a direct correlation with Sr abundance values. Thus, sites with large degrees of hydrothermal alteration and low levels of strontium are most promising for REY extraction/development.

The second hypothesis, that spatial proximity to Hicks dome would correlate with higher Σ REY abundances proved false. There was no relationship seen between Σ REY abundance and proximity to Hicks Dome. Indeed, concentrations of REY and other economic metals were lowest on average in region 1 where Hicks Dome resides. Antithetically, the greatest REY abundances are instead found in region 3, in the far northern edge of the basin. The second greatest abundances are similarly found far from the purported source of enrichment, in region 2, the southwestern portion of the basin.

Instead it is suggested that the Σ REY enrichment may have occurred as separate events throughout the basin associated with hydrothermal solutions, with sites impacted most greatly by

MVT type mineralization having generally, the greatest abundances of REY.

5.2 Comments and Future Considerations

Apart from natural factors that influence the site to site heterogeneity of the weathering matrices, including various degrees of detrital input or hydrothermal alteration, the human element further complicates the matter. Since the rise of the industrial revolution in the mid-1800s, the considerable resources of bituminous coal in the Pennsylvanian rocks of the Illinois basin have been developed by a variety of means (underground, pit, strip mining, etc.) and histories are many times unknown or poorly documented for these drainages. Illinois CMD reflects a staggering array of geochemical environments resulting from diverse mining histories with multiple coal seams mined by a variety of methods, creating CMD with sometimes drastically different weathering matrices and environments, ranging from hills of inverted strata at former strip mines, to tailings ponds, to mine portals sealed with coal fines or other mining refuse. Previous efforts of AMD remediation, including addition of limestone aggregate and/or biowastes, seem to provide meaningful impact on REY abundance / pattern.

Reflection on this study with an objective eye bears to mind several things. An early self-criticism of the study was poor representation of circumneutral/alkaline across all three regions. Few circumneutral samples were collected, four within Region 1: (SIU-1, SIU-4, SIU-18, and SIU-22), one from the bioreactor outlet at Tab Simco (SIU-8) and two (otherwise) unreported drainage samples from Region 2: SIU-33 (pH=7.28) and SIU-34 (pH=7.95). Of these, only the R1-CMD and TS-CMD samples were sent for ICP-MS, with budgetary concerns precluding the further analysis of circumneutral R2-CMD.

Another shortcoming of this study is the lack of numerical flowrate data. While the narrative field notes on sampling conditions that were taken were useful in interpretations,

objective observations would have been useful in the valance of both specific drainages and basin wide resources. This ties in with another issue, the variability of flowrate/dryness at sites. There is a concern that the concentrations seen in samples from slow seeps may not be indicative of the general chemistry of the drainage, especially at higher flow rates. SIU 36 was stagnant at the time of sampling and, similarly, SIU 41 was a very slow seep. The variability and impact of flowrate at these sites warrants further investigation. Furthermore, past studies of TS-CMD show that while enrichments of dissolved metals Fe, Al, Si, Zn, Cd, Cu, Ni, Sr, K are relatively unwavering, there have been sporadic episodes of relative enrichments, for Cd and Cu on 9/26/12, and periods of relative depletions, as seen for Ni throughout Q4 of 2012, as well as seasonal effects of temperature on dissolved oxygen, vigor of sulfate-reducing bacteria, and ORP (Lefticariu et al., 2015). It might be warranted to explore if this geochemical consistency found at Tab-Simco might be a characteristic that is typical of other Illinois CMD. In this same vein, more drainages in the northern extent of the basin should be sampled to determine whether all AMD of the region share the abundances, and perhaps more importantly, the distinct critical-REY enrichment seen within the few samples of R3-CMD.

5.3 Economic Viability

Owing to the severity of demand of the thusly named *critical*-REY, REY pattern is a prime aspect of consideration when it comes to feasibility, with an eye for preferential Y (MREY) over Ce (LREY) type enrichment. Flowrate is another factor, though conceivably this could be remedied by injection wells (i.e., enhanced in-situ leaching), perhaps with the assistance of environmentally friendly ‘green’ chelating agents or microbiotic technologies that have been developed in recent years (Asemave, 2018).

The most obvious factor impacting economic viability is \sum REY abundance. \sum REY is

highly variable within Illinois AMD, containing ~1mg/L on average with outputs just under 10 mg/L in at least 1 locale. In traditional production of REY, a considerable effort is undertaken in the process of mining, processing, and leaching ore in order to arrive at the same point where we are in Illinois CMD, an aqueous solution rich in dissolved REY and other economic metals.

Weathering processes have already leached the elements that are critical in this burgeoning era of high technology and renewable energy from the same Pennsylvanian rocks that fueled the industrial revolution of our ancestors. As the global shift towards renewable energy and technologies continues, the same waters that pollute local ecosystems could instead be remediated, providing simultaneously the benefits of domestic production of critical REY as well as lessened anthropogenic impact. Thus, in-state REY production might thus double as remediation efforts, ushering in the prospect of subsidization by a variety of state and federal actors, for both economic and environmental reasons, and would yield substantial benefits in both theaters.

REFERENCES

- Alonso, E., Sherman, A.M., Wallington, T.J., Everson, M.P., Field, F.R., Roth, R., and Kirchain, R.E., 2012, Evaluating Rare Earth Element Availability: A Case with Revolutionary Demand from Clean Technologies: *Environmental Science & Technology*, v. 46, p. 3406–3414, doi:10.1021/es203518d.
- Asemave, K., 2018, Greener Chelators for Recovery of Metals and Other Applications: *Organic & Medicinal Chemistry International Journal*, v. 6, doi:10.19080/OMCIJ.2018.06.555694.
- Ayora, C., Macías, F., Torres, E., and Nieto, J.M., 2015, Rare Earth Elements in Acid Mine Drainage, in XXXV Reunión de la Sociedad Española de Mineralogía, Spain, http://www.uhu.es/fexp/sem2015/arc/seminarios/seminario_3.pdf (accessed May 2017).
- Bau, M., 1999, Scavenging of dissolved yttrium and rare earths by precipitating iron oxyhydroxide: experimental evidence for Ce oxidation, Y-Ho fractionation, and lanthanide tetrad effect: *Geochimica et Cosmochimica Acta*, v. 63, p. 67–77, doi:10.1016/S0016-7037(99)00014-9.
- Bau, M., and Dulski, P., 1995, Comparative study of yttrium and rare-earth element behaviours in fluorine-rich hydrothermal fluids: *Contributions to Mineralogy and Petrology*, v. 119, p. 213–223, doi:10.1007/BF00307282.
- Bauer, D., Diamond, D., Li, J., Sandalow, D., Telleen, P., and Wanner, B., 2010, U.S. Department of Energy Critical Materials Strategy: 1000846, 1000846 p., doi:10.2172/1000846.
- Behum, P.T., Lefticariu, L., Bender, K.S., Segid, Y.T., Burns, A.S., and Pugh, C.W., 2011, Remediation of coal-mine drainage by a sulfate-reducing bioreactor: A case study from the Illinois coal basin, USA: *Applied Geochemistry*, v. 26, p. S162–S166, doi:10.1016/j.apgeochem.2011.03.093.
- Bigham, J.M., and Nordstrom, D.K., 2000, Iron and Aluminum Hydroxysulfates from Acid Sulfate Waters: *Reviews in Mineralogy and Geochemistry*, v. 40, p. 351–403, doi:10.2138/rmg.2000.40.7.
- Bradbury, J.C., Baxter, J.W., and others, 1992, Intrusive breccias at Hicks Dome, Hardin County, Illinois: Circular no. 550, <https://www.ideals.illinois.edu/bitstream/handle/2142/44637/intrusivebreccia550brad.pdf?sequence=2> (accessed June 2017).

- Chehreh Chelgani, S., and Hower, J.C., 2018, Estimating REY content of eastern Kentucky coal samples based on their associated ash elements: *Journal of Rare Earths*, v. 36, p. 1234–1238, doi:10.1016/j.jre.2018.02.015.
- Chu, S., 2011, *Critical materials strategy*: DIANE Publishing.
- Cobb, J.C., 1981, *Geology and geochemistry of sphalerite in coal*: University of Illinois at Urbana Champaign, Illinois.
- Dai, S., Chekryzhov, I.Yu., Seredin, V.V., Nechaev, V.P., Graham, I.T., Hower, J.C., Ward, C.R., Ren, D., and Wang, X., 2016a, Metalliferous coal deposits in East Asia (Primorye of Russia and South China): A review of geodynamic controls and styles of mineralization: *Gondwana Research*, v. 29, p. 60–82, doi:10.1016/j.gr.2015.07.001.
- Dai, S., Graham, I.T., and Ward, C.R., 2016b, A review of anomalous rare earth elements and yttrium in coal: *International Journal of Coal Geology*, v. 159, p. 82–95, doi:10.1016/j.coal.2016.04.005.
- Dai, S., Xie, P., Jia, S., Ward, C.R., Hower, J.C., Yan, X., and French, D., 2017, Enrichment of U-Re-V-Cr-Se and rare earth elements in the Late Permian coals of the Moxinpo Coalfield, Chongqing, China: Genetic implications from geochemical and mineralogical data: *Ore Geology Reviews*, v. 80, p. 1–17, doi:10.1016/j.oregeorev.2016.06.015.
- Denny, F.B., Guillemette, R.N., and Lefticariu, L., 2015, Rare Earth Mineral Concentrations in Ultramafic Alkaline Rocks and Fluorite Within the Illinois-Kentucky Fluorite District: Hicks Dome Cryptoexplosive Complex, Southeast Illinois and Northwest Kentucky (USA), *in* Lasemi, Z. ed., Champaign, Illinois, Illinois State Geological Survey, v. Circular 587, https://www.researchgate.net/profile/Liliana_Lefticariu/publication/272820495_Rare_earth_mineral_concentrations_in_ultramafic_alkaline_rocks_and_fluorite_within_the_Illinois-Kentucky_Fluorite_District_Hicks_Dome_cryptoexplosive_complex_southeast_Illinois_and_Northwest_Kentucky_/links/55944a6a08ae5d8f392f6362/Rare-earth-mineral-concentrations-in-ultramafic-alkaline-rocks-and-fluorite-within-the-Illinois-Kentucky-Fluorite-District-Hicks-Dome-cryptoexplosive-complex-southeast-Illinois-and-Northwest-Kentucky.pdf (accessed June 2017).
- Dewil, R., Baeyens, J., Roels, J., and Steene, B.V.D., 2008, Distribution of Sulphur Compounds in Sewage Sludge Treatment: *Environmental Engineering Science*, v. 25, p. 879–886, doi:10.1089/ees.2007.0143.

- Generalic, E. Rare earth elements: EniG. Periodic Table of the Elements, Calculators, and Printable Materials, https://www.periodni.com/rare_earth_elements.html (accessed April 2019).
- Gimeno Serrano, M.J., Auqué Sanz, L.F., and Nordstrom, D.K., 2000, REE speciation in low-temperature acidic waters and the competitive effects of aluminum: *Chemical Geology*, v. 165, p. 167–180, doi:10.1016/S0009-2541(99)00166-7.
- Goodarzi, F., and Swaine, D.J., 1994, The influence of geological factors on the concentration of boron in Australian and Canadian coals: *Chemical Geology*, p. 18.
- Goodenough, K.M., Wall, F., and Merriman, D., 2018, The Rare Earth Elements: Demand, Global Resources, and Challenges for Resourcing Future Generations: *Natural Resources Research*, v. 27, p. 201–216, doi:10.1007/s11053-017-9336-5.
- Gromet, L.P., Haskin, L.A., Korotev, R.L., and Dymek, R.F., 1984, The “North American shale composite”: Its compilation, major and trace element characteristics: *Geochimica et Cosmochimica Acta*, v. 48, p. 2469–2482, doi:10.1016/0016-7037(84)90298-9.
- Hower, J.C., Eble, C.F., Dai, S., and Belkin, H.E., 2016a, Distribution of rare earth elements in eastern Kentucky coals: Indicators of multiple modes of enrichment? *International Journal of Coal Geology*, v. 160–161, p. 73–81, doi:10.1016/j.coal.2016.04.009.
- Hower, J.C., and Gayer, R.A., 2002, Mechanisms of coal metamorphism: case studies from Paleozoic coalfields: *International Journal of Coal Geology*, v. 50, p. 215–245, doi:10.1016/S0166-5162(02)00119-2.
- Hower, J., Granite, E., Mayfield, D., Lewis, A., and Finkelman, R., 2016b, Notes on Contributions to the Science of Rare Earth Element Enrichment in Coal and Coal Combustion Byproducts: *Minerals*, v. 6, p. 32, doi:10.3390/min6020032.
- Hower, J.C., Greb, S.F., Cobb, J.C., and Williams, D.A., 2000, Discussion on origin of vanadium in coals: parts of the Western Kentucky (USA) No. 9 coal rich in vanadium: *Special Publication* No. 125, 1997, 273–286: *Journal of the Geological Society*, v. 157, p. 1257–1259, doi:10.1144/jgs.157.6.1257.
- Hower, J.C., Ruppert, L.F., and Eble, C.F., 1999, Lanthanide, yttrium, and zirconium anomalies in the Fire Clay coal bed, Eastern Kentucky: *International Journal of Coal Geology*, v. 39, p. 141–153, doi:10.1016/S0166-5162(98)00043-3.

- Hower, J.C., Williams, D.A., Eble, C.F., Sakulpitakphon, T., and Moecher, D.P., 2001, Brecciated and mineralized coals in Union County, Western Kentucky coal field: *International Journal of Coal Geology*, v. 47, p. 223–234, doi:10.1016/S0166-5162(01)00047-7.
- Huang, Z., Fan, M., and Tian, H., 2020, Rare earth elements of fly ash from Wyoming's Powder River Basin coal: *Journal of Rare Earths*, v. 38, p. 219–226, doi:10.1016/j.jre.2019.05.004.
- IDNR Abandoned Mine Lands:., <https://www.dnr.illinois.gov/mines/AML/Pages/default.aspx> (accessed June 2017).
- IUPAC, 2005, Nomenclature of Inorganic Chemistry – IUPAC Recommendations 2005: *Chemistry International -- Newsmagazine for IUPAC*, v. 27, doi:10.1515/ci.2005.27.6.25.
- King, H.M. REE - Rare Earth Elements - Metals, Minerals, Mining, Uses: *Geology and Earth Science News and Information*, <https://geology.com/articles/rare-earth-elements/> (accessed April 2019).
- Kolata, D.R., and Nelson, W.J., 1997, Role of the Reelfoot Rift/Rough Creek Graben in the evolution of the Illinois Basin, *in* Special Paper 312: Middle Proterozoic to Cambrian rifting, central North America, *Geological Society of America*, v. 312, p. 287–298, doi:10.1130/0-8137-2312-4.287.
- Kolker, A., Scott, C., Lefticariu, L., Mastalerz, M., Drobniak, A., and Scott, A., 2020, Geochemical data for Illinois Basin coal samples, 2015-2018:
- Lefticariu, L., Klitzing, K.L., and Kolker, A., 2020, Rare Earth Elements and Yttrium (REY) in coal mine drainage from the Illinois Basin, USA: *International Journal of Coal Geology*, v. 217, p. 103327, doi:10.1016/j.coal.2019.103327.
- Lefticariu, L., Sutton, S.R., Bender, K.S., Lefticariu, M., Pentrak, M., and Stucki, J.W., 2017, Impacts of detrital nano- and micro-scale particles (dNP) on contaminant dynamics in a coal mine AMD treatment system: *Science of The Total Environment*, v. 575, p. 941–955, doi:10.1016/j.scitotenv.2016.09.154.

- Lefticariu, L., Walters, E.R., Pugh, C.W., and Bender, K.S., 2015, Sulfate reducing bioreactor dependence on organic substrates for remediation of coal-generated acid mine drainage: Field experiments: *Applied Geochemistry*, v. 63, p. 70–82, doi:10.1016/j.apgeochem.2015.08.002.
- Long, K.R., Van Gosen, B.S., Foley, N.K., and Cordier, D., 2010, The Principal Rare Earth Elements Deposits of the United States: A Summary of Domestic Deposits and a Global Perspective, *in* Sinding-Larsen, R. and Wellmer, F.-W. eds., *Non-Renewable Resource Issues*, Dordrecht, Springer Netherlands, p. 131–155, doi:10.1007/978-90-481-8679-2_7.
- Manceau, A., Merkulova, M., Murdzek, M., Batanova, V., Baran, R., Glatzel, P., Saikia, B.K., Paktunc, D., and Lefticariu, L., 2018, Chemical Forms of Mercury in Pyrite: Implications for Predicting Mercury Releases in Acid Mine Drainage Settings: *Environmental Science & Technology*, v. 52, p. 10286–10296, doi:10.1021/acs.est.8b02027.
- Misono, M., Ochiai, E., Saito, Y., and Yoneda, Y., 1967, A new dual parameter scale for the strength of lewis acids and bases with the evaluation of their softness: *Journal of Inorganic and Nuclear Chemistry*, v. 29, p. 2685–2691, doi:10.1016/0022-1902(67)80006-X.
- Moorehead, A., 2013, IGNEOUS INTRUSIONS AT HICKS DOME, SOUTHERN ILLINOIS, AND THEIR RELATIONSHIP TO FLUORINE-BASE METAL-RARE EARTH ELEMENT MINERALIZATION, <http://opensiuc.lib.siu.edu/theses/1240>.
- Palmer, C.A., Mroczkowski, S.J., Kolker, A., Finkelman, R.B., and Bullock Jr., J.H., 2001, Chemical analysis and modes of occurrence of selected trace elements in a Powder River basin coal and its corresponding simulated cleaned coal: Open-File Report Report 2000–323, doi:10.3133/ofr00323.
- Pentrák, M., Czímerová, A., Madejová, J., and Komadel, P., 2012, Changes in layer charge of clay minerals upon acid treatment as obtained from their interactions with methylene blue: *Applied Clay Science*, v. 55, p. 100–107, doi:10.1016/j.clay.2011.10.012.
- Plumlee, G.S., Goldhaber, M.B., and Rowan, E.L., 1995, The potential role of magmatic gases in the genesis of Illinois-Kentucky fluorspar deposits; implications from chemical reaction path modeling: *Economic Geology*, v. 90, p. 999–1011, doi:10.2113/gsecongeo.90.5.999.
- Schatzel, S.J., and Stewart, B.W., 2003, Rare earth element sources and modification in the Lower Kittanning coal bed, Pennsylvania: implications for the origin of coal mineral matter and rare earth element exposure in underground mines: *International Journal of Coal Geology*, v. 54, p. 223–251, doi:10.1016/S0166-5162(03)00038-7.

- Seid, M.J., Denny, F.B., and Devera, J.A., 2013, Bedrock Geology of Cave-in-Rock Quadrangle: Illinois State Geological Survey.
- Seredin, V.V., and Dai, S., 2012a, Coal deposits as potential alternative sources for lanthanides and yttrium: *International Journal of Coal Geology*, v. 94, p. 67–93, doi:10.1016/j.coal.2011.11.001.
- Seredin, V. V, and Dai, S., 2012b, Coal deposits as potential alternative sources for lanthanides and yttrium: *International Journal of Coal Geology*, v. 94, p. 67–93, doi:10.1016/j.coal.2011.11.001.
- Smith, P.A., 2002, CHARACTERIZATION OF AN ACID MINE DRAINAGE SITE IN SOUTHERN ILLINOIS: *Journal American Society of Mining and Reclamation*, v. 2002, p. 472–486, doi:10.21000/JASMR02010472.
- Stewart, B.W., Capo, R.C., Hedin, B.C., and Hedin, R.S., 2017, Rare earth element resources in coal mine drainage and treatment precipitates in the Appalachian Basin, USA: *International Journal of Coal Geology*, v. 169, p. 28–39, doi:10.1016/j.coal.2016.11.002.
- Thompson, A., Amistadi, M.K., Chadwick, O.A., and Chorover, J., 2013, Fractionation of yttrium and holmium during basaltic soil weathering: *Geochimica et Cosmochimica Acta*, v. 119, p. 18–30, doi:10.1016/j.gca.2013.06.003.
- USGS, 2019, Mineral commodity summaries 2019: U.S. Geological Survey: Mineral Commodity Summaries Report, 200 p., <https://doi.org/10.3133/70202434>.
- Verplanck, P.L., Nordstrom, D.K., Taylor, H.E., and Kimball, B.A., 2004, Rare earth element partitioning between hydrous ferric oxides and acid mine water during iron oxidation: *Applied Geochemistry*, v. 19, p. 1339–1354, doi:10.1016/j.apgeochem.2004.01.016.
- Weng, Z., Jowitt, S.M., Mudd, G.M., and Haque, N., 2015, A Detailed Assessment of Global Rare Earth Element Resources: Opportunities and Challenges: *Economic Geology*, v. 110, p. 1925–1952, doi:10.2113/econgeo.110.8.1925.
- Williams-Jones, A.E., Migdisov, A.A., and Samson, I.M., 2012, Hydrothermal Mobilisation of the Rare Earth Elements - a Tale of “Ceria” and “Yttria”: *Elements*, v. 8, p. 355–360, doi:10.2113/gselements.8.5.355.

Yang, M., Liu, G., Sun, R., Chou, C.-L., and Zheng, L., 2012, Characterization of intrusive rocks and REE geochemistry of coals from the Zhuji Coal Mine, Huainan Coalfield, Anhui, China: *International Journal of Coal Geology*, v. 94, p. 283–295, doi:10.1016/j.coal.2011.06.012.

Zhao, F., Cong, Z., Sun, H., and Ren, D., 2007, The geochemistry of rare earth elements (REE) in acid mine drainage from the Sitai coal mine, Shanxi Province, North China: *International Journal of Coal Geology*, v. 70, p. 184–192, doi:10.1016/j.coal.2006.01.009.

APPENDIX A

MAPS

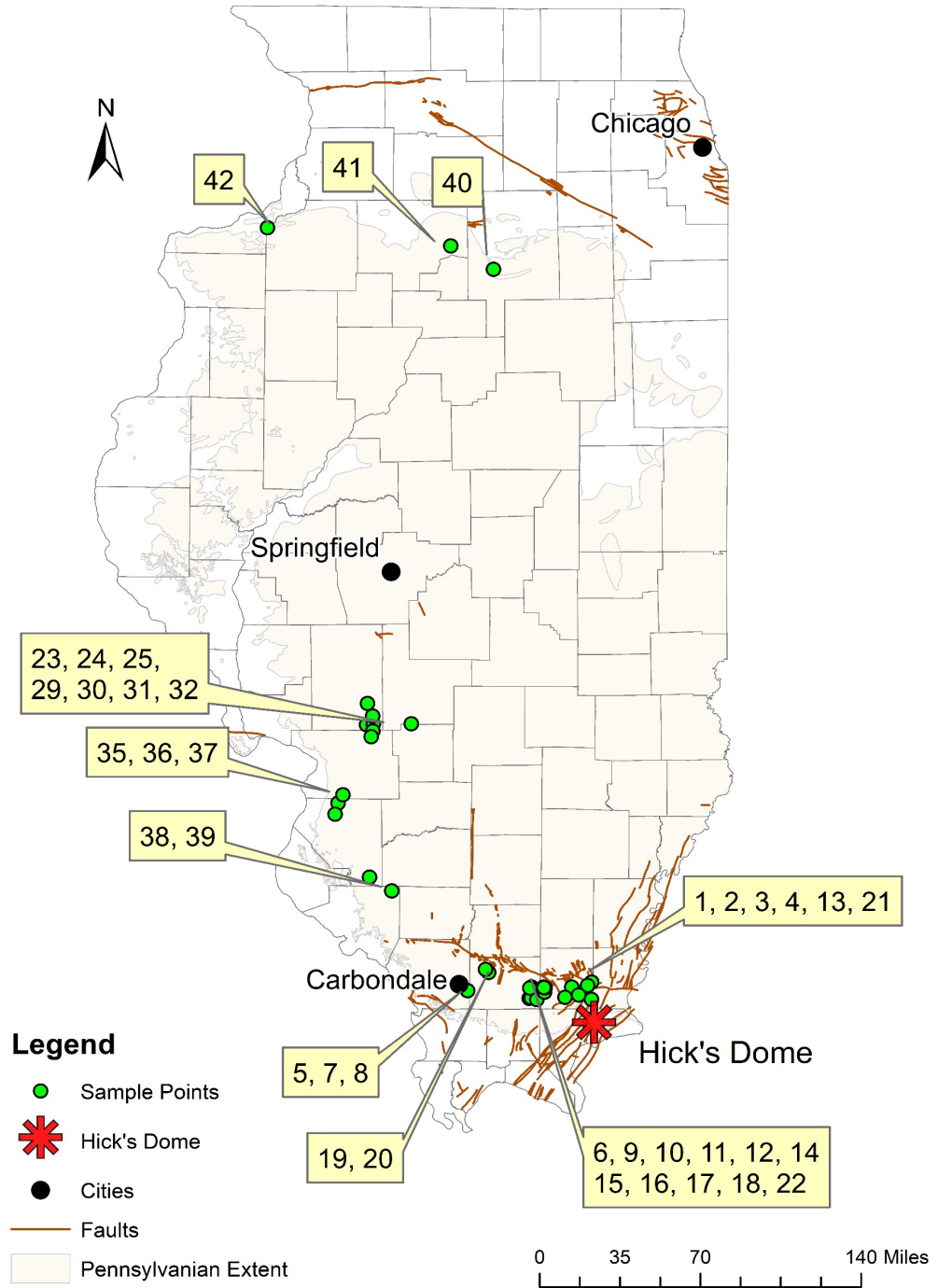


Figure A1: Map of sampling locations across the greater Illinois Basin.

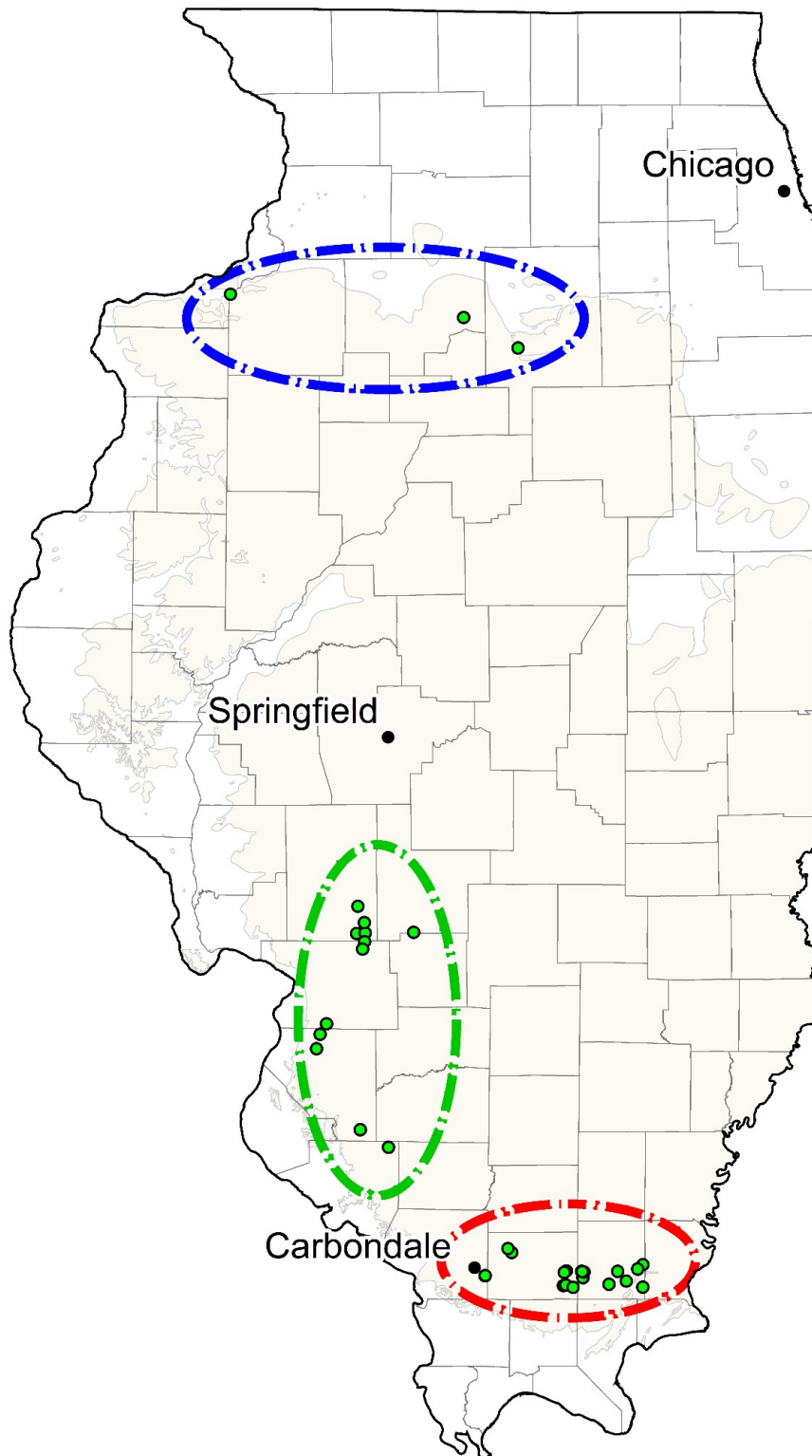


Figure A2: Map illustrating the three sampling areas in the Illinois Basin.

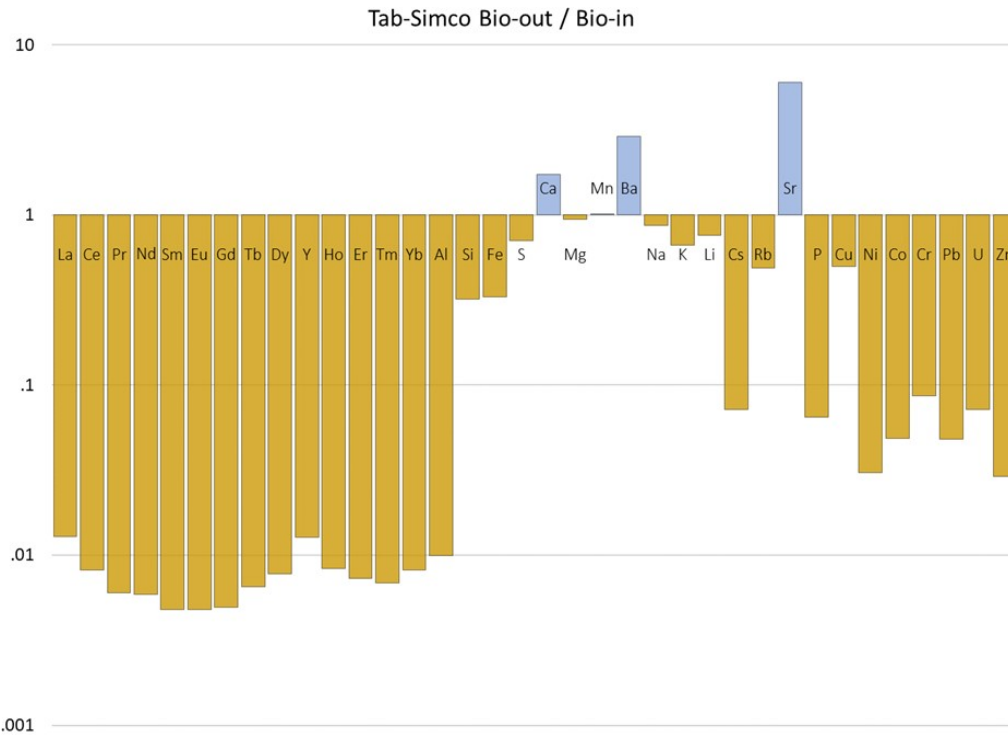


Figure A3: Depletions/enrichment effects of remediation at Tab-Simco

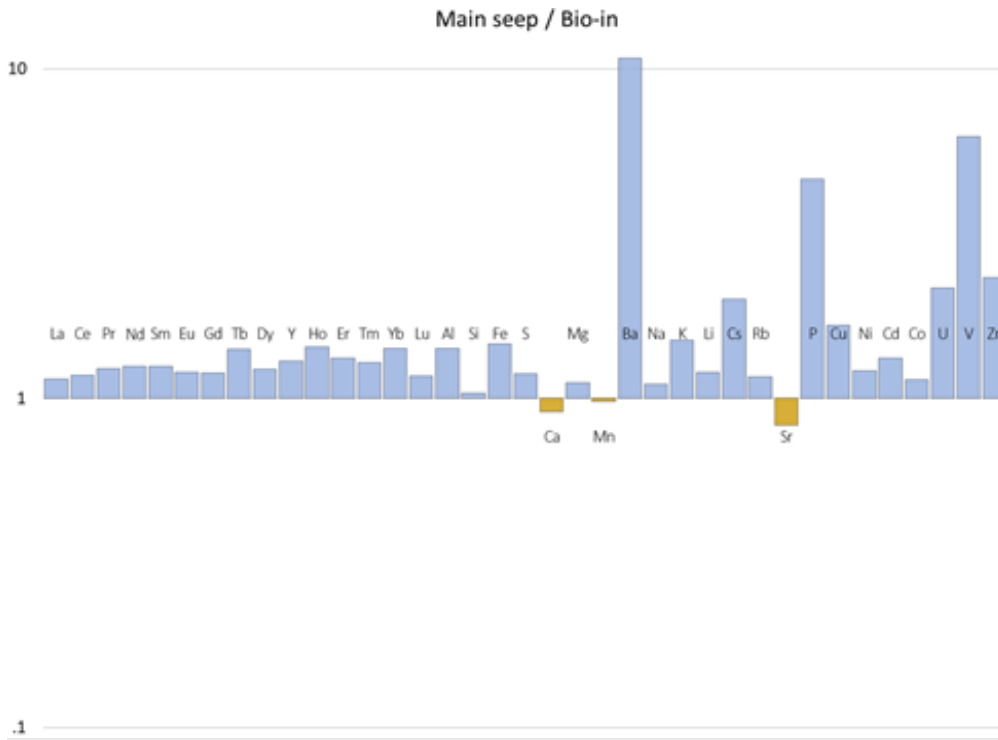


Figure A4: Enrichments of the main seep vs combined seeps

APPENDIX B

COPYRIGHT PERMISSIONS

Permission to use Illinois structural map from Kolata and Nelson (1997).



Marketplace™

Geological Society of America - License Terms and Conditions

This is a License Agreement between Kyle Klitzing ("You") and Geological Society of America ("Publisher") provided Clearance Center ("CCC"). The license consists of your order details, the terms and conditions provided by Geologi and the CCC terms and conditions.

All payments must be made in full to CCC.

Order Date	12-Oct-2020	Type of Use	Repu
Order license ID	1069400-1		thes
ISBN-13	9780813723129	Publisher	Geol
		Portion	Imag

LICENSED CONTENT

Publication Title	Middle Proterozoic to Cambrian rifting, central North America	Country	Unit
Author/Editor	Green, John C., Dickas, Albert Brinkley, Ojakangas, Richard W.	Rights holder	Geol
Date	12/31/1996	Publication Type	Book
Language	English		

REQUEST DETAILS

Portion Type	Image/photo/illustration	Distribution	World
Number of images / photos / illustrations	1	Translation	Original
Format (select all that apply)	Print, Electronic	Copies for the disabled?	No
Who will republish the content?	Academic institution	Minor editing privileges?	No
Duration of Use	Life of current edition	Incidental promotional use?	No
Lifetime Unit Quantity	Up to 250,000	Currency	USD
Rights Requested	Main product		

NEW WORK DETAILS

Title	REY in Acid Mine Drainages of the Illinois Basin	Institution name	South Carb
Instructor name	Dr. Liliana Lefticariu	Expected presentation date	2020

ADDITIONAL DETAILS

Order reference number	N/A	The requesting person / organization to appear on the license	Kyle
------------------------	-----	---	------

Permission to use figures of Appalachian drainages (Stewart et al., 2017)

ELSEVIER LICENSE TERMS AND CONDITIONS

This Agreement between Mr. Kyle Klitzing ("You") and Elsevier ("Elsevier") consists of your license detail: conditions provided by Elsevier and Copyright Clearance Center.

License Number	4926431088783
License date	Oct 12, 2020
Licensed Content Publisher	Elsevier
Licensed Content Publication	International Journal of Coal Geology
Licensed Content Title	Rare earth element resources in coal mine drainage and treatment precip Appalachian Basin, USA
Licensed Content Author	Brian W. Stewart,Rosemary C. Capo,Benjamin C. Hedin,Robert S. Hedin
Licensed Content Date	Jan 2, 2017
Licensed Content Volume	169
Licensed Content Issue	n/a
Licensed Content Pages	12
Start Page	28
End Page	39
Type of Use	reuse in a thesis/dissertation
Portion	figures/tables/illustrations
Number of figures/tables/illustrations	3
Format	both print and electronic
Are you the author of this Elsevier article?	No
Will you be translating?	No
Title	REY In Acid Mine Drainages of the Illinois Basin
Institution name	Southern Illinois University - Carbondale
Expected presentation date	Nov 2020
Order reference number	KKLITZ2020
Portions	Figures 5, 8, & 10

Permission to use figures of Spanish AMD from Ayora et al. 2015

Re: Permission to use figures in thesis

1 message

carlos ayora <cayora1@gmail.com>
To: Kyle Klitzing <kklitzing@gmail.com>

1

Dear Kyle,
Of course, you can use any of the Figures. Thank you for your interest. Good luck with the defense.
Regards,
Carlos

Missatge de Kyle Klitzing <kklitzing@gmail.com> del dia dl., 12 d'oct. 2020 a les 13:09:

Buenos Dias,
I would like permission to use a couple figures in the introduction chapter of my master's thesis titled REY in Acid Mine Drainage in the Illinois Basin for my degree at Southern Illinois University - Carbondale. I hope to defend it at the end of this month.
I would like to use figures 2 and 4 from the conference paper titled Rare Earth Elements in Acid Mine Drainage made for Mineralogy between June 30 and July 3, 2015, of which you are listed as the principal author.

A copy of the paper (for your quick reference) can be found here: <https://www.uhu.es/fexp/sem2015/arc/seminarios/semi>
May you kindly provide permission for me to re-use these figures as long as I properly attribute this work? If there is any me to use, please let me know.

¡Muchas gracias!

Que tenga un buen dia,
Kyle Klitzing

--

Permission to use Hicks Dome schematic from (Plumlee et al., 1995).



Society of Economic Geologists
Advancing Science and Discovery: 1920-2020

[Sign In](#) [Contact](#) [Join/Renew](#) [Contribute](#)

[About](#) [Membership](#) [Events](#) [Publications](#) [Students & Early Career](#)

Copyright

Permissions ▼

Fair Use Permission ▲

Use of up to three figures, a brief paragraph (up to 300 words), a single table, or the abstract from a single SEG publication is considered to be fair usage, and no formal permission is needed. If formal permission is required, please make your request as indicated below ("Usage Fees"). Fees may be assessed. We expect the SEG publication to be cited with appropriate credit, i.e., fully and prominently.

Copying and Use in the Classroom ▼

Posting on a Website ▼

Usage Fees ▼

Electronic Usage ▼

Open Access (OA)

OA Publishing Policy

How can I tell if a paper is OA?

What can I do with an OA paper?

How much does it cost?

How do I select this option?

Will paying for OA make any difference in the review process or publication time?

Will the SEG OA policy comply with funding requirements?

Can I use material from elsewhere in my paper?

Green Open Access

SEG also has a Green Open Access option, whereby the manuscript is published with the usual copyright restrictions, but authors are allowed to place a post-peer reviewed version of the manuscript online after an embargo period of time of manuscript publication—the month given on the cover of the issue (or first month listed, for two-month embargo). The version is that which the editor has approved for publication and for which he has given instructions to the author along to production, but which has not been through copyediting, layout, final proofing, and publishing with the

Permission to use figure of chondrite normalized samples from (Denny et al., 2015).

10/13/2020

Illinois State Geological Survey Terms of Use | ISGS

Copyright and Licensing

ISGS electronic services and most information contained therein are copyrighted with all rights reserved. Copyright may be held by the Board of Trustees of the University of Illinois, a different institution, or the item may be in the public domain. It is your responsibility to determine the copyright holder for any particular item and to determine what permissions may be needed to reproduce it. Individuals or entities may make fair use of copyrighted ISGS information, such as reproducing a single figure or table, or using a brief quotation, without obtaining formal permission, but in all cases the Illinois State Geological Survey must be credited as the source of the material. To reproduce ISGS information beyond the fair use exception, permission must be obtained from the ISGS Information Office, 615 East Peabody Drive, Champaign, Illinois 61820, 217-333-4747, info@isgs.illinois.edu. License fees and a license agreement may be required, depending on the proposed usage.

Permission to use map of the Tab Simco AMD site from (Behum et al., 2011)

License Number 4934190231608

License date Oct 22, 2020

 Licensed Content

Licensed Content Publisher Elsevier
 Licensed Content Publication Applied Geochemistry
 Licensed Content Title Remediation of coal-mine drainage by a sulfate-reducing bioreactor: A case study from the Illinois coal basin, USA
 Licensed Content Author Paul T. Behum, Liliana Lefticariu, Kelly S. Bender, Yosief T. Segid, Andrew S. Burns, Charles W. Pugh
 Licensed Content Date Jun 1, 2011
 Licensed Content Volume 26
 Licensed Content Issue n/a
 Licensed Content Pages 5
 Journal Type S&T

 About Your Work

Title REY In Acid Mine Drainages of the Illinois Basin
 Institution name Southern Illinois University - Carbondale
 Expected presentation date Nov 2020

 Requestor Location

Mr. Kyle Klitzing
 305 Robinson Circle Apt A-E
 Requestor Location Carbondale, IL 62901

 Order Details

Type of Use reuse in
 Portion figures/t
 Number of figures/tables/illustrations 1
 Format both prir
 Are you the author of this Elsevier article? No
 Will you be translating? No

 Additional Data

Order reference number KYLK202
 Portions Fig. 1. Pl
 showing

 Tax Details

Publisher Tax ID 98-03976

Permission to use photo and schematic diagram of the Tab Simco remediation site (Lefcariu et al., 2017)

License Number	4933950359524		
License date	Oct 21, 2020		
📄 Licensed Content		📄 Order Details	
Licensed Content Publisher	Elsevier	Type of Use	reuse in a tl
Licensed Content Publication	Science of The Total Environment	Portion	figures/tabl
Licensed Content Title	Impacts of detrital nano- and micro-scale particles (dNP) on contaminant dynamics in a coal mine AMD treatment system	Number of figures/tables/illustrations	1
Licensed Content Author	Liliana Lefcariu, Stephen R. Sutton, Kelly S. Bender, Mihai Lefcariu, Martin Pentrak, Joseph W. Stucki	Format	both print a
Licensed Content Date	Jan 1, 2017	Are you the author of this Elsevier article?	No
Licensed Content Volume	575	Will you be translating?	No
Licensed Content Issue	n/a		
Licensed Content Pages	15		
Journal Type	S&T		
📄 About Your Work		📄 Additional Data	
Title	REY In Acid Mine Drainages of the Illinois Basin	Order reference number	KYLK2020
Institution name	Southern Illinois University - Carbondale	Portions	Figure 1: vie
Expected presentation date	Nov 2020		
📍 Requestor Location		📄 Tax Details	
	Mr. Kyle Klitzing 305 Robinson Circle Apt A-E	Publisher Tax ID	98-0397604
Requestor Location	Carbondale, IL 62901 United States		

VITA

Graduate School
Southern Illinois University

Kyle L. Klitzing

Kyle.Klitzing@gmail.com

Lake Land College
Associate of Science, Mathematics, May 2013

Southern Illinois University Carbondale
Bachelor of Science, Geology, December 2015
Minor in Mathematics, December 2015

Special Honors and Awards:

Southern Illinois University

1. College of Engineering Academic Excellence Scholarship, Fall 2013
2. Dean's Transfer Scholarship, Fall 2013
3. College of Science Scholarship, Spring, Fall 2014
4. Porter Jobling Research Grant 2016

Thesis Paper Title:

Rare Earth Elements and Yttrium in Acid Mine Drainages of the Illinois Basin.

Major Professor: Dr. Liliana Lefticariu

Publications:

1. Lefticariu, L., Klitzing, K.L., and Kolker, A., 2020, Rare Earth Elements and Yttrium (REY) in coal mine drainage from the Illinois Basin, USA: *International Journal of Coal Geology*, v. 217, p. 103327, doi:10.1016/j.coal.2019.103327.

Presentations:

2. Klitzing, K.L., Kolker, A., Geboy, N.J., Vancil, G., and Lefticariu, L., (2016) Rare Earth and Strategic Elements in Illinois Coal Deposits and Coalmine Waste. GSA North-Central Section - 50th Annual Meeting in Urbana-Champaign, Illinois, 18 April 2016, doi:10.1130/abs/2016NC-275380.
3. Klitzing, K.L., Lefticariu, L., Kolker, A., and Mick, A., (2018) Rare Earth Element and Yttrium Resources in Acid Mine Drainage in the Illinois Basin, USA. GSA Annual Meeting in Indianapolis, Indiana, 06 November 2018, doi:10.1130/abs/2018AM-320174.